Synthesis, Characterization, and Utilization of Photocatalytic Property of Titanium Oxalate Complex

Tanin Tudrabiab

A Thesis Submitted in Partial Fulfillment of the Requirements for the Degree of Master of Science in Inorganic Chemistry

Prince of Songkla University

2014

Thesis Title Synthesis, Characterization, and Utilization of Photocatalytic Property of Titanium Oxalate Complex

Author Mr.Tanin Tudrabiab

Major Program Inorganic Chemistry

Major Advisor :

……...

(Assoc.Prof.Dr.Sumpun Wongnawa)

Examining Committee :

……...……Chairperson

(Dr.Anob Kantacha)

...……..……..Committee

(Assoc.Prof.Dr.Sumpun Wongnawa)

…...……Committee

(Asst.Prof.Dr.Sumetha Suwanboon)

....……...……....Committee

(Dr.Uraiwan Sirimahachai)

The Graduate School, Prince of Songkla University, has approved this thesis as partial fulfillment of the requirements for the Master of Science Degree in Inorganic Chemistry.

…….....

(Assoc.Prof.Dr.Teerapol Srichana)

Dean of Graduate School

I hereby certify that this work has not been accepted in substance for any degree, and is not being currently submitted in candidature for any degree.

_____Signature

(Mr.Tanin Tudrabiab)

Candidate

This is to certify that the work here submitted is the result of the candidate's own investigations. Due acknowledgement has been made of any assistance received.

_____Signature

(Assoc.Prof.Dr.Sumpun Wongnawa)
Major Advisor

_____Signature

(Mr.Tanin Tudrabiab)
Candidate

ชื่อวิทยานิพนธ์ การสังเคราะห์การศึกษาคุณลักษณะและการนำสมบัติทางโฟโตคะตะไลติกของสารเชิงซ้อนไทเทเนียมออกซาเลตมาใช้ประโยชน์

ผู้เขียน นายธานินทร์ ทัดระเบียบ

สาขาวิชา เคมีอินทรีย์

ปีการศึกษา 2556

บทคัดย่อ

ได้ทำการสังเคราะห์สารเชิงซ้อนไทเทเนียมออกซาเลตเป็นรูปแบบโครงผลึกด้วยวิธีการสังเคราะห์ที่ต่างจากที่เคยมีการรายงานไว้แล้วโดยการเติมสารละลาย $TiOSO_4.2H_2O$ ลงในสารละลายกรดออกซาลิกที่มีเอทานอลเป็นตัวทำละลายในช่วงแรกขณะที่ทิ้งสารไว้ในสารละลายผงตะกอนที่เกิดขึ้นเกิดเป็นรูปแบบอสัญฐานแต่เมื่อเวลาเพิ่มขึ้นผงตะกอนจะเปลี่ยนรูปแบบเป็นรูปแบบโครงผลึกศึกษาคุณลักษณะของสารเชิงซ้อนไทเทเนียมออกซาเลตที่ได้ทั้งทางกายภาพและทางเคมีโดยใช้เทคนิค XRD, BET, TGA, DSC, SEM, EDX และFT-IR สำหรับข้อมูลจากXRDพบว่าสารเชิงซ้อนไทเทเนียมออกซาเลตที่ได้มีสูตรทางเคมีคือ $Ti_2O_2(C_2O_4)(OH)_2.H_2O$ โดยตรงกับในระบบฐานข้อมูล JCPDS เลขที่ 00-048-1164 ซึ่งแสดงระบบโครงผลึกเป็นแบบออร์โทรอมบิคมีค่าคงที่แลตติสคือ a=1.0503 nm, b=1.5509 nm และc=0.9700 nm. และในการศึกษาปฏิกิริยาโฟโตคะตะไลติกนั้นศึกษาการสลายสีของสารละลายไอโอดีน (ทิงเจอร์ไอโอดีน 2%) ในน้ำทิ้งพบว่าสารเชิงซ้อนไทเทเนียมออกซาเลตนี้สามารถสลายสีสารละลายไอโอดีนจากสีส้มเข้มกลายเป็นใสไม่มีสีภายใต้การฉายแสงยูวีและความเข้มข้นสูงสุดของสารละลายไอโอดีนที่สลายได้คือ 3×10^{-4}M โดยใช้เวลาการฉายแสงยูวี 6 ชั่วโมงสารเชิงซ้อนไทเทเนียมออกซาเลตนี้สามารถนำกลับมาใช้ซ้ำในการสลายสีสารละลายไอโอดีนได้อีก

Thesis Title	Synthesis, Characterization, and Utilization of Photocatalytic Property of Titanium Oxalate Complex
Author	Mr.Tanin Tudrabiab
Major Program	Inorganic Chemistry
Academic Year	2013

Abstract

Titanium(IV) oxalate was successfully synthesized in a polycrystalline form by adding $TiOSO_4.2H_2O$ solution to an ethanol solution of oxalic acid which was a different method from those reported in the literatures.During the first ageing period, the initial precipitate exhibited poor crystallinity. The powder turned into a crystalline phase after the ageing time was increased.The physico-chemical properties of the synthesized titanium(IV) oxalate compound were studied by XRD, BET, TGA, DSC, SEM, EDX, and FT-IR techniques. From the X-ray data the product can be assigned as $Ti_2O_2(C_2O_4)(OH)_2.H_2O$, titanium oxide oxalate hydroxide hydrate, in JCPDS No.00-048-1164 which exists in the orthorhombic crystal system with lattice constants of a=1.0503 nm, b=1.5509 nm and c=0.9700 nm. The photocatalytic reaction was studied via degradation of aqueous solution of iodine (tincture iodine 2%) which was used as model for wastewater. The titanium oxalate product could convert dark-orange iodine solution to colorless iodide by means of UV-light irradiation. The maximum initial concentration of aqueous iodine solution on the photodegradation by crystalline titanium oxalate complex which turned from dark-orange to colorless in 6 hours was 3×10^{-4} M. In addition, the titanium oxalate complex could be used repeatedly to degrade the iodine solution.

.

ACKNOWLEDGEMENTS

The completion of this thesis would be impossible without the help of many people, whom I would like to thank.

I would like to express my sincere thanks to my advisor, Associate Professor Dr. Sumpun Wongnawa, who accepted this research problem from my proposal, for the valuable suggestions, for all the help and guidance over the years, for never failing to answer those annoying questions I kept wondering, for all excellent teaching and supervision, encouragement and criticism without which I would have been unable to complete this work.

Thanks are also extended to examination committee members of this thesis for their valuable time.

I would like to thank the Department of Chemistry, Faculty of Science, Prince of Songkla University, for all necessary laboratory facilities used throughout this research.

I am deeply indebted to the Center of Excellence for Innovation in Chemistry: PERCH-CIC, and the Graduate School, Prince of Songkla University, for the financial supports of this research.

My acknowledgements are extended to all of my collaborators who helped create an enjoyable atmosphere to be working in and for their many helpful in many countless ways throughout the years.

And last but not least, I would like to express my great debt of gratitude and dedication to my parents, sister, spouse and son who help me walk through the path of life to reach this stage.

Tanin Tudrabiab

THE RELEVANCE OF THE RESEARCH WORK TO THAILAND

Chemical industries produce paint and chemicals for photography, batteries, lubricants and other purposes from iodine. Radioactive iodine is applied in medicine, for example in thyroid cancer treatment. It can be released during nuclear accidents. Iodine often ends up in surface water from waste water treatment plants, including radioactive isotopes. High iodine concentrations may be present near chemical waste dumps.The release of this colored wastewater into the eco-system is maianly the environmental problem.Iodine is attributed to water hazard class 1 meaning that it is only slightly harmful when dissolved in water. However, reactions with alkali metals, aluminum, mercury, fluorine or turpentine may increase the risk.

No interest has been paid to titanium(IV) oxalate compound in the area of pollution control as well as utilizing its photodegradation propertyto cope with pollutants has been rarely reported.

This work used tincture of iodine solution as a model for wastewater discharged from places like hospitals or medicinal-oriented laboratories. The photodegradation studies showed that the synthesized titanium oxalate complex could degrade the aqueous iodine solution via photocatalytic reaction under UV irradiation. In addition, the titanium oxalate complex could be used several times to degrade the iodine solution under UV irradiation, though the photodegradation activities decreased with number of repeated used.These results point to possible use oftitanium oxalate complex for photodegradation treatment of wastewater from such places and we hope that this method might be used widely in the future as Thailand is growing and increasingly known as the medical hub of this region of the world.

CONTENTS

CONTENTS (continued)

CONTENTS (continued)

LIST OF FIGURES

LIST OF FIGURES (Continued)

LIST OF FIGURES (Continued)

LIST OF TABLES

LIST OF ABBRAVIATION AND SYMBOLS

α	=	Alpha
β	=	Beta
%	=	Percentage
°	=	Degree
λ	=	Wavelength
δ	=	Bending vibration
ν	=	Streching vibration
Å	=	Angstrom
A.R.	=	Analytical Reagent
BET	=	Brunauer-Emmett-Teller
cm	=	Centimeter
cm^{-1}	=	Wavenumber
°C	=	Degree Celsius
CPX	=	Complex
d	=	Diameter
DSC	=	Differential scanning calorimeter
EDX	=	Energy dispersive X-ray spectroscopy
FWHM	=	Full width at half-maximum
FT-IR	=	Fourier-transformed infrared spectroscopy
g	=	Gram
g/L	=	Gram per litre
h	=	Hour
hv	=	Photon energy
JCPDS	=	Joint Committee on Powder Diffraction Standard
K	=	Kelvin
M	=	Molar
m	=	Meter

LIST OF ABBRAVIATION AND SYMBOLS (Continued)

mg	=	Milligram
mL	=	Milliliter
mM	=	Millimolar
MW	=	Molecular weight
min	=	Minute
n	=	Number
nm	=	Nanometer
ppm	=	Part per million
SEM	=	Scanning electron microscopy
T	=	Temperature
TGA	=	Thermogravimetric analysis
UV	=	Ultraviolet
W	=	Watt
XRD	=	X-ray powder diffraction

CHAPTER 1
INTRODUCTION

1.1 Introduction

1.1.1 Background information

Titanium is the first member of the d-block transition elements and has four valence electrons $3d^2 4s^2$. Titanium, the world's fourth most abundant metal (exceeded only by aluminium, iron, and magnesium) and the ninth most abundant element (constituting about 0.63% of the Earth's crust), was discovered in 1791 in England by Reverend William Gregor who recognized the presence of a new element in ilmenite. The element was rediscovered several years later by the German chemist Heinrich Klaporth in rutile ore who named it after Titans, mythological first sons of the goddess Ge (Earth in Greek mythology). Titanium(IV) is the most stable and common oxidation state; compound in lower oxidation states, -I, 0, II and III, are quite readily oxidized to Ti(IV) by air, water, or other reagents. The energy for removal of four electrons is high, so the Ti(IV) is not found unbound to other elements that are present in various igneous rocks and sediments and Ti(IV) compounds are generally covalent. The estimated ionic radii for Ti(IV) is 0.68 Å and the octahedral covalent radii is 1.36 Å (Cotton, *et al*., 1972). Extremely pure titanium(IV) can be made on laboratory scale by the van Arkel-de Boer method, also used for other metals, in which TiI_4 that has been carefully purified is vaporized and decomposed on a hot wire in the vacuum (Tornqvist, *et al*., 1979).

Titanium compounds occur primarily in minerals like rutile, ilmenite, leucoxene, anatase, brookite, perovskite, and sphene, and it is found in titanates and many iron ores. The metal was also found in meteorites and has been detected in the Sun and M-type stars. Rocks brought back from the Moon during the Apollo 17 mission have 12.1% TiO_2. Titanium is also found in coal, ash, plants, and even in the human body (Albert Stwertka, 1998).

Titanium is well known for its excellent corrosion resistance (almost as resistant as platinum) being able to withstand attack by acid, moist chlorine gas, and

common salt solutions. Pure titanium is not soluble in water but soluble in concentrated acids (Lide, D. R., 2005). It is a light strong metal with low density (40% as dense as steel) that, when pure, is quite ductile (especially in an oxygen-free environment), easy to work, lustrous, and metallic-white in color. The relatively high melting point of this element makes it useful as a refractory metal. Titanium is as strong as steel, but 45% lighter, 60% heavier than aluminium, and twice stronger. These properties make it very resistant to the usual kinds of metal fatigue (Krebs, *et al*. 2006). Some of its properties are given in Table 1.1.

Table 1.1 Properties of titanium

Property	value
[a]Electronic structure	$3d^2 4s^2$
[b]Melting point, °C	1668 ± 5
[b]Boiling point, °C	3260
[b]Density, g/cm^3	
α phase at 20 °C	4.507
β phase at 885 °C	4.35
[b]Thermal conductivity at 25 °C, W/(m·K)	21.9
[b]Electrical resistivity at 20 °C, nΩ·m	420
[b]Magnetic susceptibility, mks	180 x 10^{-6}
[b]Modulus of elasticity, Gpa	
tension	*ca.* 101
compression	103
shear	44
[a]Metallic redius (Å)	1.47
[a]Entropy S°_{298} (cal/deg/mol)	7.33
[a]$E^\circ(M^{2+}/M)$ volts , 25 °C	-1.63
[a]$E^\circ(M^{3+}/M^{2+})$ volts , 25 °C	-0.37
[a]Heat of atomisation (kcal/g·atom)	112.6

[a](Clark, *et al.*, 1968), [b] (Kiriakidou, *et al.*, 1999).

Crystal structure studies on a number of titanium (IV) complexes or organometallic compounds have shown that most of them are not monomer in the solid state. Well known groups of compounds with tetrameric or dimeric structure are represented by alkoxides (Clark, *et al*., 1968).

The dicarboxylic ($C_2O_4^{2-}$) or oxalato anion (ox^{2-}) or ethanedioate ion has σ donor properties. The appearance of conjugated double bond shows π electron delocalization of oxalate ligand (I) (Zhou, *et al*., 1989). It can be electron donor and often functions as bidentate bridging ligand. Complexes formed by the oxalate ion describe below are of this type, with the possibility of π-bonding from the 2*p* orbitals on the oxygen making some contribution to the overall bond. The oxalate anion can coordinate to metal as monodentate (II) or bidentate ligand (III): the bidentate chelate structure (III) is the most common one (Nakamoto, K. *et al*., 1978).

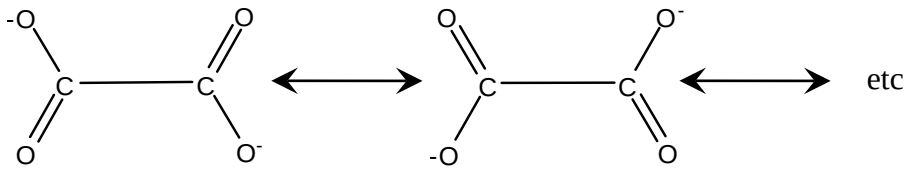

I

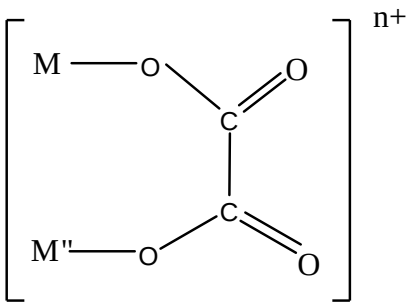

II

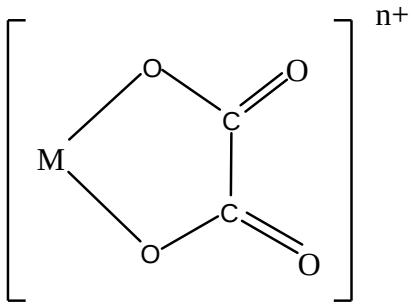

III

Oxalate, anion obtained from oxalic acid, occurs widely in nature, most notably fat hen (lamb's quarters), sorrel, and Oxalis species (wood sorrels). The root and/or leaves of rhubarb and buckwheat are listed as being high in oxalic acid (Streitweiser, *et al*., 1976). It arises biosynthetically via the incomplete oxidation of

carbohydrates. Other edible plants that contain significant concentrations of oxalic acid include star fruit (carambola), black pepper, parsley, poppy seed, amaranth, spinach, chard, beets, cocoa, chocolate, most nuts, most berries, New Zealand Spinach (Tetragonia tetragonioides) and beans. The gritty “mouth feel” one experiences when drinking milk with a rhubarb dessert is caused by precipitation of calcium oxalate. Thus, even dilute amounts of oxalic acid can readily "crack" the casein found in various dairy products. Leaves of the tea plant (*Camellia sinensis*) contain among the greatest measured concentrations of oxalic acid relative to other plants. However, the infusion beverage typically contains only low to moderate amounts of oxalic acid per serving, due to the small mass of leaves used for brewing.

1.1.2 Photochemical Reaction (William Reusch, 2009)**.**

Photochemistry is the underlying mechanism for all of photobiology. When a molecule absorbs a photon of light, its electronic structure changes, and it reacts differently with other molecules. The energy that is absorbed from light can result in photochemical changes in the absorbing molecule, or in an adjacent molecule (e.g., photosensitization). The energy can also be given off as heat, or as lower energy light, i.e., fluorescence or phosphorescence, in order to return the molecule to its ground state. Each type of molecule has a different preference for which of these different mechanisms it uses to get rid of absorbed photon energy, e.g., some prefer fluorescence over chemistry.

Photochemical reactions use the light energy to happen, however sunlight is a combination of many color lights and each color light may have different properties and different photochemical effects. Some chemical reactions that are normally very slow can be dramatically sped up by adding energy from light. For example, a gaseous mixture of hydrogen and oxygen is stable at room temperature. Occasionally, a hydrogen molecule might collide with an oxygen molecule with enough energy for them to react, but this happens very rarely. The rate at which the molecules react might be measured in years, perhaps centuries. But if you shine an ultraviolet light on the mixture, oxygen and hydrogen molecules combine explosively to form water. The ultraviolet light in the aforementioned chemical reaction provided the activation energy required to stimulate the reaction of hydrogen and oxygen.

Photochemical reactions are familiar to all of us. When the skin tans after exposure to sunlight, the tanning is the result of biological pathways that were stimulated by ultraviolet light. And photosynthesis, where carbon dioxide is converted into starch, is completely dependent on sunlight.

A. The Basic Laws of Photochemistry

The First Law of Photochemistry states that light must be absorbed for photochemistry to occur. Although this is a very simple law, some people in Low Level Light Therapy believe that light can produce effects without being absorbed. More education is required.

The Second Law of Photochemistry states that for each photon of light absorbed by a chemical system, only one molecule is activated for a photochemical reaction. This law is true for ordinary light intensities, however, with high-powered lasers, two-photon reactions can occur, i.e., the molecule is raised to a higher energy state than produced by single-photon absorption.

The Bunsen-Roscoe Law of Reciprocity states that a photochemical effect is directly proportional to the total energy dose, irrespective of the time required to deliver the dose. This law is true for chemicals in a test tube, but the response of cells to radiation usually involves a sequence of interacting biological reactions, making a linear "dose x time" relationship highly unlikely. There is no reciprocity when damage is produced, e.g., DNA damage, but there can be reciprocity over a narrow range of doses for photoreceptors that trigger a response, such as phytochrome (Wayne, *et al*., 1996).

B. Electromagnetic Radiation

Electromagnetic radiation consists of waves of electric and magnetic fields traveling in space at right angles to one another (see Figure 1.1).

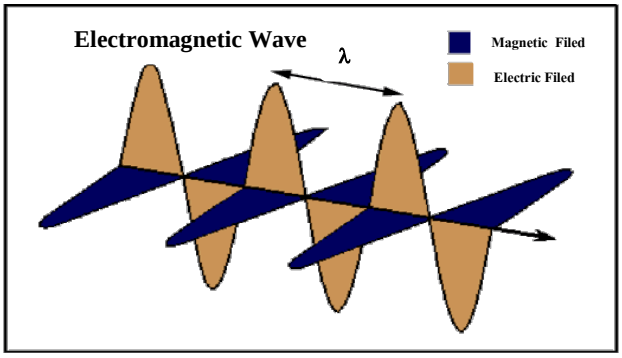

Figure 1.1 An electromagnetic wave showing the perpendicularly-oriented waves of electric and magnetic fields, and the characteristic wavelength (λ) of the radiation (Klessinger, *et al*., 1995).

The electromagnetic spectrum is composed of different wavelengths of light having different photon energies, and is classified into the regions shown in Figure 1.2. Note that the regions of interest for photochemistry, i.e., visible and ultraviolet (UV), are only a small part of the full electromagnetic spectrum. Longer wavelengths, e.g., far infrared, tend to cause the vibrational excitation of molecules, which results in heating. Shorter wavelength X-ray causes ionization.

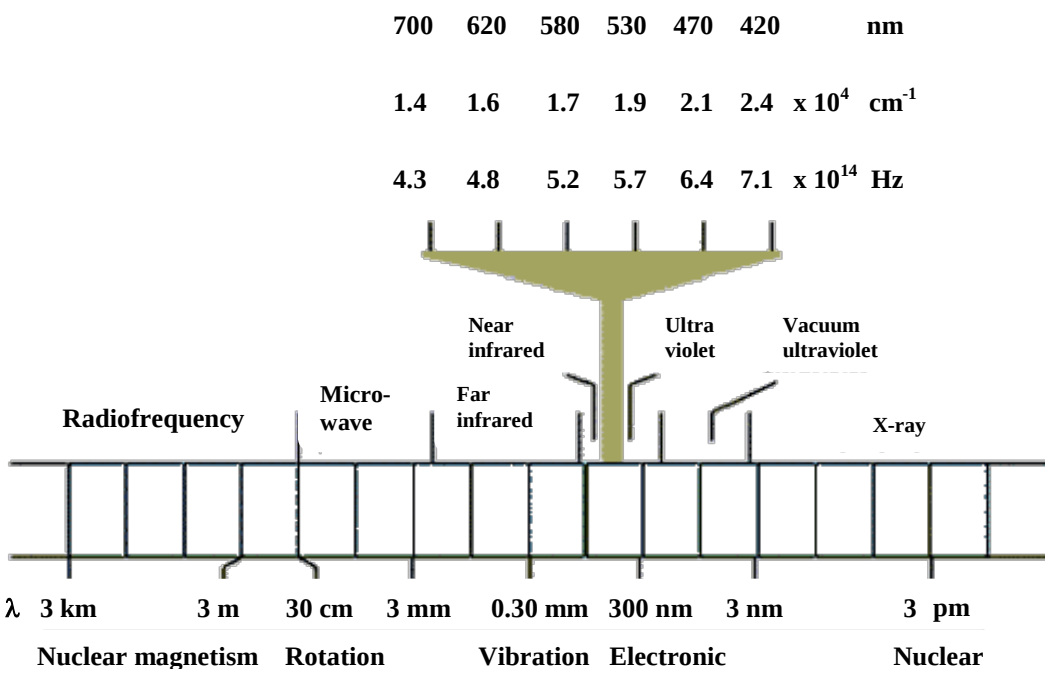

Figure 1.2 The electromagnetic spectrum and the highlighted visible region (Klessinger, *et al*., 1995).

C. Spectral regions

Photochemistries typically work in only a few sections of the electromagnetic spectrum. Some of the most widely used sections, and their wavelengths, are the following:

- Ultraviolet: 100–400 nm.
- Visible Light: 400–700 nm.
- Near infrared: 700–2500 nm.

D. The Jablonski Diagram

The energy gained by a molecule when it absorbs a photon causes an electron to be promoted to a higher electronic energy level. Figure 1.3 illustrates the principal photophysical radiative and non-radiative processes displayed by organic molecules in solution. The symbols S_0, S_1, T_2, etc., refer to the ground electronic state

(S_0), first excited singlet state (S_1), second excited triplet state (T_2), and so on. The horizontal radiative transitions and curly arrows indicate non-radiative transitions. The boxes detail the electronic spins in each orbital, with electrons shown as up and down arrows, to distinguish their spin. Note that all transitions from one electronic state to another originate from the lowest vibrational level of the initial electronic state. For example, fluorescence occurs only from S_1, because the higher singlet states (S_2, etc.) decay so rapidly by internal conversion that fluorescence from these states cannot compete.

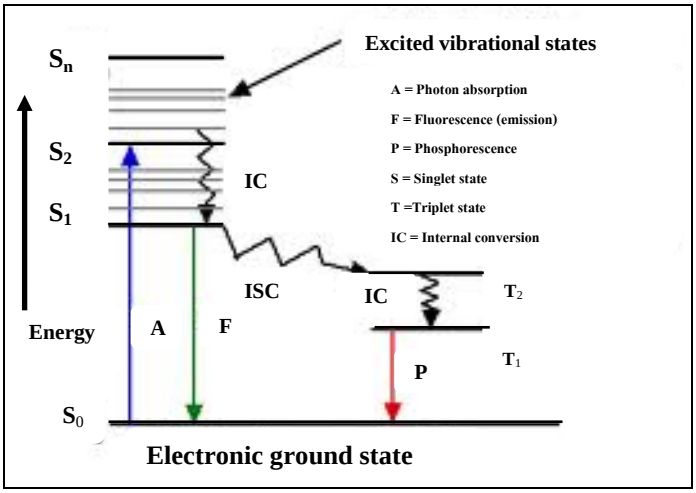

Figure 1.3 The Jablonski diagram (Thomas, 1998).

E. Electronically Excited States

The absorption of a UV or visible photon by a molecule produces an electronically excited state. The distribution of the electrons surrounding the nuclei change, as well as the forces between the atomic nuclei of a molecule. As a result, molecules in electronically excited states often have very different chemical and physical properties than their electronic ground states. For example, α-hydroxy naphthalene becomes a strong acid in its excited state. The ground state of α-hydroxy naphthalene has a pK_a of 9.2, but this is reduced to 0.4 in the excited singlet state. Molecules such as this are known as photoacids.

F. The Beer-Lambert Law

The absorption of photons of light is described by the Beer-Lambert Law, a relationship that indicates a decrease in intensity as a beam passes through a medium that can absorb it. Consider a parallel beam of monochromatic light of initial intensity, I_0, passing through a homogeneous absorbing medium (Figure 1.4).

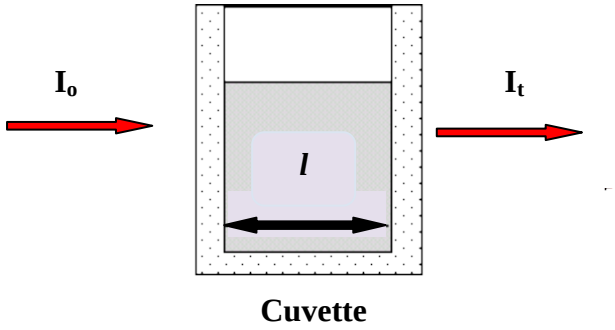

Figure 1.4 Schematic representation showing that light of initial intensity, I_o, passing through an absorbing medium in a cuvette with light path, I, will emerge with a final intensity, I_t (Wayne, *et al*., 1996).

In spectroscopy, absorbance, A, and optical density, OD, are used somewhat interchangeably. Optical density can be expressed as;

$$OD = \log (1/T) \qquad (1.1)$$

where T is the transmittance. It can also be expressed as:

$$A = OD = -\log(I_t / l_o) \qquad (1.2)$$

Note the log scale that an OD of 1 will have a transmittance of 0.1, and a % transmission of 10, but at OD = 2, the transmittance is 0.01, and the % transmission = 1. Another way of expressing this information is to use the Beer-Lambert Law. It states that the absorbance, A, of a molecular species is linearly related to the path

length (centimeter), l, the absorber concentration (moles/liter), c, and the proportionality constant, called the molar extinction coefficient of the absorbing molecular species (liters/mole-cm) [a measure of how strongly a chemical species absorbs light at a given wavelength].

$$A = \varepsilon . c . l \qquad (1.3)$$

G. Energy Level Diagram

One way to view the properties of molecular excited states is shown by the potential energy diagram in Figure 1.5. This diagram, known as a Franck-Condon energy level diagram, shows potential energy curves for the ground state (S_0), and first excited singlet state (S_1) of an organic molecule as a function of nuclear configuration. These curves are sometimes referred to as potential energy wells, because of their shape. The horizontal lines within each curve represent the vibrational levels of each electronic state. The lowest vibrational state for each energy level is designated as 0, and the levels above it are successively 1, 2, etc. The band assignments in brackets (e.g., (0, 1)) indicate, respectively, the vibrational level of the initial state, and of the final state involved in a transition.

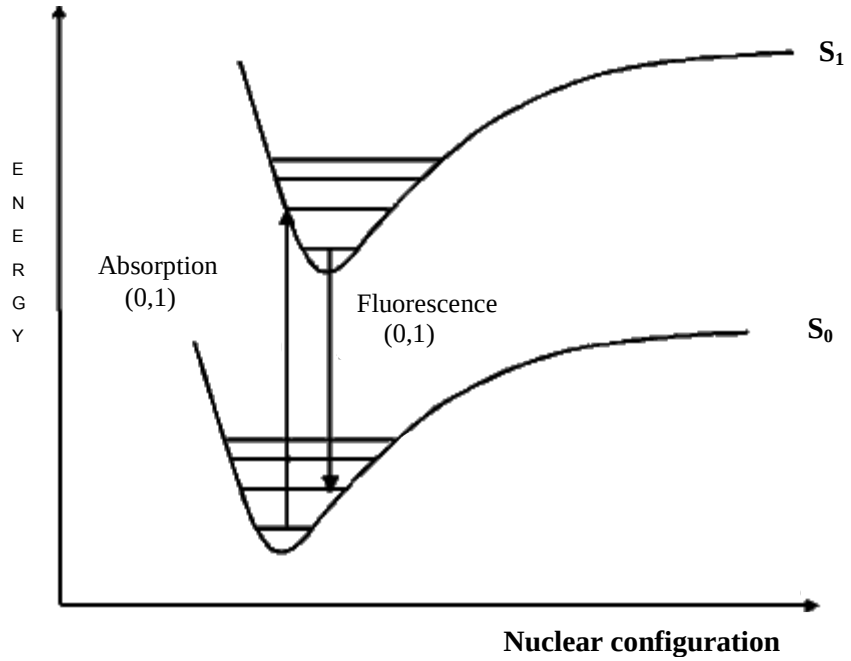

Figure 1.5 Franck-Condon Energy Level Diagram **(**William Reusch, 2009).

The horizontal axis is the nuclear configuration, which can be thought of as the distance between nuclei. When considering two atoms bonded to each other, the bottom of the well corresponds to the equilibrium bond length. Because excitation involves the movement of charge density into an antibonding orbital, the equilibrium bond length in S_1 is generally longer than in S_0. This is illustrated in the diagram by the displacement of the S_1 well to the right of the S_0 well.

The absorption of light takes place on a much faster time scale (approximately 10^{-15} s) than molecular vibration (approximately 10^{-12} s), and hence the initially formed excited state must have the same nuclear configuration as the ground state. This transition is called the vertical or Franck-Condon transition, and results in the molecule having excess vibrational energy. The excess vibrational energy can be dissipated through the process of vibrational relaxation, i.e., the process of internal conversion, which returns the molecule to the lowest vibrational level of S_1. Fluorescence usually occurs from the lowest vibrational level of S_1. Because these transitions occur at lower energies than absorption, fluorescence is observed at longer

wavelengths (λ) than absorption (i.e., lower energy), as shown in the lower right corner of Figure 1.5.

F. Quantum Yields and Lifetimes

The energy that a molecule gains when it absorbs light is subsequently lost by a molecule in one of several ways. As shown graphically in the Jablonski diagram (Figure 1.3), it can lose the energy as heat as it returns to the ground state (internal conversion). Alternately, it can lose the energy as light (fluorescence), usually on a nanosecond time scale. A third pathway is intersystem crossing to a triplet state, from which energy can also be lost as light (phosphorescence), but over much longer times (microseconds or longer). And finally, the energy can be transferred to another molecule.

The quantum yield of a process is the probability that an absorbed photon undergoes one particular process. Thus, one can define a quantum yield for fluorescence, a quantum yield for phosphorescence, or a quantum yield for other pathways. Each quantum yield is typically a number between 0 and 1 (except under unusual circumstances), and the total of all quantum yields for a particular absorption event should sum to one. Note that these processes are competing. If conditions are altered such that the quantum yield for fluorescence is increased, then the quantum yield for some other process (es) must decrease.

Consider a molecule, M, that is exposed to light, and absorbs photons at the rate, I_{abs}. As shown in the following formulas, the excited singlet state of the molecule, $^1M^*$, can fluoresce emitting a photon, $h\nu_f$. It can lose energy as heat, and move to the triplet excited state, $^3M^*$, by intersystem crossing (isc). Finally, it can lose energy as heat, and move to the ground state by internal conversion (ic). The rate of each of these loss processes will be proportional to the concentration of the excited singlet state, $^1M^*$, and a rate constant, k, for each process, as given in the second column below.

					Rate	
M	$\rightarrow$	$^1M^*$			I_{abs}	(1.4)
$^1M^*$	$\rightarrow$	M	+	$h\nu_f$	$k_f[^1M^*]$	(1.5)
$^1M^*$	$\rightarrow$	$^3M^*$	+	heat	$k_{isc}[^1M^*]$	(1.6)
$^1M^*$	$\rightarrow$	M^*	+	heat	$k_{ic}[^1M^*]$	(1.7)

Because the lifetime of the singlet excited state is relatively short, we can assume that the entire excited singlet states that are formed by light absorption will rapidly decay through one of the three means just described. This is the "steady state" approximation. Since the rate of formation of the excited singlet state is I_{abs} , then the sum of the rates of loss, each given above, must be equal to the rate of formation.

$$I_{abs} = \sum k_i [^1M^*] \qquad (1.8)$$

From this relationship, one can determine the quantum yield for each process. It is simply the rate of that process as a fraction of all pathways for the loss of energy.

G. Intermolecular Processes: Excited State Quenching.

When a second molecule interacts with a molecule in an excited state, new ways may be created for the excited state species to lose its energy of excitation. Such interactions (collisions) can induce the loss of energy in the form of heat, which is called physical quenching, or it can cause the energy to be transferred to the second molecule with or without the transfer of an electron. The former is called simply energy transfer, and the latter electron transfer. Formally, one can write:

M^*	+	Q	$\rightarrow$	M	+	Q	+	heat	
								physical quenching	(1.9)
M^*	+	Q	$\rightarrow$	M	+	Q^*		energy transfer	(1.10)
M^*	+	Q	$\rightarrow$	M^*	+	Q^-		electron transfer	(1.11)

When this kind of quenching occurs it reduces the concentration of the excited state more rapidly than if the quencher were not present. This means that fluorescence, which is proportional to the concentration of the excited state, will also be reduced. By monitoring fluorescence from the excited state molecule, one can determine the concentration of a quencher, if its rate constant of interaction with the excited state is known. Once again, consider the molecule, M, that can decay by fluorescence, intersystem crossing or internal conversion. Now add a fourth possiblility, quenching. The reactions and rates are then given by:

					Rate	
M	$\rightarrow$	$^1M^*$			I_{abs}	(1.12)
$^1M^*$	$\rightarrow$	M	+	$h\nu_f$	$k_f[^1M^*]$	(1.13)
$^1M^*$	$\rightarrow$	$^3M^*$	+	heat	$k_{isc}[^1M^*]$	(1.14)
$^1M^*$	$\rightarrow$	M	+	heat	$k_{ic}[^1M^*]$	(1.15)
$^1M^*$	+	Q	$\rightarrow$	quenching	$k_q[^1M^*][Q]$	(1.16)

Note that the quenching reaction rate depends on 2 reactants, M and Q, and the rate constant is a bimolecular rate constant. Once again, one can make the steady state approximation, and compare the rate of fluorescence, $k_f[^1M^*]$ in the presence of the quencher to the same quantity in the absence of the quencher. This leads to the following relationship:

$$\frac{I_f^o}{I_f} = 1 + k_q \tau_f [Q] \qquad (1.17)$$

where I_f^0 is the intensity, or rate of fluorescence, without a quencher; I_f is the intensity, or rate of fluorescence, with a quencher; k_q is the quencher rate coefficient; τ_f is the fluorescence lifetime of A without a quencher present, and [Q] is the concentration of the quencher. This relationship is referred to as the Stern-Volmer equation.

H. Photochemical Reactivity

The chemical reactivity of molecule is determined principally by its electron distribution. In the case of transition-metal complexes, it is well known that the widely ranging rates of their thermal reactions may be qualitatively (or semi-quantitatively) explained on the basis of the *d*-electron configuration of the central atom. For example, the kinetic inertness of the $(t_{2g})^6$ octahedral complexes can be accounted for on the basis of ligand field arguments, which show that the rearrangement of the ground-state octahedral structure to any transition state, whether of coordination number five or seven, would inevitably involve large activation energy.

In the excited states, the electron distribution is more or less changed with respect to the ground state and, therefore, the reactivity is also changed. A full theory of exited state reactivity is also changed. A full theory of excited state reactivity would begin with a calculation of the electron distribution in the excited state and would be followed by an account of the time-dependent nuclear configurations which follow as the molecule relaxes towards equilibrium with its environment. Such a possibility, however, seems to be a very remote one for polynuclear molecules in general, and even more so for coordination compounds. At the present time, we can only try to infer something on the reactivities of the excited states from an approximate and qualitative examination of their electron distribution (Gilbert, 1993).

For this purpose, it is again convenient to classify the electron electronically excited states in terms of “localized” MO configurations (*via supra*) as ligand- field, charge-transfer, and intra-ligand excited states.

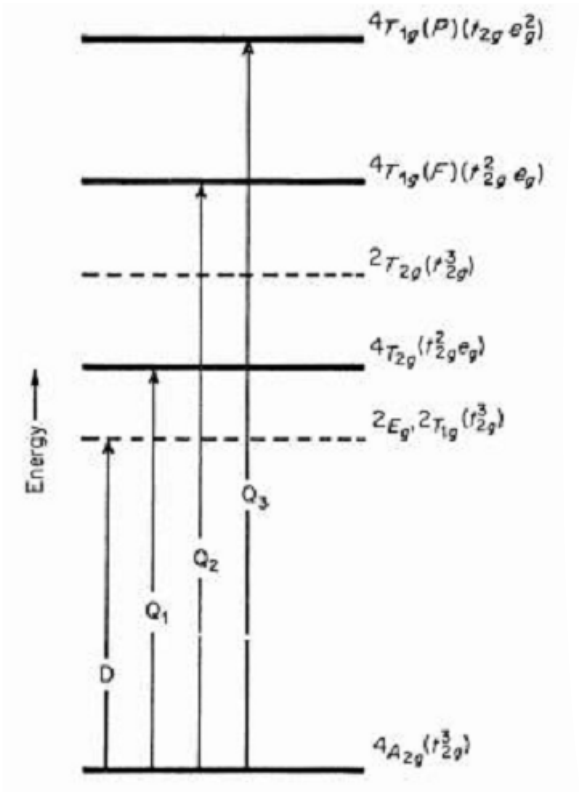

Figure 1.6 Schematic energy level diagram for octahedral Cr(III) complexes (d^3 electronic configuration)(Kagan, 1993).

(i) Ligand-Field Excited States

At a first approximation, the ligand-field (metal-centered) excited states arise from electron transition occurring between "metal" *d* orbitals (*vide supra*). With respect to the ground-state electron distribution, these transitions result in an *angular* electron rearrangement, which does not modify the charge distribution between ligands and metal. Therefore, since the ground state of complexes is usually stable towards intramolecular oxidation-reduction process (i.e. towards the homolytic fission of metal-ligands bonds), it is to be expected that the ligand-field excited states will also be stable towards this type of reactivity.

The angular rearrangement of the metal electrons, however, can cause important consequences as far as the reactivity towards ligand substitution or isomerization reactions is concerned. Such consequences can be easily visualized, for

example, in the case of strong field octahedral complex, such as those of Cr(III). The ground state of these complex, $^2A_{2g}$ belongs to the $(t_{2g})^3$ configuration (Figure 1.7). The spin-allowed transitions, such as the $^2A_{2g}\,(t_{2g})^3 \rightarrow {}^4T_{2g}\,(t_{2g})^2\,(e_g)$ one, correspond to the promotion of an electron from the t_{2g} to the e_g orbitals. This promotion will strongly affect the metal-ligand bonds. In a crystal field picture, the promotion of an electron from a t_{2g} orbital, which is direct away from the ligand, to an e_g orbital, which is directed towards the ligands, is expected to cause: (i) an increase in the metal-ligand repulsion, and then, either some lengthening of metal-ligend distances (and, eventually the detachment of a ligand) or a rearrangement of the molecule towards a more stable structure (isomerization); (ii) a decrease of electron density in some directions between the ligands, which will facilitate a nucleophilic attack on the central metal by solvent molecule or other ligands present in the solution (substitution reaction). A molecule orbital approach leads to parallel results. The e_g orbitals are strongly σ-antibonding, so that their partial occupation is expected to weaken some metal-ligand bonds. On the other hand, the presence of an empty t_{2g} orbital, available for bond making, will facilitate the entering of a new ligand. Note that, in the case of intraconfiguration transitions, such as $^2A_{2g}\,(t_{2g})^3 \rightarrow {}^2E_g\,(t_{2g})^3$ one in Cr(III) complexes, the above consideration do not apply.

(ii) Charge-Transfer Excited States

These states arise from transition between MO's principally localized on the metal and MO's principally localized on the ligands. Such transitions cause a radical redistribution of the electronic charge between the central metal and ligands and thus, a change in their oxidation state. It follows that the charge-transfer exited states will be particularly inclined to give intramolecular oxidation-reduction processes, resulting in the reduction of the metal and oxidation of a ligand, or viceversa. The tendency of the charge-transfer exited states to give such redox processes will be influenced by a number of factor, such as: (i) the stability of upper and lower oxidation states of the metal and ligands; (ii) the effective amount of charge transfer induced by irradiation; (iii) whether or not the charge-transfer is localized between *one* particular ligand and metal ($X \rightarrow M$ charge-transfer states in $ML_{n-1}X$ complexes); (iv) environmental condition (solvent reactivity, etc.).

The above discussion shows that, going from the ground state to charge-transfer exited states, one must expect principally a strong increase in the reactivity towards oxidation-reduction reaction. However, other features of the charge-transfer exited states should be pointed out. First of all, one can expect that there will be an increase in the reactivity towards substitution reactions. In fact, because of the charge-transfer process, the oxidation state of the metal is charge and, as a consequence, an inert complex may be change into a labile one. For example, LMCT transition in Co(III) complexes lead to Co(II) species which are kinetically labile. More specifically, it should also be considered that: (i) the MLCT transition increase the positive charge of the metal, so that a nucleophilic attack by other ligands could be facilitated; (ii) in most LMCT transition, the transferred electron goes into a metal orbital which points in the direction of the ligands (i.e. in a e_g σ-antibonding orbital): a metal-ligand repulsion could then result, analogously to what happens in the case of the ligand- field exited states. Moreover, charge-transfer transitions are expected to cause a strong change in the acid strength of complexes which contain "protogenic" ligands, such as H_2O, NH_3, en, etc.

As we have mentioned above, intermolecular charge-transfer transitions can also occur. For example, in ion-pair systems involving a complex cation, the excited states corresponding to such transitions are inclined to give redox processes

which result in the formation of a reduced form of the complex that, if it is unstable, will undergo decomposition. Of course, the actual occurrence of the redox process will depend on intrinsic properties of the ion-pair and on environmental conditions. Similarly, charge-transfer to solvent transitions will lead to an oxidized form of the complex and a solvated electron.

Finally, it is worth-while emphasizing the relation between the position of the charge-transfer bands and the thermal stability towards redox reactions. If a system shows a charge-transfer band at sufficiently long wavelengths, it means that the energy which must be supplied to make an oxidation-reduction reaction possible is relatively small. Thus, a similar system, containing a more oxidizable (anionic) ligand, is expected to undergo a spontaneous (i.e. thermal) redox reaction. This is true in a number of system; for example copper(II) bromide is dark red and copper(II) iodide is also “black” that it does not exist at all. Of course, a similar behavior may be observed in a series of complexes which contain the same anionic ligand and different metal ions.

(iii) Intra-Ligand Excited States

Intra-ligand (or ligand-centered) excited states arise from electrons occurring between two MO’s which may be considered as mainly localized on the ligand system. It is difficult to make general predictions on the reactivity of intra-ligand excited states because these states may occur in a variety of different ligands. At a first approximation, the intra-ligand transition neither change the charge distribution between the ligands and metal, nor affect the bonding structure of complex in the direct way. However, the change in the electronic structure of the ligand can cause important changes in it donor or acceptor properties, equilibrium geometry, dipole moment, acid strength, etc., so that these excited states could be unstable towards metal-ligand dissociation. Moreover, the ligand itself may be photosensitive in the particular reaction medium, and this will certainly affect the stability of the complex.

1.1.3 Iodine (I_2)

Iodine was discovered in 1811 by French chemist Curtois during the process of manufacturing potassium nitrate, with which he supplied the Napoleon armies (Week, M. E., 1945). While washing seaweed ashes (used to conserve potash in the process) with sulfuric acid, he notice violet fumes that condensed on his copper equipment and caused corrosion. Later, Gay-Lussac and Davy recognized it as a new element and named it after the Greek word for violet. Shortly after, polyiodide chemistry was discovered when Pelletier and Caventou showed that the addition of iodine to strychnine triiodide, which they named “hydroiodure iodure” (Pelletier, et *al.*, 1819). The reaction between metal halides and iodine, as well as the increased solubility of iodine in different solvents on the addition of potassium iodide also attracted early attention. Several investigators considered the increase in solubility a consequence of the formation of triiodide ions. However, many researchers were reluctant of accept this explanation. The first systematic investigation was initiated in 1839 by Jörgensen (Jörgensen, S. M., 1870). He proposed that polyiodide alkaloids contain iodide as well as iodine.

Even at an early stage in their history, polyiodides found applications in several areas. The blue starch-iodine complex (believed to consist of polyiodide fragments) was discovered already in 1814, and in that same year was employed as a sensitive analytical test for iodine (Greenwood, *et al*., 1990). A more unusual application for polyiodides was found during the extermination of stray dogs undertaken by the Paris police in 1830. They used strychnine-containing derivatives, and it was not long before an antidote was requested. Donne found that a solution of iodine in potassium iodide (potassium triiodide) was an appropriate antidote for the poisoning. The same mixture (tincture of iodine) has also been applied to the treatment of goiter (Coindet. 1820).

Polyiodide have earned much deserved attention because of their fascinating structural chemistry. Examples of everything from very simple discrete unit to one-dimensional chains and complicated two and three-dimensional networks all occur. Already in 1933, the first complete structural determination of a polyiodide, ammonium triiodide [$(NH_4)I_3$], was reported. Up until now, a large number of

polyiodide ions have been structurally characterized and anions in the range from I_2^- to I_{293}^- have been established. The great variety of possible polyiodide structures is a consequence of the ability of iodine to catenate through donor-acceptor interactions combined with the influence of counterions. These features have been rationalized and utilized in template synthesis, as well as in molecular and crystal engineering, where different cations are used to achieve special structural feature (Bally, *et al*., 1998). A apart from cation variation, it is also possible to substitute the polyiodide building blocks for other donor and acceptor species in order to modify the structural properties. Polyiodides are hypervalent, and many large polyiodide structures cannot be explained by simple covalent bonding models. The nature of the bonding in polyiodides has therefore been the object of much theoretical speculation (Landrum, *et al*., 1997). The interest in polyiodides has also been focused on mixed-valence, donor-acceptor materials (organic metals) where iodine is used as the acceptor. These materials often exhibit unusually high electronically conductivity. Several of these mix-valence compounds have been found to be superconductors with a T_c typically at 2-8 K. The use of iodine to dope conjugated polymers (where polyiodides are formed via charge transfer) to form conducting polymers has been an area of great interest, and the 2000 Nobel Prize in Chemistry to A. J. Heeger, A. G. MacDiarmid, and H. Shirakawa was awarded for research in this area.

Many of the properties mentioned above suggest potential technical applications in a great variety of areas. Indeed, polyiodides have found such applications in electronics, fuel cells, batteries, solar cells, optical devices, etc. (Rajpure, *et al*., 2000).

Iodine is strongly reactive, even though it is less extreme for iodine than for other halogens. Iodine cannot be found as an element, but rather as I_2 molecules, as I^- ions, or as iodate (a salt of iodinic acid with IO_3^- anion). When iodine is added to water the following reaction results (http://www.lenntech.com /periodic/water/iodine/iodine-and water.gtm# ixzz0pVrHMe34):

$$I_{2\,(l)} + H_2O_{\,(l)} \rightarrow OI^-_{\,(aq)} + 2H^+_{\,(aq)} + I^-_{\,(aq)} \qquad (1.30)$$

I_2 molecules and water molecules react to substances such as hypoiodite (OI^-). The reaction can move both ways of the equilibrium, depending on the pH of the solution. Iodine may also occur as I_3^-, HIO, IO^- and HIO_3. Iodine can bind to many different substances, for example other halogens. The compounds that are form behave differently when they come in contact with water.

Solubility of iodine and iodine compounds in water is determined by temperature (25^oC) and pressure (1 bar), and is relatively low. Iodine is better soluble in iodine solutions. The following reaction mechanism occurs:

$$I_2 + I^- \rightarrow I_3^- \qquad K = 723 \pm 10\ (25^oC) \qquad (1.31)$$

Most iodine compounds are readily soluble in water or alcohol. Inorganic iodine is highly water soluble.

Anthropogenic activities add iodine to the environment. Iodine is applied for different purposes, such as iodine x-rays, which are applied to patients in large doses (up to 200 g), and then excreted through urine. This and other medicinal applications may end up in groundwater through wastewater discharge. Iodine is applied for cleansing and disinfecting wounds, and is added to facial soap and band aids. Iodine disinfection mechanisms are ascribed to oxygen release from water molecules.

Chemical industries produce paint and chemicals for photography, batteries, lubricants and other purposes from iodine. Radioactive iodine is applied in medicine, for example in thyroid cancer treatment. It can be released during nuclear accidents. Iodine often ends up in surface water from waste water treatment plants, including radioactive isotopes. Iodine is retained by sludge for 2-25%. The residue remains in water, causing effluents to contain between 1 and 16 μg/L. High iodine concentrations may be present near chemical waste dumps.

Iodine is attributed to water hazard class 1. This means it is only slightly harmful when dissolved in water. However, reactions with alkali metals, aluminum, mercury, fluorine or turpentine may increase the risk. Environmental risks may differ between iodine substances. The LD_{50} value for rats (oral uptake) is about 14,000 mg/kg. The most commonly known environmental impact of radioactive iodine

was the nuclear reactor explosion at Chernobyl in 1986. The iodine isotope ^{131}I was released in large amounts. The isotope has a half life of 8 days, and it can be taken up by cows and other cattle, thereby moving into human milk and water supplies. In the Ukraine radioactive iodine in flowing water still causes problems. Most rivers flow south. High tide erases radioactivity of the mainland. Normally, humans hardly ever come into contact with radioactive iodine, unless there is a work-related reason or some kind of medical treatment.

The health effects of iodine in water fumes cause eye and lung irritation. As a pure element, iodine is toxic, even amounts as small as 2 g may be lethal. In an alcoholic solution an amount of 30 ml may be lethal. Iodines are relatively harmless in comparison. However, rat experiments point out these may influence female fertility.

A. Tincture of Iodine

Tincture of iodine can generally be described as a disinfectant, usually 2-7% elemental iodine, along with potassium iodide or sodium iodide, dissolved in a mixture of ethanol and water. As in the case of Lugol's iodine, the role of iodide and water in the solution is to increase the solubility of the elemental iodine, by turning it to the soluble triiodide anion I_3^-. However, since iodine has moderate solubility in ethanol, it is also assisted by this solvent directly(http://en.wikipedia.org/wiki/ Tincture_iodine).

Figure 1.7 The photograph of tincture iodine solution.

Thus, iodine tincture solutions are characterized by the presence of alcohol, and about the same amount (weight % content) of elemental iodine as iodide. Lugol's iodine, by contrast, has no alcohol, and has twice the amount of iodide as elemental iodine.

USP formulas of tincture of iodine is defined in the U.S. National Formulary (NF) as containing in each 100 mL, 1.8 to 2.2 grams of elemental iodine, and 2.1 to 2.6 grams of sodium iodide. Alcohol is 50 ml and the balance is purified water. This "2% free iodine" solution provides about one mg of free iodine per drop.

USP strong iodine tincture is defined in the NF as containing in each 100 mL, 6.8 to 7.5 gram of iodine, and 4.7 to 5.5 gram of potassium iodide. Purified water is 50 mL and the balance is alcohol. This 7% tincture solution is about 3.5 times more concentrated than USP 2% tincture.

As both USP solutions contain elemental iodine, which is moderately toxic when ingested in amounts larger than those required to disinfect water, tincture of iodine is sold labeled "for external use only," and used primarily as a disinfectant. Small amounts may be added to suspect drinking water as a disinfectant (typically 5 mg free iodine per liter, or 5 drops of 2% tincture).

Iodine tincture is not a recommended source of solely-nutritional iodine. Nutritional iodine is better supplied in the form of the less toxic iodide or iodate salts, which the body can easily convert to thyroid hormone.

Nevertheless, the iodide in tincture of iodine used as a water disinfectant does supply more than adequate nutritional iodine, perhaps 30 or more RDA per liter or quart. Application of tincture or Lugol's to the skin also results in absorption and bioavailability of some moderate fraction of the iodine. The absorption time (disappearance of the skin stain) depends on the level of iodine already in the body as well as the condition of the skin, and varies from one or two hours in iodine-deficient persons to many hours in those having normal levels.

Tincture of iodine is often found in emergency survival kits, used both to disinfect wounds and to sanitize surface water for drinking. When an alcohol solution is not desirable for this purpose, the alcohol-free Lugol's iodine, an aqueous

solution of iodine in potassium iodide solution, or else povidone iodine (Betadine), a povidone iodine solution, can be used.

1.2 Review of Literatures

1.2.1 General Remark

In the previous recent decades, oxalate-based compounds were often used in low-temperature routes to prepare nanocrystalline oxides. A representative example was the formation of pure barium titanate from the thermal decomposition of the complex barium titanyl oxalate hydrate. Similarly, in a systematic study of new compounds involving lead and zirconium and/or titanium, precursors of PZT type oxides, new mixed oxalates have been prepared, e.g., lead zirconium oxalate. In the course of this chemical synthesis investigation, some oxalate derivatives have also been obtained, such as lead nitrate oxalate and a titanium compound, whose structural and thermal properties are reported here. There are only a few inorganic oxalate-based titanium(IV) compounds for which the crystal structure is known. Kolen' ko, *et al*., (2004) reported that all of them are mixed oxalates, such as $M^{I}_{2}TiO(C_2O_4)_2 \cdot H_2O$ with M^{I} = NH_4, K and $BaTiO(C_2O_4)_2 \cdot 4.5H_2O$. The structure of these compounds contains tetramers Ti_4O_{20} based on four vertex sharing TiO_6 distorted octahedra, a wide range of Ti---O clusters which form -O-Ti-O- rings have also been obtained. Only a few studies for titanium oxalate involving synthesis, and some photochemistry degradation of other pollutants have been reported as follows.

Velde, *et al*., (1974) reported that Ti(IV) could be formed with oxalate ion to obtain colorless single crystal of titanyl oxalate using $TiCl_4$ and oxalic acid solution as precursors and controlled the pH in narrow range. It was identified to be ammonium titanyl oxalate monohydrate $(NH_4)_2TiO(C_2O_4)_2$. H_2O whose structure was monoclinic in the space group $P2_1/c$ with Z=8, d_c=1.808 g/cm^3 and d_m = 1.80 g/cm^3. The anion consisted of cyclic tetranuclear complexes $[TiO_{1/2}O_{1/2}(C_2O_4)_2]_4^{8-}$ with l symmetry. The titanium atoms had six-coordination with two bridging oxygen atoms cis to one another and four oxygen atoms of bidentate oxalate groups, together forming a distorted octahedral. Titanium atoms were part of cyclic tetrameric anions

with a central eight-ring (-Ti-O-)$_4$. The actual name of the compound should therefore be: ammonium cyclotetra-di-μ-oxo-cis-dioxalatotitanate (IV) tetra-hydrate.

Daniele, *et al*., (1983) studied the formation and stability of Li^+, Na^+, and K^+ complexes with oxalate or dicarboxylate ligand potentiometrically at various temperature and ionic strengths. It was found that the protonation constants obtained in different background salts followed in the order, almost invariably, $K^+ > Na^+ \geq Li^+$, suggesting that they were weak complexes. The stabilities of the alkali metal complexes with dicarboxylate ligand were $Li^+ > Na^+ \geq K^+$.

Hee-Lack, *et al*., (1999) investigated titanium oxalate powder by addition of $TiO(NO_3)_2$ solution to an ethanol solution of oxalic acid, white powder was precipitated and ripened in the mother solution with/without ultrasound at various temperatures. The powder was transformed from a poor cystallinity in the initial to an unknown crystalline phase, which was named *Y-phase*. The treatment of ultrasound during the ripening reaction accelerated the dissolution rate of the initial precipitated particles, so that the formation of the crystalline phase was hastened. The influences from various factors were observed such as reaction temperature and ripening time, as well as the effect of ultrasonic treatment in the solution.

Potdar, *et al*., (1999) developed the chemical coprecipitation route to synthesize a mixed oxalates [BaC_2O_4 + $TiO(C_2O_4)(H_2O)_2$] precursor. Ti(IV) always forms complex compounds with oxalate ions in ethanol. All complexes were shown to be titanyl compounds with formula $TiOC_2O_4 \cdot nH_2O$ if the Ti : C_2O_4 ratio 1 : 1 and pH < 2 was maintained. In that route, titanyl oxalate, $TiO(C_2O_4).nH_2O$ was prepared by reaction between alcoholic solution of butyl titanate monomer and oxalic acid. With excess oxalate concentration where Ti : $C_2O_4^{2-}$ ratio was maintained as 1 : 2 , the precipitate formed was further converted into soluble sodium titanyl oxalate, $Na_2TiO(C_2O_4)_2$ by reaction with sodium oxalate solution. It is reasonable to expect the formation of $Na_2TiO(C_2O_4)_2$ as titanium has tendency to form anionic oxalate complex species with a large number of coordinated oxalate ion. The fraction of $TiOC_2O_4$ species decreased rapidly with increasing pH whereas the anionic $TiO(C_2O_4)_2^{2-}$ builds up and approaches 100% in the pH 2.5–3.5 (stable over narrow pH range). The produced were destabilized by maneuvering pH conditions with the adding of aqueous solution of barium acetate to form insoluble $TiO(C_2O_4)(H_2O)_2$ and

oxalic acid. When barium acetate solution with pH = 6.9 – 7.1 was added to solution containing anionic $TiO(C_2O_4)_2^{2-}$ species, white precipitate was formed due to destabilization of anionic species. The pH after precipitation was 5.2. The *in-situ* regenerated oxalic acid reacted with Ba^{2+} ions to precipitate BaC_2O_4 simultaneously. The pyrolysis of mixed oxalate [BaC_2O_4 + $TiO(C_2O_4)(H_2O)_2$] in air were calcined at various temperature for 5 h to study crystallization and structure evolution behaviour. The system produced $BaTiO_3$ powders at ≥ 750 ^oC, size range 0.2-0.5 μm with spherical morphology. Formation of a mixed oxalates [BaC_2O_4 + $TiO(C_2O_4)(H_2O)_2$] precursor can be demonstrated by the following reactions;

$$(C_4H_9O)_4Ti + H_2C_2O_4.2H_2O + (CH_3)_2CHOH \rightarrow TiOC_2O_4 + 4C_4H_9OH \quad (1.32)$$

$$TiOC_2O_4 + Na_2C_2O_4 \rightarrow Na_2TiO(C_2O_4)_2 \quad (1.33)$$

$$Na_2TiO(C_2O_4)_2 \rightarrow 2Na^+ + TiO(C_2O_4)_2^{2-} \quad (1.34)$$

$$TiO(C_2O_4)_2^{2-} + 2H_2O \rightarrow TiO(C_2O_4)(H_2O)_2 + C_2O_4^{2-} \quad (1.35)$$

$$Ba(CH_3COO)_2 \rightarrow Ba^{2+} + 2CH_3COO^- \quad (1.36)$$

$$Ba^{2+} + C_2O_4^{2-} \rightarrow BaC_2O_4 \quad (1.37)$$

$$2Na^+ + 2CH_3COO^- \rightarrow 2CH_3COONa \quad (1.38)$$

$$BaC_2O_4 + TiO(C_2O_4)(H_2O)_2 \rightarrow BaC_2O_4 + TiOC_2O_4 + 2H_2O \quad (1.39)$$

$$BaC_2O_4 + TiOC_2O_4 \rightarrow BaCO_3 + TiO_2 + 2CO + CO_2 \quad (1.40)$$

$$BaCO_3 + TiO_2 \rightarrow BaTiO_3 + CO_2 \quad (1.41)$$

Chaouki, *et al*., (2003) reported the synthesis of the titanium (IV) oxalate, $[Ti_2O_3(H_2O)_2](C_2O_4).H_2O$, in a polycrystalline form in the course of the study of precursors of PZT type oxide. Its crystal structure was solved *ab initio* from powder diffraction data collected with conventional monochromatic X-rays. The symmetry was orthorhombic, space group *Cmca*, with cell dimensions a = 15.494(2) Å, b = 10.491(1) Å, c = 9.700(1) Å and Z = 8. The structures consisted of inorganic corrugated layers of corner-sharing TiO_6 octahedra, which formed infinite –Ti-O-Ti- connections, linked together by the oxalate anions. The titanium environment was discussed with regard to bond-valence calculations. The thermal behavior of this compound had been studied by temperature-dependent X-ray diffraction and thermal analyses. In the course of the dehydration process, the partially dehydrated phase $[Ti_2O_3(H_2O)_2](C_2O_4)$ had been isolated and its structure was solved from *in situ* X-ray powder diffraction data. Its crystal structure determination showed that the framework of the precursor was preserved. The complete decomposition scheme into anatase was also described.

Kolen' ko, *et al*., (2004) showed data on the phase composition and physicochemical properties of nanocrystalline TiO_2 powder prepared via hydrothermal treatment of aqueous titanyl sulfate ($TiOSO_4$), titanyl nitrate ($TiO(NO_3)_2$), and aqua complex titanyl oxalate acid ($H_2TiO(C_2O_4)_2$) solution and amorphous titanyl hydroxide ($TiO_2 \cdot nH_2O$) gel (synthesized by precipitation H_2TiCl_6 with an excess of aqueous ammonia) at 423 and 523 K for 10 min to 6 h at solution concentrations from 0.07 to 0.5 M. The synthesized samples were characterized by X-ray diffraction, thermogravimetry, transmission electron microscopy, and nitrogen BET surface area measurements. It was shown that, independent of the precursor, short-term (10 min) hydrothermal treatment led to the formation of nanocrytalline anatase (crystalline sized d = 10-30 nm), a metastable form titania. Upon increasing hydrothermal-treatment time to 6 h, the systems studied exhibited different behaviors. Nanocrytalline anatase might persist (titanyl sulfate solutions and amorphous titanyl hydroxide gel) or transformed into rutile (d= 50-100 nm).

Salah, *et al*., (2009) found that the performance of TiO_2 photocatalysts in eliminating organic compounds in water could be improved by combining them with calcium oxalate. The adsorption maximum capacity of Orange II on various pure

photocatalysts was dependent on the specific area. Concerning the mixed TiO_2/calcium oxalate catalysts, they observed that adsorption was still higher than that of pure correspondent photocatalysts. The influence of the sacrificial agent differed according to the photocatalyst used. Thus performance of the P25-TiO_2 photocatalyst was positive and slightly affected by the presence of calcium oxalate, whereas with TiO_2 –PC500 a decline in photocatalytic activity was noted. The use of calcium oxalate significantly improved the performance of titanium dioxide prepared by sol-gel. They observed similar results with the kinetics of mineralization. It seems that the effect of oxygen was the same whether pure TiO_2 samples or 70%TiO_2/30% calcium oxalate mixtures were used, regarding the rate of conversion of Orange II after 30 min of irradiation.

Wang, *et al*., (2009) investigated on oxalic acid used for removal from the intermediates of ilmenite leached by KOH liquor. Various parameters, such as pH, temperature, initial oxalate concentration, and illumination were included. Up to 96.5% of ilmenite was decomposed by KOH leaching method with the main products being $K_4Ti_3O_8$ and hematite. The optimum factors investigated were 90-100^oC, pH = 1.1, initial oxalate concentration, C_{ox} = 1.2 M, and under light illumination. In addition, it was found that the orthorhombic crystal $Ti_2O_2(OH)_2(C_2O_4).H_2O$ formed during the leaching process, which proceeded through three stages: (1) dissolution of the initial crystal $K_4Ti_3O_8$; (2) formation of clusters of particles; and (3) formation of $Ti_2O_2(OH)_2(C_2O_4).H_2O$ with good crystallinity. At low temperature ~ 60^oC, it often needed days to form a good crystallinity of $Ti_2O_2(OH)_2(C_2O_4).H_2O$, while only a few hours was enough at high temperature ~ 100^oC. The crystallinity of $Ti_2O_2(OH)_2(C_2O_4).H_2O$ remained unchanged with heat treatment at 180^oC, while it was destroyed at 190^oC, respectively. The reaction occurring in the process can be described as follows:

$$12\ FeTiO_3 + 16\ KOH + 3\ O_2 \rightarrow 4\ K_4Ti_3O_8 + 6\ Fe_2O_3 + H_2O \qquad (1.42)$$

$$Fe_2O_3 + H_2C_2O_4 \rightarrow 2\ [Fe(C_2O_4)_2]^{2-} + 3\ H_2O + 4\ H^+ + 2\ CO_2 \qquad (1.43)$$

$$Fe_2O_3 + H_2C_2O_4 + 4H^+ \rightarrow 2\ [FeHC_2O_4]^{2+} + 3\ H_2O \qquad (1.44)$$

$$2\ K_4Ti_3O_8 + 7\ H_2C_2O_4 \rightarrow 3\ Ti_2O_2(OH)_2(C_2O_4).H_2O + H_2O + 4\ K_2C_2O_4 \qquad (1.45)$$

Yogesh, *et al*., (2009) examined whether a single crystal precursor of the type $MTiO(C_2O_4)_2.H_2O$ could be obtained by simple salt elimination reaction between divalent transition metal chlorides and titanyl oxalate ion in an aqueous solution by addition of divalent transition metal chlorides to yield a molecular precursor. However, a mixture of transition metal titanyl oxalate was obtained insted. They suggest that molecular precursor of the formula $M\ [TiO(C_2O_4)_2].xH_2O$ might not be possible for M = Mn, Fe, Co, Ni and Cd by the reaction of their chlorides with potassium titanyl oxalate solution in the pH range 2–3. The addition of transition metal chlorides solution did not facilitate to stabilize the $TiO(C_2O_4)_2^{2-}$species so as to result in the molecular precursor. The narrow pH range of the stability of the titanyl species might be one of the reasons for the unsuccessful attempt towards the molecular precursor preparation but this could also arise from structural considerations. In the reported single crystal structure of $BaTiO(C_2O_4)_2$, the Ba^{2+}ion was both nine and ten coordinated by oxygen. The ionic radius of Ba^{2+}, 1.50 Å, is comparable to the potassium ion under similar coordination environments. However, the ionic radii of the metal ions, Co^{2+}, Ni^{2+}, Fe^{2+}, $Mn^{2+}$and $Cd^{2+}$are much smaller compared with either the Ba^{2+} or K^+ ion. The smaller size of these ions might be destabilizing the molecules and consequently might prevent the molecular precursor formation.

Wojciech Macyk, *et al*., (2009) reported that oxalic acid was the simplest example of a dicarboxylic acid. This model compound undergoes a strong dissociative adsorption onto the Ti(IV) surface. Several studies (ATR-FTIR) indicated that strong inner-sphere surface complexes were generated. Three different structures of these surface species were proposed: bidentate chelating and/or bidentate bridging where two oxygen atoms of each carboxyl group were attached to the same or adjacent Ti atoms while two remaining oxygen atoms were turned away from the surface (Figure 9), and monodentate (protonated adsorbed oxalate and/or strongly hydrogen-bonded oxalate or protonated oxalate) which might appear at low pH.

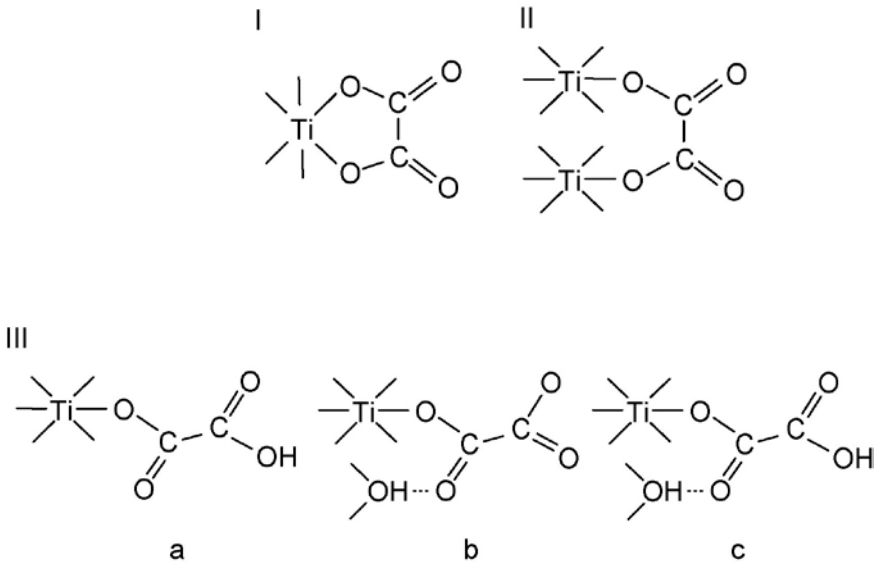

Figure 1.8 Types of Ti(IV)-oxalate surface complexes bidentate chelating(I), bidentate bridging(II) and proposed monodentate structures(III): protonated adsorbed oxalate (a), strongly hydrogen-bonded oxalate (b) or protonated oxalate (c).

Sophie, *et al*., (2011) studied the oxalic precipitation usually applied in nuclear industry Ti process radioactive wastes or to recover actinides from a multicomponent solution. These work dealt with the development of methods adapted to a nuclear environment in order to study the agglomeration phenomena during actinide oxalic precipitation. These methods were previously set up with harmless elements that simulate the actinide behavior: the lanthanide. A parametric study was carried out to qualify the influence of operating parameters on the agglomeration kernel and to determine a kinetic law for this mechanism. The experimental study was performed in a mixed suspension mixed product removal (MSMPR) precipitator at steady state. The method was based on the resolution of two population balances using the moment approach, one for elementary crystals and the other for agglomerates. Provided that the kinetic rates of nucleation and growth were known, the agglomeration kernel could be obtained from a mathematical treatment of the experimental particle size distributions. Results pointed out that experimental crystal sizes were consistent with an independent kernel. It appeared that the agglomeration

kernel was directly proportional to supersaturation, increased with temperature but was limited by ionic strength and shear rate.

1.2.2 Methods of dye removal from dye-containing industrial effluents

The control of water pollution has become increasingly importance in recent years. The release of dyes into the environment constitutes only a small proportion of water pollution, but dyes are visible in small quantities due to their brilliance. Tightening government legislation is forcing textile industries to treat their waste effluent to an increasingly high standard. Currently, removal of dyes from effluents is by physiochemical means. Such methods are often very costly and although the dyes are removed, accumulation of concentrated sludge creates a disposal problem. There is a need to find alternative treatments that are effective in removing dyes from large volumes of effluents and are low in cost, such as biological or combination systems. Many articles review or report the currently available technologies and suggests an effective, cheaper alternative for dye removal and decolourisation applicable on large scale.

Tim Robinson, *et al*., (2001) reviewed the critical study of the most widely used methods of dye removal from dye-containing industrial effluents. These methods have been discussed under three categories: chemical, physical and biological. Currently the main methods of textile dye treatment are by physical and chemical means with research concentrating on cheaper effective alternatives.

1.2.2.1 Chemical methods (Tim Robinson, *et al*., 2001).

A. Oxidative processes

This is the most commonly used method of decolourisation by chemical means. This is mainly due to its simplicity of application. The main oxidizing agent is usually hydrogen peroxide (H_2O_2). This agent needs to be activated by some means, for example, ultra violet light. Many methods of chemical decolourisation vary depending on the way in which the H_2O_2 is activated. Chemical oxidation removes the

dye from the dye-containing effluent by oxidation resulting in aromatic ring cleavage of the dye molecules.

B. H_2O_2–Fe(II) salts (Fenton's reagent)

Fenton's reagent is a suitable chemical means of treating wastewaters which are resistant to biological treatment or is poisonous to live biomass. Chemical separation uses the action of sorption or bonding to remove dissolved dyes from wastewater and has been shown to be effective in decolourising both soluble and insoluble dyes. One major disadvantage of this method is sludge generation through the flocculation of the reagent and the dye molecules. The sludge, which contains the concentrated impurities, still requires disposal. It has conventionally been incinerated to produce power, but such disposal is seen by some to be far from environmentally friendly. The performance is dependent on the final floc formation and its settling quality, although cationic dyes do not coagulate at all. Acid dyes, anionic dyes, mordant dyes and reactive dyes usually coagulate, but the resulting floc is of poor quality and does not settle well, yielding mediocre results.

C. Ozonation

The use of ozone was first pioneered in the early 1970s, and it is a very good oxidizing agent due to its high instability (oxidation potential, 2.07) compared to chlorine, another oxidizing agent (1.36), and H_2O_2 (1.78). Oxidation by ozone is capable of degrading chlorinated hydrocarbons, phenols, pesticides and aromatic hydrocarbons. The dosage applied to the dye-containing effluent is dependent on the total color and residual COD to be removed with no residue or sludge formation and no toxic metabolites. Ozonation leaves the effluent with no color and low COD suitable for discharge into environmental waterways. This method shows a preference for double-bonded dye molecules. One major advantage is that ozone can be applied in its gaseous state and therefore does not increase the volume of wastewater and sludge. Chromophore groups in the dyes are generally organic compounds with conjugated double bonds that can be broken down forming smaller molecules, resulting in

reduced coloration. These smaller molecules may have increased carcinogenic or toxic properties, and so ozonation may be used alongside a physical method to prevent this. Decoloration occurs in a relatively short time.

A disadvantage of ozonation is its short half-life, typically being 20 min. This time can be further shortened if dyes are present, with stability being affected by the presence of salts, pH, and temperature. In alkaline conditions, ozone decomposition is accelerated, and so careful monitoring of the effluent pH is required. Better results can be achieved using irradiation or with a membrane filtration technique. One of the major drawbacks with ozonation is cost, continuous ozonation is required due to its short half-life.

D. Photochemical

Photochemical processes are used to degrade toxic organic compounds to CO_2 and H_2O without the use of additional chemical oxidants, because the degradation is assisted by high concentrations of hydroxyl radicals ($OH^{\bullet}$) generated in the process. In this case, the photoexcitation of TiO_2 particles promotes an electron from the valence band to the conduction band, generating an electron (e_{CB}^-)/hole (h_{VB}^+) pair. Both reductive and oxidative processes can occur at or near the surface of the photoexcited TiO_2 particle. In general, oxygen is used to scavenge the conduction band electron, producing a superoxide anion radical ($O_2^{\bullet -}$), effectively preventing electron (e_{CB}^-)/hole (h_{VB}^+) recombination, and prolonging the lifetime of the hole. The photogenerated hole has the potential to oxidize several substrates by electron transfer. In aqueous solutions, oxidation of water to hydroxyl radical ($OH^{\bullet}$) by the photogenerated hole appears to be the predominant pathway. Hydroxyl radicals ($OH^{\bullet}$) and, to a lesser extent, superoxide anion can act as oxidants, ultimately leading to the mineralization of organic compounds (Gomes de Moraes, *et al.*, 2000).

The mineralization of most of the organic pollutants could be degraded following the usually proposed mechanism;

1. Absorption of efficient photons ($h\nu > Eg = 3.2$ eV) by titanium dioxide

$$TiO_2 + h\nu \rightarrow e_{CB}^- + h_{VB}^+ \quad (1.46)$$

2. Oxygen ionosorption (first step of oxygen reduction; oxidation state of oxygen changes from 0 to -1/2)

$$(O_2)_{ads} + e_{CB}^- \rightarrow O_2^{\bullet -} \quad (1.47)$$

3. Neutralization of OH^- groups by photoholes which produces $OH^\bullet$ radicals

$$(H_2O \rightarrow H^+ + OH^-)_{ads} + h_{VB}^+ + \rightarrow H^+ + OH^\bullet \quad (1.48)$$

4. Neutralization of $O_2^{\bullet -}$ by protons

$$O_2^{\bullet -} + H^+ \rightarrow HO_2^\bullet \quad (1.49)$$

5. Transient hydrogen peroxide formation and dismutation of oxygen

$$2\ HO_2^\bullet \rightarrow H_2O_2 + O_2 \quad (1.50)$$

6. Decomposition of H_2O_2 and second reduction of oxygen

$$H_2O_2 + e^- \rightarrow OH^\bullet + OH^- \quad (1.51)$$

7. Oxidation of the organic reactant via successive attacks by $OH^\bullet$ radicals

$$R + OH^\bullet \rightarrow R^\bullet + H_2O \quad (1.52)$$

8. Direct oxidation by reaction with holes

$$R + h^+ \rightarrow R^{+\bullet} \rightarrow \text{degradation products} \quad (1.53)$$

As an example of the last process, holes can react directly with carboxylic acid generating CO_2:

$$RCOO^- + h^+ \rightarrow R^\bullet + CO_2 \quad (1.54)$$

This causes the chemical oxidation of organic materials.

Photocatalysis has recently become a common word and various products using photocatalytic functions have been commercialized. Among many candidates for photocatalysts, TiO_2 is almost the only material suitable for industrial use at present and also probably in the future. This is because TiO_2 has the most efficient photoactivity, the highest stability and the lowest cost. More significantly, it has been used as a white pigment from ancient times, and thus, its safety to humans and the environment is guaranteed by history. There are two types of photochemical reaction proceeding on a TiO_2 surface when irradiated with ultraviolet light. One includes the photo-induced redox reactions of adsorbed substances, and the other is the photo-induced hydrophilic conversion of TiO_2 itself. The former type has been known since the early part of the 20^{th} century, but the latter was found only at the end of the

century. The combination of these two functions has opened up various novel applications of TiO_2, particularly in the field of building materials.

Instead, the research shifted to the utilization of the strong photoproduced oxidation power of TiO_2 for the destruction of pollutants. The first such reports were those of Frank and Bard in 1977, in which they described the decomposition of cyanide in the presence of aqueous TiO_2 suspensions (Frank, *et al*., 1980). In the 1980s, detoxications of various harmful compounds in both water and air were demonstrated using powdered TiO_2 actively as potential purification methods of waste water and polluted air (Fox, *et al*., 1980).When the purpose shifted to the oxidation reaction of harmful compounds, the reduction reaction was not necessarily hydrogen production anymore. The ionization of TiO_2 was not necessary in this case, and TiO_2 powder itself was used under ambient condition. Now both the reduction and oxidation sites are located on the TiO_2 surface, and the reduction of adsorbed oxygen molecules proceeds on the TiO_2 surface. As already mentioned, the holes (h^+) generated in TiO_2 were highly oxidizing, and most compounds were essentially oxidized completely. In addition, various forms of active oxygen, such as O_2^-,·OH, HO_2· and O·, produced by the following processes may be responsible for the decomposition reactions.

$$e^- + O_2 \rightarrow O_2^- \text{ (ad)} \qquad (1.55)$$

$$O_2^- \text{ (ad)} + H^+ \rightarrow HO_2 \text{ (ad)} \qquad (1.56)$$

$$h^+ + H_2O \rightarrow {}^-OH \text{ (ad)} + H^+ \qquad (1.57)$$

$$h^+ + O_2\text{(ad)} \rightarrow 2\cdot O \text{ (ad)} \qquad (1.58)$$

For the purpose of easy handling of photocatalysts, the immobilization of TiO_2 powders on supports was carried out in the late 1980s. Although many research studies were on the purification of wastewater and polluted air, TiO_2 photocatalysis could not be developed to the stage of a real industrial technology in the 1980s.

In recent years attention has been focused on heterogeneous photocatalysis for the treatment of recalcitrant chemical present in the wastewater. Among these heterogeneous photocatalysis in the presence of irradiated semiconductors (TiO_2, WO_3, SnO_2, ZnO, CdS, and others), TiO_2 has been successfully

used to decolorize and mineralize many organic pollutants including several dyes and their intermediates present in aqueous systems using both artificial light and under sunlight using solar technology (Muruganandham, *et al*., 2005). TiO_2 is the most widely used photocatalyst because of its good activity, chemical stability, commercial availability and inexpensiveness. It is generally used as a photocatalyst for environmental applications such as air purification, water disinfection, hazardous waste remediation and water purification (Nagaveni, *et al*., 2004). The efficiency of advanced oxidation processes for degradation of recalcitrant compounds has been extensively documented. Photochemical processes are used to degrade toxic organic compounds to CO_2 and H_2O without the use of additional chemical oxidants, because the degradation is assisted by high concentrations of hydroxyl radicals (OH·) generated in the process. In this case, the photoexcitation of TiO_2 particles promotes an electron from the valence band to the conduction band, generating an electron (e_{CB}^-) /hole (h_{VB}^+) pair. Both reductive and oxidative processes can occur at or near the surface of the photoexcited TiO_2 particle. In general, oxygen is used to scavenge the conduction band electron, producing a superoxide anion radical ($O_2{\cdot}^-$), effectively preventing electron (e_{CB}^-) /hole (h_{VB}^+) recombination, and prolonging the lifetime of the hole. The photogenerated hole has the potential to oxidize several substrates by electron transfer. In aqueous solutions, oxidation of water to hydroxyl radical (OH·) by the photogenerated hole appears to be the predominant pathway. Hydroxyl radicals (OH·) and, to a lesser extent, superoxide anion can act as oxidants, ultimately leading to the mineralization of organic compounds (Gomes de Moraes, *et al*., 2000).

E. Sodium hypochloride (NaOCl)

This method attacks at the amino group of the dye molecule by the Cl^+. It initiates and accelerates azo-bond cleavage. This method is unsuitable for disperse dyes. An increase in decoloration is seen with an increase in Cl concentration. The use of Cl for dye removal is becoming less frequent due to the negative effects it has when released into waterways and the release of aromatic amines which are carcinogenic, or otherwise toxic molecules.

F. Cucurbituril

Cucurbituril was first mentioned by Behrand (1905), and then rediscovered in the 1980s by Freeman (1981). It is a cyclic polymer of glycoluril and formaldehyde. Cucurbituril, so named, because its structure is shaped like a pumpkin (a member of the plant family *Cucurbitaceae*). The uril, indicates that a urea monomer is also part of this compound. Buschmann (1992) showed extraordinarily good sorption capacity of cucurbituril for various types of textile dyes. Cucurbituril is known to form host-guest complexes with aromatic compound and this may be the mechanism for reactive dye adsorption. Another proposed mechanism is based on hydrophobic interactions or the formation of insoluble cucurbituril-dye-cation aggregates since adsorption occurs reasonably fast. To be industrially feasible, cucurbituril would need to be incorporated into fixed bed sorption filters. Like many other chemical methods, cost is a major disadvantage.

G. Electrochemical destruction

This is a relatively new technique, which was developed in the mid 1990s. It has some significant advantages for use as an effective method for dye removal. There is little or no consumption of chemicals and no sludge build up. The breakdown metabolites are generally not hazardous leaving it safe for treated wastewaters to be released back into water ways. It shows efficient and economical removal of dyes and a high efficiency for color removal and degradation of recalcitrant pollutants. Relatively high flow rates cause a direct decrease in dye removal, and the cost of electricity used is comparable to the price of chemicals.

1.2.2.2 Physical treatments

A. Adsorption

Adsorption techniques have gained favor recently due to their efficiency in the removal of pollutants too stable for conventional methods.

Adsorption produces a high quality product, and is a process which is economically feasible. Decolourisation is a result of two mechanisms: adsorption and ion exchange, and is influenced by many physio-chemical factors, such as, dye/sorbent interaction, sorbent surface area, particle size, temperature, pH, and contact time.

B. Activated carbon

This is the most commonly used method of dye removal by adsorption and is very effective for adsorbing cationic, mordant, and acid dyes and to a slightly lesser extent, dispersed, pigment and reactive dyes. Performance is dependent on the type of carbon used and the characteristics of the wastewater. Removal rates can be improved by using massive doses, although regeneration or re-use results in a steep reduction in performance, and efficiency of dye removal becomes unpredictable and dependent on massive doses of carbon. Activated carbon, like many other dye-removal treatments, is well suited for one particular waste system and ineffective in another. Activated carbon is expensive. The carbon also has to be reactivated otherwise disposal of the concentrates has to be considered. Reactivation results in 10–15% loss of the sorbent.

C. Peat

The cellular structure of peat makes it an ideal choice as an adsorbent. It has the ability to adsorb transition metals and polar organic compounds from dye-containing effluents. Peat may be seen as a viable adsorbent in countries such as Ireland and UK, where it is widely available. Peat requires no activation, unlike activated carbon, and also costs much less. Due to activated carbon’s powdered nature, it has a much larger surface area, and hence has a better capacity for adsorption. Spent peat may be burned and utilized for steam rising, or, potentially, as substrate in SSF, for protein enrichment.

D. Wood chips

They show a good adsorption capacity for acid dyes although due to their hardness, it is not as good as other available sorbents and longer contact times are required. Adsorbed wood is conventionally burnt to generate power although there is potential for SSF of the dye-adsorbed wood chips.

E. Fly ash and coal (mixture)

A high fly ash concentration increases the adsorption rates of the mixture due to increasing the surface area available for adsorption. This combination may be substituted for activated carbon, with a ratio of fly ash:coal, 1:1.

F. Silica gel

An effective material for removing basic dyes, although side reactions, such as air binding and air fouls with particulate matter, prevents it being used commercially.

G. Other materials

The use of these substrates such as natural clay, corn cobs, rice hulls etc., for dye removal is advantageous mainly due to their widespread availability and cheapness. They are economically attractive for dye removal, compared to activated charcoal, with many comparing well in certain situations. These materials are so cheap regeneration is not necessary and the potential exists for dye-adsorbed materials to be used as substrates in solid state fermentation (SSF) for protein enrichment.

H. Membrane filtration

This method has the ability to clarify, concentrate and, most importantly, to separate dye continuously from effluent. It has some special features unrivalled by other methods; resistance to temperature, an adverse chemical environment, and microbial attack. The concentrated residue left after separation poses disposal problems, and high capital cost and the possibility of clogging, and membrane replacements are its disadvantages. This method of filtration is suitable for water recycling within a textile dye plant if the effluent contains low concentration of dyes, but it is unable to reduce the dissolved solid content, which makes water re-use a difficult task.

I. Ion exchange

Ion exchange has not been widely used for the treatment of dye-containing effluents, mainly due to the opinion that ion exchangers cannot accommodate a wide range of dyes. Wastewater is passed over the ion exchange resin until the available exchange sites are saturated. Both cation and anion dyes can be removed from dye-containing effluent this way. Advantages of this method include no loss of adsorbent on regeneration, reclamation of solvent after use and the removal of soluble dyes. A major disadvantage is cost. Organic solvents are expensive, and the ion exchange method is not very effective for disperse dyes.

J. Irradiation

Sufficient quantities of dissolved oxygen are required for organic substances to be broken down effectively by radiation. The dissolved oxygen is consumed very rapidly and so a constant and adequate supply is required. This has an effect on cost. Dye-containing effluent may be treated in a dual-tube bubbling rector. This method showed that some dyes and phenolic molecules can be oxidized effectively at a laboratory scale only.

K. Electrokinetic coagulation

This is an economically feasible method of dye removal. It involves the addition of ferrous sulphate and ferric chloride, allowing excellent removal of direct dyes from wastewaters. Unfortunately, poor results with acid dyes, with the high cost of the ferrous sulphate and ferric chloride, means that it is not a widely used method. The optimum coagulant concentration is dependent on the static charge of the dye in solution and difficulty in removing the sludge formed as part of the coagulation is a problem. Production of large amounts of sludge occurs, and this results in high disposal costs.

1.2.2.3 Biological treatments

A. Decolourisation by white-rot fungi

White-rot fungi are those organisms that are able to degrade lignin, the structural polymer found in woody plants. The most widely studied white-rot fungus, in regards to xenobiotic degradation, is *Phanerochaete chrysosporium*. This fungus is capable of degrading dioxins, polychlorinated biphenyls (PCBs) and other chloro-organics. Davis, *et al*., (1993) also showed the potential of using *P. sordida* to treat creosote contaminated soil. Kirby (1999) has shown that *P. chrysosporium* had the ability to decolorize artificial textile effluent by up to 99% within 7 days. White-rot fungi are able to degrade dyes using enzymes, such as lignin peroxidases (LiP), manganese dependent peroxidases (MnP). Other enzymes used for this purpose include H_2O_2-producing enzymes, such as, glucose-1-oxidase and glucose-2-oxidase, along with laccase, and a phenoloxidase enzyme. These are the same enzymes used for the lignin degradation. Azo dyes, the largest class of commercially produced dyes, are not readily degraded by micro-organisms but these can be degraded by *P. chrysosporium* (Paszczynski and Crawford, 1995). Other fungi such as, *Hirschioporus larincinus*, *Inonotus hispidus*, *Phlebia tremellosa* and *Coriolus versicolor* have also been shown to decolorize dye-containing effluent.

Although white-rot fungi have been shown to decolorize dyes in liquid fermentations, enzyme production has also been shown to be unreliable. This is mainly due to the unfamiliar environment of liquid fermentations. The ability to utilize these fungi in their natural environment means that they are more likely to be more effective in SSF.

B. Other microbial cultures

Mixed bacterial cultures from a wide variety of habitats have also been shown to decolorize the diazo-linked chromophore of dye molecules in 15 days Nigam, *et al.*, Marchant (1995) and Nigam, *et al.*, (1996) demonstrated that a mixture of dyes were decolorized by anaerobic bacteria in 24–30 h, using free growing cells or in the form of biofilms on various support materials. Ogawa, *et al.*, (1990) also demonstrated the use of bacteria for azo dye biodegradation. These microbial systems have the drawback of requiring a fermentation process, and are therefore unable to cope with larger volumes of textile effluents. The ability of bacteria to metabolize azo dyes has been investigated by a number of research groups. Under aerobic conditions azo dyes are not readily metabolized although Kulla (1981) reported the ability of *Pseudomonas* strains to aerobically degrade certain azo dyes. However, the intermediates formed by these degradative steps resulted in disruption of metabolic pathways and the dyes were not actually mineralized. Under anaerobic conditions, such as anoxic sediments, many bacteria gratuitously reduce azo dyes reportedly by the activity of unspecific, soluble, cytoplasmic reductases, known as azo reductases. These enzymes are reported to result in the production of colourless aromatic amines which may be toxic, mutagenic, and possibly carcinogenic to animals.

Increasingly literature evidence suggests that additional processes may also be involved in azo dye reduction. It has been reported that many bacteria reduce a variety of sulfonated and non-sulfonated azo dyes under anaerobic conditions without specificity of any significance. In addition many highly charged and high molecular-sized sulfonated and polymeric azo dyes are unlikely to pass the cell membrane.Taken together both pieces of evidence point to the existence of a reducing activity which is not dependent on the intracellular availability of the azo dye. This hypothesis was

supported by work at the University of Stuttgart, Germany, which isolated a strain of *Sphingomonas* capable of using redox mediators generated during the aerobic metabolism of 2-naphthalenesulfonate to facilitate a 20-fold increase in its ability to reduce the sulfonated azo dye amaranth. These redox mediators were found to be decomposition products of 1, 2-dihydroxynaphthalene and were able to anaerobically shuttle reduction equivalents from the bacterial cells to the extracellular azo dye. Subsequently this group found that their isolate *Sphingomonas* sp strain BN6 possessed both cytoplasmic and membrane-bound azo-reductase activities. Yeasts, such as *Klyveromyces marxianus*, are capable of decolorizing dyes. Banat et al. (1999) showed that *K. marxianus* was capable of decolorizing Remazol Black B by 78–98%. Zissi et al. (1997) showed that *Bacillus subtilis* could be used to break down *p*-aminoazobenzene, a specific azo dye. Further research using mesophilic and thermophilic microbes has also shown them to degrade and decolorize dyes.

C. Adsorption by living/dead microbial biomass

The uptake or accumulation of chemicals by microbial mass has been termed biosorption (Hu, 1992; Hu, 1996; Tsezos, *et al.*, 1989; Kumar, *et al.*, 1998). Dead bacteria, yeast and fungi have all been used for the purpose of decolorizing dye-containing effluents.

Textile dyes vary greatly in their chemistries, and therefore their interactions with micro-organisms depend on the chemistry of a particular dye and the specific chemistry of the microbial biomass. Depending on the dye and the species of micro-organism used different binding rates and capacities will be observed. It can be said that certain dyes have a particular affinity for binding with microbial species.

It had been observed that biomass derived from the thermotolerant ethanol-producing yeast strain, *K. marxianus* IMB3, exhibited a relatively high affinity for heavy metals. Biosorption capacities showed that this type of biomass had a significantly high affinity for dye removal, and so widened the spectrum of use for biomass.

The use of biomass has its advantages, especially if the dye-containing effluent is very toxic. Biomass adsorption is effective when conditions are not always

favorable for the growth and maintenance of the microbial population. Adsorption by biomass occurs by ion exchange.

Hu (1992) demonstrated the ability of bacterial cells to adsorb reactive dyes. Zhou, *et al.*, (1993) used actinomyces as an adsorbent for decolonization of effluents containing anthroquinone, phalocyanine and azo dyes.

Biosorption tends to occur reasonably quickly: a few minutes in algae to a few hours in bacteria (Hu, 1996). This is likely to be due to an increase in surface area caused by cell rupture during autoclaving.

D. Anaerobic textile-dye bioremediation systems

Azo dyes make up 60–70% of all textile dyestuffs. Azo dyes are soluble in solution, and are not removed via conventional biological treatments. Reactive dyes have been identified as the most problematic compounds in textile dye effluents. Anaerobic bioremediation allows azo and other water-soluble dyes to be decolorized. This decolorisation involves an oxidation–reduction reaction with hydrogen rather than free molecular oxygen in aerobic systems. Typically, anaerobic breakdown yields methane and hydrogen sulphide. Azo dye acts as an oxidizing agent for the reduced flavin nucleotides of the microbial electron chain and is reduced and decolorized concurrently with reoxidation of the reduced flavin nucleotides. In order for this to occur, additional carbon is required in order for decolorisation to proceed at a viable rate. This additional carbon is converted to methane and carbon dioxide, releasing electrons. These electrons cascade down the electron transport chain to a final electron acceptor, in this case, the azo-reactive dye. The electrons react with the dye reducing the azo bonds, and ultimately causing decolorisation.

In lab-scale studies glucose has been added to provide a source of carbon. This additional carbon supplementation may be a limiting factor when this technology is scaled-up. Anaerobic degradation of textile dyes yields only azo reduction. Mineralisation does not occur. It has been shown that azo- and nitro-components are reduced in the sediments and in the intestinal environment, resulting in the regeneration of the parent toxic amines. Therefore, careful monitoring is required before treated wastewater is released into waterways. A major advantage of

this anaerobic system, apart from the decolourisation of soluble dyes, is the production of biogas. Biogas can be reused to provide heat and power, and will reduce energy costs.

Recently, there has been increasing interest in application of nanocrystalline materials for catalyst, supports, ceramics, inorganic membranes, gas sensing, water purification, and solar energy conversion (Yanqing, *et al.*, 2001). Furthermore, photocatalysis of nanocrystalline titanium dioxide has a great many advantage on waste water treatment such as high catalysis efficiency, energy saving, no pollution, etc. and can degrade all kinds of organic pollutants from water effectively. All of those merits make photocatalysis of water treatment and it is supposed to be used widely in the future (Balong, *et al.*, 2003).

Coloration is a key factor in the commercial success of textile products, particularly those with high fashion content, especially garments, furnishings and upholstery. The business generated by the dye industry over the last two years was approximately US$ 22 billion, and constituted a total employment of about 1.45 million people. Excluding fluorescent brighteners, the dye consumption per capita is approximately 150 g per year, serving an average consumption of textile fiber of about 14.0 kg per year per inhabitant. Despite, the high economic importance of the textile industry in the world, this industry is responsible for around 700,000 ton of about 10,000 different types of dyes on pigments produced each year. During dye use among the several industries responsible for pollution of the aquatic ecosystems, the textile dyeing and printing industries are major players, around a half of a tone of these dyestuffs are lost per day to the environment. Approximately 200l of water are required, for every kilogram of finished cotton fabric. The reactions necessary to fix these dyes to the fibers are not very efficient. Therefore, residual dyes, several types of chemicals and salts are dumped into the water and are discharged in the wastewater system. At least 20% of those not used dye might enter the environment through effluents from wastewater treatment plants (Carneiro, *et al.*, 2004).

Removal of color in wastewater generated by the textile industries is color issue of discussion and regulation all over the world. Among the relative dyes, the textile azo dyes with synthetic intermediates as contaminant and its degradation product have undoubtedly attracted the most attention with regard to high

environmental impact, because of their widespread use, their potentiality to form toxic aromatic products (carcinogenicity and mutagenicity properties) and their low removal rate during primary and secondary treatment. They represent about 50% of the worldwide production and correspond to an important source of contamination considering that a significant part of the synthetic textile dyes are lost in waste streams during manufacturing or processing operations. Therefore, it is important to develop effective wastewater remediation technologies for these compounds.

Various chemical and physical treatment processes are currently proposed for these dyes. These largely fall into the categories of direct precipitation or elimination by adsorption, flocculation, membrane separation, coagulation and chlorination. These methods have been largely incomplete and ineffective because the problem is not completely resolved, being required further treatment. A number of biological processes, such as sequenced anaerobic / aerobic digestion, have been proposed in the treatment of textile wastewater, but they are limited due to the fact that many of the dyes are xenobiotic and non-biodegradable. Alternative methods based on advanced oxidation processes combining ultraviolet irradiation and oxidative agents for dye treatment have been also investigated, but the presence of intermediates arising from the photodegradation reaction could be more harmful than the pollutant itself.

Several of titanium oxalate compounds have been reported as mixed oxalates, such as $MI_2TiO(C_2O_4)_2.H_2O$ with MI = NH_4, K and $BaTiO(C_2O_4)_2.4.5H_2O$. The structure of these compounds contain tetramers Ti_4O_2 based on four vertex sharing TiO_6 distorted octahedra, a wide range of Ti---O clusters which form -O-Ti-O- rings have also been obtained (Kolen' ko, et al., 2004). Only a few studies for titanium oxalate involving synthesis reported in the JCPDS. No interest has been paid to these compounds in the area of pollution control in some photocatalytic degradation of other pollutants have been reported as follows. Therefore, we deem that the photodegradation aspect of compound of this type should be investigated. Furthermore, photocatalysis of nanocrystalline titanium dioxide has a great many advantage on waste water treatment such as high catalysis efficiency, energy saving, no pollution, etc. and can degrade all kinds of organic pollutants from water effectively. All of those merits make photocatalysis of water treatment and it is supposed to be used widely in the future (Balong, et al., 2003).

The aim of this work is to study the effect of varying reaction condition in the synthesis of titanium oxalate. In this work, the precipitation and ageing reactions are investigated. I have prepared titanium oxalate using $TiOSO_4.2H_2O$ with aim to use it as a new precursor. In $TiOSO_4.2H_2O$ structure there are infinite zigzag chains of -Ti-O-Ti-O- chains with SO_4^{2-}ion and H_2O coordinated to complete octahedral environment about the Ti atom (Kharkar, *et al.*, 1957). Oxalic acid dihydrate plays the role as source of oxalate ligand. The study aims at finding the influence of temperature, time, concentration ratio, and Ti(IV) precursor on hydrothermal crystallization of titanium oxalate complex and the morphological changes occurring during titanium oxalate complex formation. The Ti(IV) to oxalate anion ratio is to be varied from 0.5, 1, and 2 ($Ti:C_2O_4^{2-}$). The synthesized titanium oxalate sample will be characterized by several techniques such as XRD, BET, TGA, DSC, SEM, EDX, and FT-IR technique.

Finally, the photodegradation of aqueous iodine solution (tincture iodine 2%) which is used as model for wastewater under UV irradiation will be investigated, employing a UV light source and titanium oxalate based products, and comparing with commercial Degussa P25 TiO_2 photocatalyst under the same treatments.

1.3 Objectives

The objectives of this research are as follows.

(1) To prepare titanium oxalate complex powders by using oxalic acid and $TiOSO_4.2H_2O$ as precursors.

(2) To study effect of temperature, time, and concentration ratio on the synthesis of titanium oxalate complex.

(3) To characterize and study some physical properties of synthesized titanium oxalate powder.

(4) To investigate the photochemistry activity of the synthesized titanium oxalate complex in the photodegradation of aqueous iodine solution (tincture iodine 2%) (model for wastewater) under UV irradiation and compare with commercial Degussa P25 TiO_2 under the same conditions and, finally, to investigate its reclyclability.

CHAPTER 2
EXPERIMENTAL AND CHARACTERIZATION TECHNIQUES

2.1 Synthesis of titanium oxalate complex

2.1.1 Chemicals

(1) Barium chloride, $BaCl_2$, A.R., code no. 1.01716.0500, Merck, Germany.

(2) Ethanol, $CH_3(OH)CH_3$, A.R., code no. 1.00983.2500, Merck, Germany.

(3) Oxalic acid dihydrate, $(COOH)_2$. $2H_2O$, A.R. , code no 1.00495.0500, Merck, Germany.

(4) Titanium(IV) oxysulfate dihydrate, $TiOSO_4.2H_2O$, A.R., code no. 14023, Riedel-De Haen, Germany.

(5) Tincture iodine, I_2 2%, Siribuncha, Bangkok, Thailand.

(6) Titanium dioxide (P25), AR., code no. D-60267, Degussa AG, Frankfurt, Germany.

(7) Sodium hydroxide, NaOH, A.R., BDH, England.

2.1.2 Instruments

A. Department of Chemistry, PSU.

(1) Analytical balance, AE 200S, SNR M 10802, Mettler Toledo A.G., Switzerland.

(2) Centrifuge, EBA 20, Hettich, Germany.

(3) Magnetic stirrer, Jenway 1000, JENWAY, UK.

(4) pH meter, pHTestr 10, Eutech Instrument/ Oakton Instrument, U.S.A.

(5) Photoreactor compartment (0.75 m x 0.75 m x 0.75 m) with 5 tubes of fluorescence blacklight (20 watts each), F20T12-BLB, GE, U.S.A.

B. Scientific Equipment Center, PSU.

(1) X-ray diffractometer, XRD, PHILIPS X'Pert MPD, the Netherlands.

(2) Scanning electron microscope/Energy dispersive x-ray fluorescence, SEM/EDX; SEM, JSM-5800LV, JEOL, Japan, and EDX, Oxford ISIS 300, Oxford Instruments (UK) Ltd., England.

C. Central Equipment Unit, Faculty of Science, PSU.

(1) Ultraviolet-visible spectrophotometer, HP 8453, Hewlett Packard, Canton, Massachusetts, USA.

2.1.3 Method

This work is divided into 2 parts: part 1 encompasses synthesis of titanium oxalate complexes under different times, temperatures, and ratios of titanium(IV) oxysulfate dihydrate to oxalic acid dehydrate; part 2 encompasses study of photocatalytic activity of the product from part 1 under UV light irradiation.

2.1.3.1 Preparation of titanium oxalate complex

All chemicals used in this work were of analytical grade and were used without further purification. Titanium(IV) oxysulfate dihydrate was used as a starting material, 0.075 mol(11.9947 g) of $TiOSO_4.2H_2O$ was dissolved in 150 mL of distilled water and poured into 0.075 mol of oxalic acid dihydrate in150 mL of ethanol. The mixture was agitated with a magnetic stirrer and kept at various temperatures and times. The merit of using ethanol because oxalic acid easily dissolves in this solvent while titanium compound is almost insoluble(Sivalingam, *et al*., 2003). The precipitate was aged and refluxed in the solution for 1(*TiOX-01*), 5(*TiOX-02*), and 8(*TiOX-03*) hours at 60 °C and 1(*TiOX-04*), 2(*TiOX-05*) , and 4(*TiOX-06*) hours at 70 °C, respectively. Subsequently, the white precipitate formed and was separated from the solution by using Whatman filter paper No.42 under vacuum-filtered. Then the white precipitate was washed with ethanol several times until no sulfate ion was found by $BaCl_2$ solution test. Finally, the washed product were dried for 2 days in air at room temperature. The final products were obtained as air-dried fine powder. The experimental procedure is schematically shown in Figure 2.1.

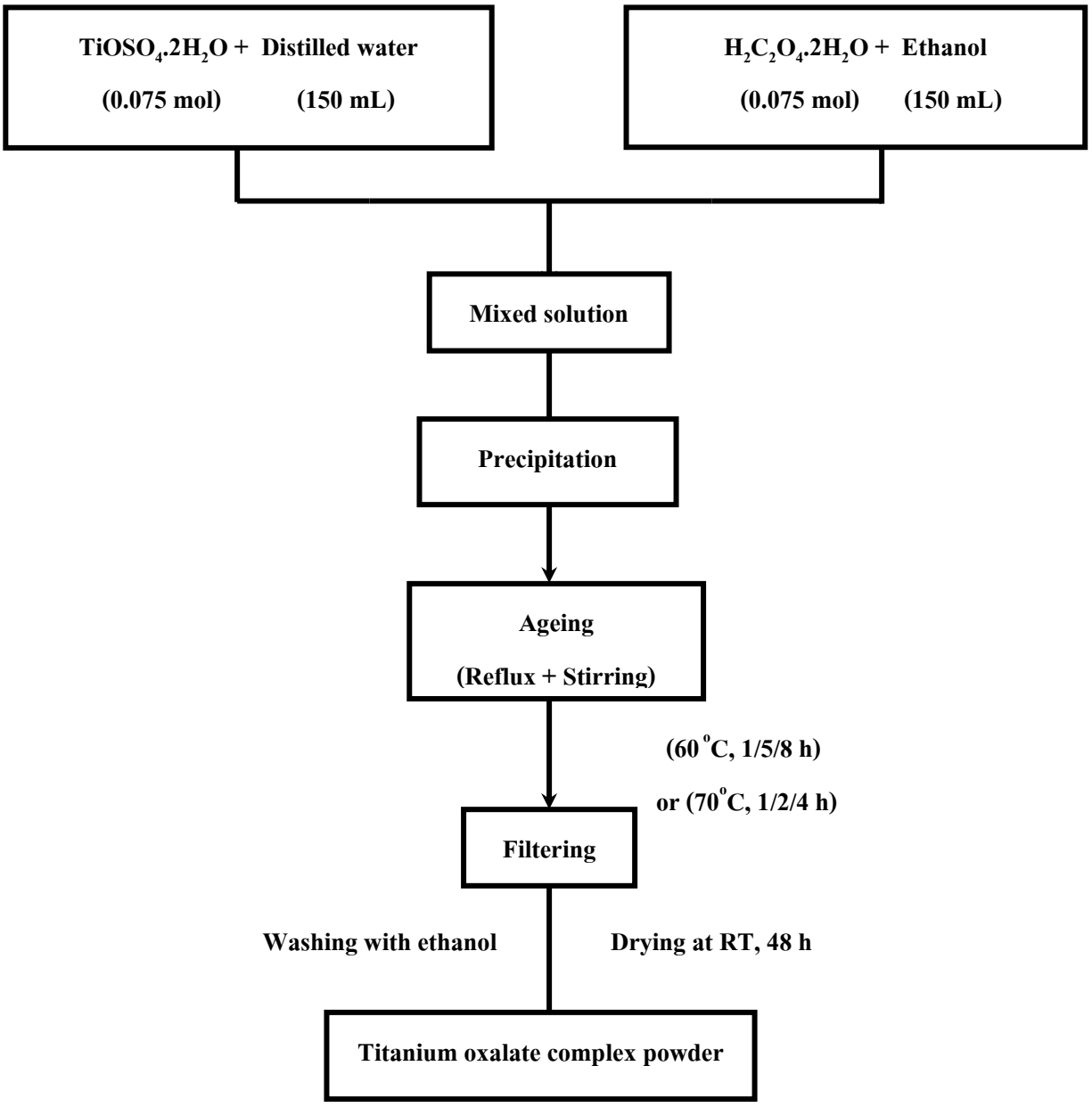

Figure 2.1 Flow chart of the preparation of titanium oxalate complex powder

2.1.3.2 Preparation of titanium oxalate complexes with different ratio of titanium(IV) oxysulfate dihydrate to oxalic acid dihydrate

In this study, we investigated the effect of ratio of titanium(IV) oxysulfate dihydrate to oxalic acid dihydrate. In a typical preparation, 0.075 (or 0.15, and 0.33) mol of $TiOSO_4.2H_2O$ was dissolved in 150 mL of distilled water and poured into the solution of 0.15 mol oxalic acid dihydrate in 150 mL of ethanol. The mixture was agitated with a magnetic stirrer and kept for 8 hours at 60 °C. (Sivalingam, *et al*., 2003). The precipitate was aged and heated in the solution. Subsequently, the white precipitate formed was separated from the solution by using Whatman filter paper No.42 under vacuum-filtered. Then the white precipitate was washed with ethanol several times until no sulfate ion was found by $BaCl_2$ solution test. Finally, the washed products were dried for 2 days in air at room temperature to give the air-dried fine powder as final products designated as *0.5TiOX-03* for 0.075 mol of $TiOSO_4.2H_2O$, *TiOX-03* for 0.15 mol of $TiOSO_4.2H_2O$ and *2TiOX-03* for 0.3 mol of $TiOSO_4.2H_2O$, respectively. The experimental procedure is schematically shown in Figure 2.2.

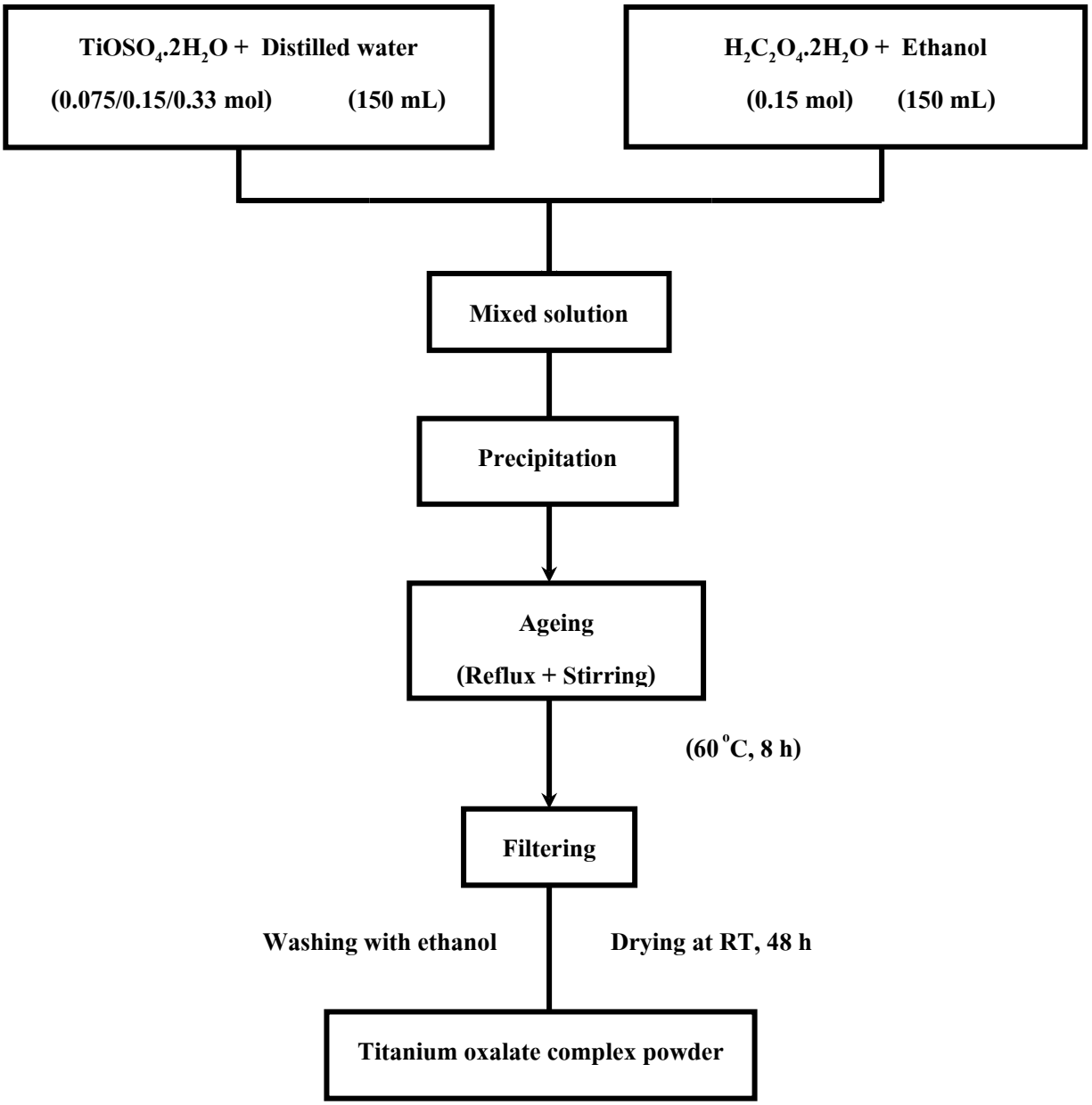

Figure 2.2 Flow chart of the preparation of titanium oxalate complex in different conditions

2.2 Characterization of samples

The synthesized titanium oxalate was characterized by various techniques like XRD, titration, EDX, SEM, TGA, DSC, FT-IR, and BET surface area techniques.

2.2.1 X-ray diffraction (XRD)

The crystallization and phase formation of the resulting titanium oxalate products were acquired on the Philips PW 3710 powder diffractometer (PHILIPS X'Pert MPD, the Netherlands) using Cu K_α radiation equipped with a Ni filter in the range 5-90^o 2θ. Diffraction patterns were compared with references in the JCPDS Powder Diffraction Files. The crystallite size was calculated by using the Scherrer's equation,

$$L = \frac{K\lambda}{\beta_{hkl} \cos\theta} \qquad (2.1)$$

where L is the average crystallite size in nm, K is a constant usually taken as 0.9, λ is the wavelength of the X-ray radiation (using Cu K_α = 0.154056 nm), β_{hkl} is the corrected band broadening (full width at half-maximum height (FWHM)) after substraction of equipment in radian, and θ is the diffracting angle (Yamamura, *et al*., 1985). All JCPDS Powder Diffraction Files were acquired by the Scientific Equipment Center, Prince of Songkla University, Hat Yai, Songkhla, Thailand.

2.2.2 Titration

Determination of the percentage of oxalate group was carried out by titration. Each titanium oxalate products was dissolved in about 50 mL of 1 M sulphuric acid in a 250 mL conical flask. The solution was heated on a hotplate to boiling temperature and titrated it with a solution of potassium permanganate which had been standardized with sodium oxalate and noted the volume of the potassium permanganate solution. For the latter purpose, 0.15 g of sodium oxalate was treated in the same way as the titanium oxalate complexes. The theoretical value of the percentage of oxalate in the complexes was calculated.

2.2.3 Scanning electron microscopy (SEM)

The surface features and morphologies of titanium oxalate products were investigated by using a scanning electron microscope (SEM) model JSM-5800 LV (Jeol Apparatus, Japan).

The elemental compositions were checked by scanning electron microscope/energy dispersive x-ray spectrometry (SEM/EDX). The energy dispersive X-ray fluorescence (EDXRF) spectrometer (Oxford ISIS 300) was attached to the SEM for this purpose.

2.2.4 Thermal gravimetric analysis (TGA)

Mass changes with temperature were studied by using a thermogravimetric analysis (TGA) model TGA7 (Perkin Elmer, USA) in the range 50-1000 °C under air atmosphere with heating rate of 10 °C per minute.

2.2.5 Differential scanning calorimeter (DSC)

The changes of energy with temperature were studied by using differential scanning calorimeter (DSC) model DSC7 (Perkin Elmer, USA) in the temperature range 50-500 ^{o}C under air atmosphere with heating rate 10 °C per minute.

2.2.6 Fourier-transformed infrared spectroscopy (FT-IR)

The Fourier-transformed infrared (FT-IR) spectra were recorded on Perkin Elmer model Spectrum GX (Perkin Elmer, U.S.A.) spectrophotometer in diffused reflectance mode at 400-4000 cm^{-1} using the pallet of the sample mixed with KBr.

2.2.7 Surface area and porosity (BET method)

The specific surface area and pore size distribution of titanium oxalate powders were characterized by analyzing the N_2 adsorption isotherms obtained at 77 K using SA 3100 (Coulter, U.S.A.) equipment. All data were acquired at Chemical Engineering Department, Faculty of Engineering, Prince of Songkla University, Hat Yai, Songkhla, Thailand, and Chemical Engineering Department, Faculty of Engineering, Kasetsart University, Bangkok, Thailand.

2.3 Photocatalytic activity tests

2.3.1 Measurement of iodine solution

The source of iodine solution used throughout this work was the aqueous iodine solution of tincture iodine (2%) manufactured by Siribuncha, Bangkok, Thailand, which hereinafter will be referred to as “iodine solution”. The calibration graph was used to find the concentration of iodine solution at any stages during the experiment. In this work, the concentrations of standard tincture iodine solutions were in the range $1x10^{-4}$ M to $1x10^{-2}$ M. The standard calibration curves of tincture iodine were constructed in two working concentrations ranges: $1x10^{-4}$ M to $1x10^{-3}$ M, and $1x10^{-3}$ M to $1x10^{-2}$ M. The calibration graphs were straight lines with R^2 = 0.998 and 0.997 as displayed in Figure 3.19 and Figure 3.20, respectively.

2.3.2 Photocatalytic activity tests

For the photocatalytic studies, the precipitates aged in the solution for 1 and 8 hours at 60 °C as titanium oxalate precipitate was tested for degradation of iodine solution. The experiments were carried out in closed compartment (0.9 m x 0.9 m x 0.9 m) to avoid interference from ambient light using 5 fluorescence blacklight (20 W, F20T12-BLB, GE, U.S.A.) tubes. Titanium oxalate powder was placed in the Erlenmeyer flask and the measured volume of iodine solution containing 100 mL was added. The amount of titanium oxalate product was 3.1062 g per liter of iodine solution. Prior to irradiation, the mixture solution was agitated with a magnetic stirrer in the dark for 1 h to reach the surfacial adsorption equilibrium. Then the mixture was irradiated with UV-light using 5 tubes of fluorescence blacklight 20 watts (λ_{max} 366 nm) (Randorn, *et al*., 2004). In these studies, the mixture solution was a magnetically stirred, before and during irradiation. At a given irradiation time interval (every 1 hour), 5 mL of mixture solution was sampled and centrifuged to separate titanium oxalate particles prior to the spectral measurement. The changes in absorbance of mixture solution were recorded using UV-Vis spectrophotometer, (SPECORD S100, Analytik Jena GmbH, Germany) at 290 nm for iodine (Svensson, *et al*., 2002). Calibration plots based on Beer-Lamberts law were established relating the absorbance to the concentration. The concentration of iodine solution was determined

quantitatively through % decolorization of iodine solution by applying the following equation;

$$\%Decolorization = \frac{C_0 - Ct}{C_0} \text{X}100 \qquad (2.2)$$

where C_0 is the initial concentration of iodine and C_t is the concentration of iodine solution at a specific sampling time.

Controlled experiments, without light or titanium oxalate complex, were carried out to demonstrate that degradation of tincture iodine solution was dependent on the presence of both light and titanium oxalate complex.

In addition, in the comparative studies with the commercial TiO_2, Degussa P25 (Degussa AG), the same experimental set up was employed as given above.

2.3.3 Studying the effect of various parameters on photocatalytic activity of titanium oxalate products

All the photocatalytic parameters including: the iodine concentrations, pH, and intensity of UV light were considered. The effect of initial iodine solution concentration was varied from $1x10^{-4}$ M to $1x10^{-3}$ M and $1x10^{-4}$ M to $1x10^{-3}$ M. The pH of aqueous iodine solution was studied in the range of neutral and base condition by adding dilute aqueous solution NaOH. The effect of intensity of UV light was studied by increasing the blacklight tubes (1, 3, and 5 tubes). Moreover, the reclyclability process was also studied by the separation of titanium oxalate powder from reaction solution and the same procedure was tested for reuse by allowing it to photodegadation new sample of aqueous iodine solution (tincture iodine 2%) again.

CHAPTER 3
RESULTS AND DISCUSSION

3.1 Synthesis of titanium oxalate complex and characterization

3.1.1 Synthesis of titanium oxalate complex

On a laboratory scale, titanium oxalate has been prepared by various methods, such as hydrothermal method, coprecipitation method, leaching method, and so on. The different preparation routes and the experimental conditions yielded titanium oxalate in products with different structures, morphologies, particle sizes and contaminations (Potdar, *et al.*, 1999; Hee-Lack Choi, *et al.*, 1999; Yu. V. Kolen' ko, A.A, *et al.*, 2004; Wang, *et al.*, 2009). $TiCl_4$ is usually used as a precursor in the synthesis of titanium oxalate complexes but the reaction condition is hard to control because of the more extreme reaction for synthesis than other precursor so it was carried out at low temperature, in an ice-bath, to avoid strong reaction. In this present study, the precipitation and ageing reactions were investigated. Titanium oxalate was prepared using titanium oxysulfate dihydrate ($TiOSO_4.2H_2O$) as a precursor. In this compound, there are infinite zigzag chains of -Ti-O-Ti-O- with SO_4^{2-}ion and H_2O coordinated to complete octahedral environment about the Ti atom. Oxalic acid dihydrate ($H_2C_2O_4.2H_2O$) plays the role as source of oxalate ligand. The use of oxalic acid dihydrate creates another advantage over using potassium oxalate or sodium oxalate as source of oxalate ligand since the two M(I)-salts cause the solution to become too basic. The oxalate anion is a good bidentate ligand that usually interlinks the metal ions into a two or three dimensional network (Evans, *et al.*, 2002; Chaiyapoom, *et al.*, 2006). The titanium oxalate complex powder exists as a white powder solid as shown in Figure 3.1.

This work involved studying the influence of temperature, time, concentration ratio, and Ti(IV) precursor crystallization of titanium oxalate complex and the morphological changes occurring during titanium oxalate complex formation. Titanium(IV) oxalate was successfully synthesized in a polycrystalline form in the

course of the study of precursor by adding $TiOSO_4.2H_2O$ solution to an ethanol solution of oxalic acid with aim to use it as a new precursor.

$$TiOSO_4.2H_2O + H_2C_2O_4.2H_2O \xrightarrow{H_2O/EtOH} TiO(C_2O_4).H_2O + H_2SO_4 + 3H_2O \quad (3.1)$$

The physico-chemical properties of the synthesized titanium(IV) oxalate compound were characterized by XRD, BET, TGA, DSC, SEM, EDX, and FT-IR.

Figure 3.1 Photograph of the synthesized titanium oxalate powder

3.1.2 Characterization of the synthesized titanium oxalate complex

The obtained product was characterized by the following techniques.

A. X-ray powder diffraction (XRD)

The identification of a species from its powder XRD diffraction pattern is based upon the position of the lines (in terms of 2θ) and their relative intensities (Skoog and Leary, 1992). The X-ray diffraction spectra of the synthesized titanium oxalate complex at various aged periods are shown in Figure 3.2 and 3.3. The X-ray data of the product are identical to that of the chemical formula $Ti_2O_2(C_2O_4)(OH)_2.H_2O$, titanium oxide oxalate hydroxide hydrate, which exists in JCPDS No.00-048-1164. The hypothetical “titanium oxalate complex” is loosely represented by $TiOC_2O_4.H_2O$. The initial formation of $TiOC_2O_4.H_2O$ has a poor crystallinity. The flat base line were detected in pattern of product in the initial

precipitate for 1 hour, Figure 3.2 and Figure 3.3 (1 h), confirming the amorphous nature of these products. As expected, with the ageing time increased, the initial precipitate changed to the phase with good crystallinity, Figure 3.2 (5, 8 h) and Figure 3.3 (4 h). When the ageing temperature was increased, 60 °C and 70 °C, the time required for the formation of crystal was shortened to form the crystal completely. Figure 3.4 shows the synthesized titanium oxalate with different ratios of Ti(IV) to oxalate precursor. At the beginning, the product formed had poor crystallinity. As the ageing time increased, the initial precipitate turned into the phase with good crystallinity.

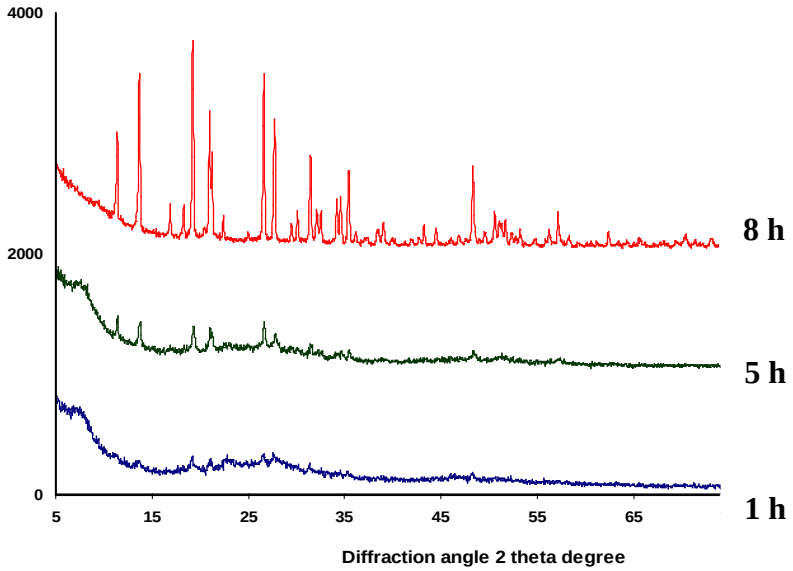

Figure 3.2 XRD patterns of the synthesized titanium oxalate complex at 60 °C under various ageing periods

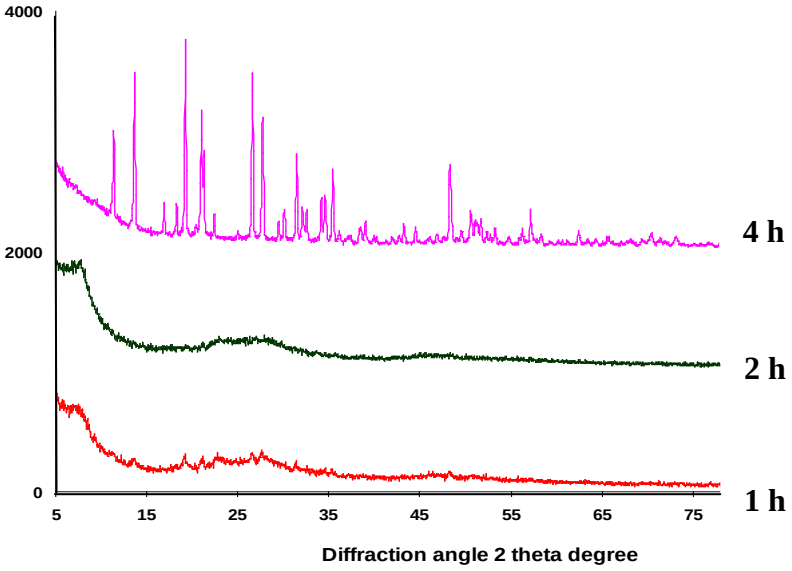

Figure 3.3 XRD patterns of the synthesized titanium oxalate complex at 70 °C under various ageing periods

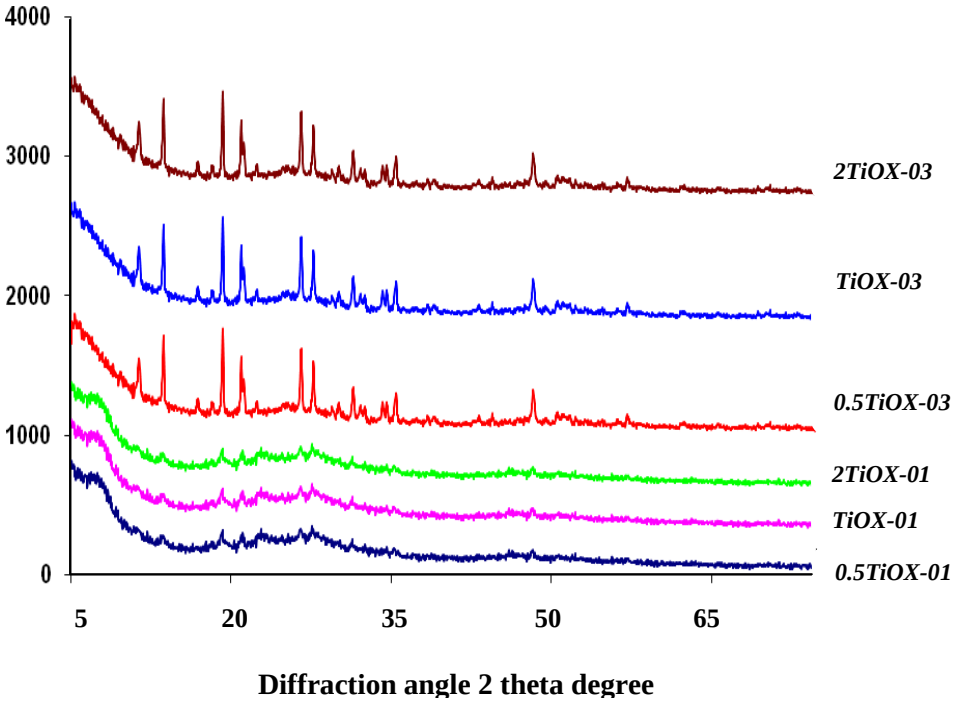

Figure 3.4 XRD patterns of the synthesized titanium oxalate complex at 60 °C with various ratio of titanium(IV) precursor

The data of the physical properties, the phase structure and average crystallite size of each sample in all synthesized titanium oxalate complexes calculated using the Scherrer equation for the main diffraction peak are given in Table 3.1 and 3.2, respectively.

Table 3.1 Effect of temperature and time on phase and average crystallite size (nm) of titanium oxalate complex samples

Sample	Temp(°C)	Time (h)	Yield(%)	Crystallite phase	Crystallite size (nm)*
TiOX-01	60	1	27.65	Amorphous	-
TiOX-02	60	5	31.88	Crystalline	19.74
TiOX-03	60	8	40.85	Crystalline	39.63
TiOX-04	70	1	28.4	Amorphous	-
TiOX-05	70	2	29.64	Amorphous	-
TiOX-06	70	4	40.81	Crystalline	39.69

* Calculated from the Scherrer's equation

Table 3.2 Effect of time and ratio of Ti(IV) to oxalate precursor at 60 °C on average crystallite size (nm) of titanium oxalate complex samples

Sample	Ratio Ti/ox	Time (h)	Yield (%)	Crystallite size (nm) *
0.5TiOX-01	0.5	1	11.57	Amorphous
0.5TiOX-03	0.5	8	23.82	54.72
TiOX-01	1	1	27.65	Amorphous
TiOX-03	1	8	40.85	39.63
2TiOX-01	2	1	15.41	Amorphous
2TiOX-03	2	8	29.73	42.16

* Calculated from the Scherrer's equation(Eq. 2.1)

The patterns of crystalline product are shown in Figure 3.5. It matches with the X-ray data of the reference material having chemical formula $Ti_2O_2(C_2O_4)(OH)_2.H_2O$, titanium oxide oxalate hydroxide hydrate, which exists in JCPDS No.00-048-1164 and the crystallographic parameters of crystalline phase are shown in Table 3.3.

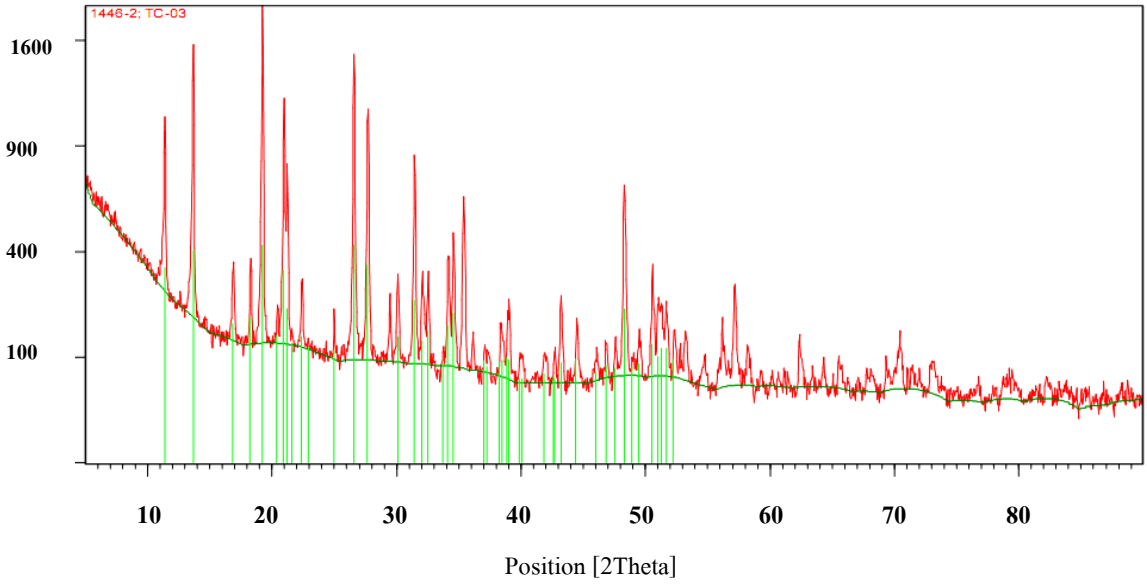

Figure 3.5 XRD patterns of the synthesized titanium oxalate complex with ageing time 8 hours at 60 °C

Table 3.3 Crystallographic parameters (JCPDS No.00-048-1164).

Parameter	Results
Crystal system	Orthorhombic
Space group	C_2^{221}
Space group number	20
a	10.503
b	15.509
c	9.700
α	90.000
β	90.000
γ	90.000

Parameter	Results
Calculate density (g/cm^3)	2.25
Volume of Cell (10^6 pm^3)	1580.04
Z	8
Color	White

The formation of product $Ti_2O_2(C_2O_4)(OH)_2.H_2O$ (*TiOX-03*) can be described based on the following two steps.

Step 1: Formation of $TiOC_2O_4$

Normally, Ti(IV) always forms complex compounds with oxalate ions in ethanol. All complexes are shown to be titanyl compounds with formula $TiOC_2O_4 \cdot nH_2O$ if the $Ti : C_2O_4$ ratio is 1 : 1 and pH < 2 is maintained. When $TiOSO_4.2H_2O$ solution was poured into a solution containing oxalic acid and pH was less than 1.5, white powder was precipitated, eq. 3.1 (Potdar, et al,1999.).

$$TiOSO_4.2H_2O + H_2C_2O_4 .2H_2O \xrightarrow{EtOH} TiO(C_2O_4).\ H_2O\ (\textit{TiOX-01}) + H_2SO_4 \quad (3.2)$$

Step 2: Ageing reaction

Formation of *TiOX-01* initially had poor crystallinity. As the ageing time increased, the initial precipitate turned to the phase with good crystallinity. If the ageing temperature was increased, the time required for the formation of crystal was shorten. From X-ray data of the aged precipitate can be assigned as $Ti_2O_2(C_2O_4)(OH)_2.H_2O$ (*TiOX-03*) which has the orthorhombic crystal system with lattice constants of a=1.0503 nm, b=1.5509 nm and c=0.9700 nm (JCPDS No.00-048-1164).

B. Surface area (BET) and pore size

The surface area is an average measurement of the external surface of a large number of particles and expressed in term of the area per unit mass (m^2/g). There

are two main analysis techniques for measuring surface area; gas adsorption and gas permeability. In this work gas adsorption surface area analysis was used. The results from surface studies, are giving in Figure 3.7-3.9 of *TiOX-01* and *TiOX-03*.

The porous nature of synthesized titanium oxalate complexes were studied by nitrogen adsorption isotherm. In order to utilize the information within the adsorption isotherms, it is necessary to inspect the shape of physisorption isotherm and the identification of the principle mechanism of adsorption. The majority of physisorption isotherms could be grouped into six types, as shown in Figure 3.6 and Table 3.4.

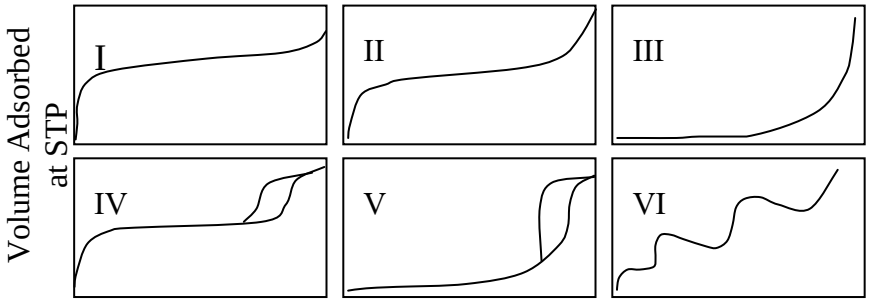

Figure 3.6 IUPAC classification of adsorption isotherms (Ryu, *et al*., 1999)

Table 3.4 IUPAC classification of the pore (Khalil, *et al*., 2001)

Porosity type	Size (d)
Ultramicropores	< typical molecule diameter of the adsorptive about 0.6 nm
Micropores	d < 2 nm
Mesopores	2 nm < d < 50 nm
Macropores	d > 50 nm

The Type I isotherm is given by microporous solids. The very steep region at low P/P_o is due to the filling of very narrow pores and limiting uptake is dependent on the accessible micropore volume rather than on the internal surface area.

The Type II isotherm is normally given by a non-porous solids which unrestricted monolayer-multilayer adsorption can occur. The Type III isotherm is generally associated with weak adsorbent-adsorbate and relatively strong adsorbate-adsorbate interactions. In this case cooperative effects lead to the development of patches of multilayer before a uniform monolayer has been formed. Type IV isotherm with hysteresis loop is the characteristic features of the adsorbate-absorbate interactions which is associated with capillary condensation. Some microporous or mesoporous solids are amongst the few adsorbents to give Type V isotherm. The Type VI isotherm is relatively rare; it presents stepwise multilayer adsorption on a uniform non-porous surface (Ryu, *et al*., 1999).

Table 3.5 Surface area of synthesized titanium oxalate complex (*TiOX-01* and *TiOX-03*)

Sample	**Surface area (m^2/g)**	**Average Pore Diameter (nm)**
TiOX-01	39.07 [a]	3.97
TiOX-03	7.89 [a]	32.2
Commercial TiO_2		
Anatase	9.65 [b]	-
Degussa P25	51.41 [b]	-

[a] Mearured using SA3100, Coulter.

[b] Reported by Choychangtong, 2004.

(1) N_2 adsorption isotherm of *TiOX-01* and *TiOX-03*

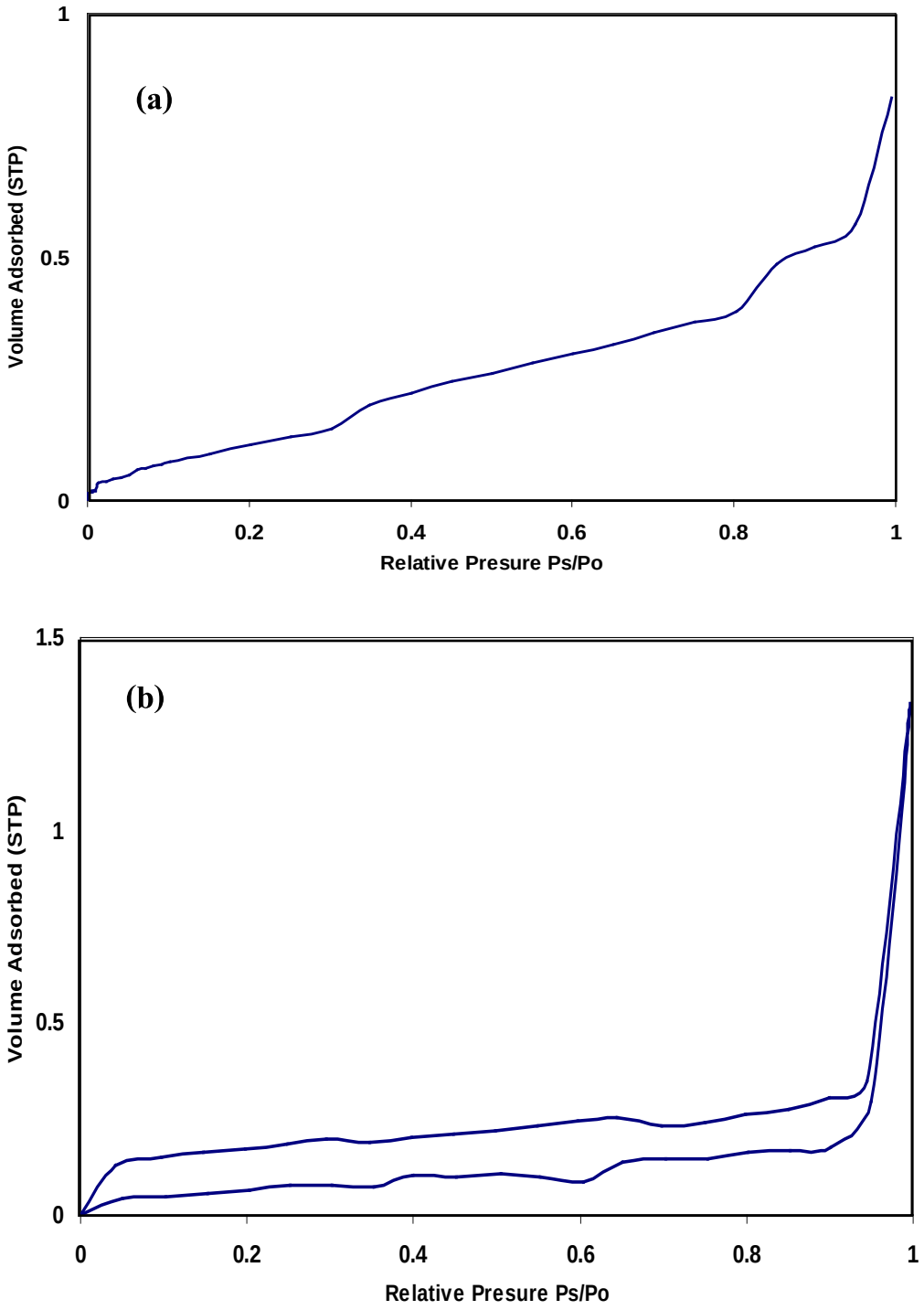

Figure 3.7 N_2 adsorption isotherm of (a) *TiOX-01*, and (b) *TiOX-03*

(2) T-plot of N_2 adsorption isotherm of *TiOX-01* and *TiOX-03*

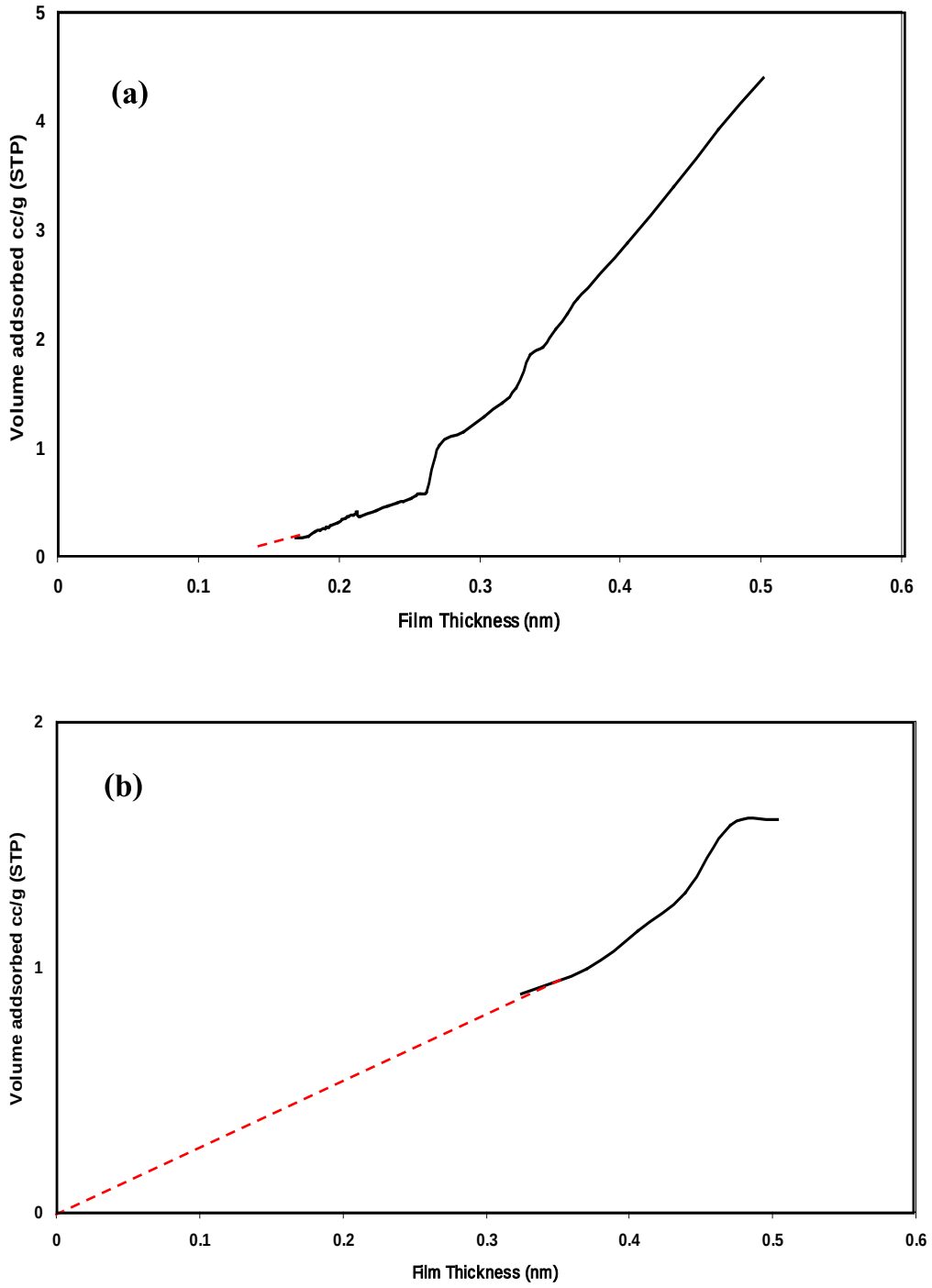

Figure 3.8 T-plot of N_2 adsorption isotherm of (a) *TiOX-01*, and (b) *TiOX-03*

(3) Pore size distribution curve of *TiOX-01* and *TiOX-03*

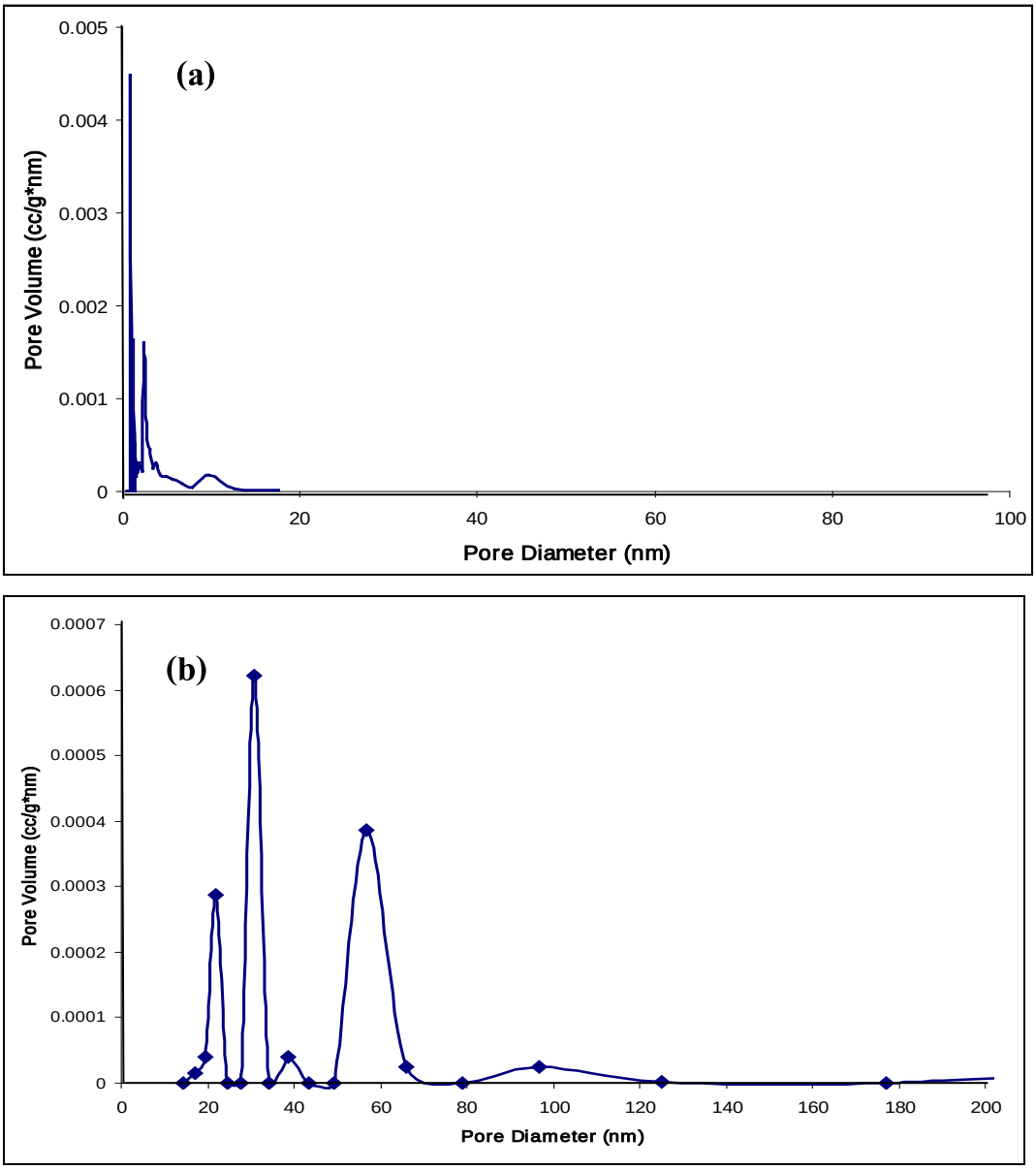

Figure 3.9 Pore size distribution curve of (a) *TiOX-01*, and (b) *TiOX-03*

The nitrogen adsorption isotherms of the synthesized titanium oxalate complex samples are shown in Figures 3.6. The isotherms of the amorphous titanium oxalate complex, *TiOX-01*, is of Type I (BDDT classification) (Ryu *et al*., 1999), indicating that the pore size is in the microporous region. For crystalline titanium oxalate complex, *TiOX-03*, the isotherm is a combination of Type I and IV (BDDT

classification) with two distinct regions; at low relative pressure, the isotherm exhibits high adsorption, indicating that the sample contains micropore (Type I). However, at high relative pressure, the curve exhibits the presence of mesopores (Type IV). The present of micropore could be checked by plotting the adsorbed layer called "*t*-plot" as seen in Figures 3.8 (a) for amorphous titanium oxalate complex, *TiOX-01*, and Figures 3.8 (b) for crystalline titanium oxalate complex, *TiOX-03,* respectively. *TiOX-01* sample showed linear t-plot not passing the origin indicating either micropore or mesopore were presence for this sample. The t-plot data of *TiOX-03* sample showed linear part passing the origin indicating that it contained both micropore or mesopore structure (Khalil, *et al*., 2001). The pore size distributions of synthesized titanium oxalate complexes are shown in Figures 3.9 for amorphous titanium oxalate complex, *TiOX-01*, and crystalline titanium oxalate complex, *TiOX-03*, respectively. The *TiOX-03* sample shows bimodal pore size distribution consisting of intra-particle pores (5-10 nm) and larger inter-particle pores (10-70 nm). Usually, there are two types of pores present in the bimodal pore size distribution. One is made from the intra-aggregated pores at lower P/P_o range (the pores within the hard aggregates) and the other is larger inter-aggregated pores in the higher P/P_o range arising from hard aggregated (the void between hard aggregates) (Yu, *et al*., 2003).

C. Scanning electron microscopy (SEM)

Figure 3.10 illustrates scanning electron micrograph of the synthesized titanium oxalate samples by refluxed. Two magnifications, 5,000x and 10,000x, were taken for each sample. From the SEM results we can see that morphologies of the samples were affected by the synthesized conditions. The precipitate of 1 hour consists of clusters of the particles which disappear with the ageing time and the morphology of the product consists of a large size and porous particles of irregular shape. On the other hand, the amount and size of the round shape particles also decrease as ageing time increase [Figure 3.10 (c), (d), (e), and (f)]. The particle sizes of samples are in the micrometer range; 1 μm for *TiOX-01*, and less than 1 μm for *TiOX-02* and *TiOX-03* samples. It is believed that a crystal phase was formed after the dissolution of the initial particles which formed the clusters at first

(a) *TiOX-01* x 5,000

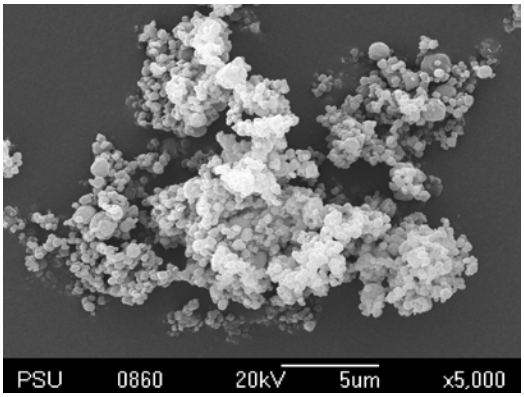

(b) *TiOX-01* x 10,000

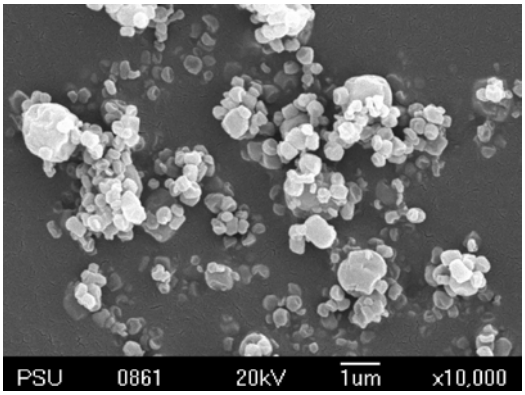

(c) *TiOX-02* x 5,000

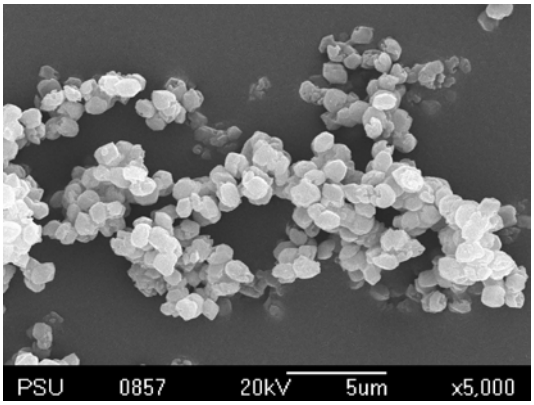

(d) *TiOX-02* x 10,000

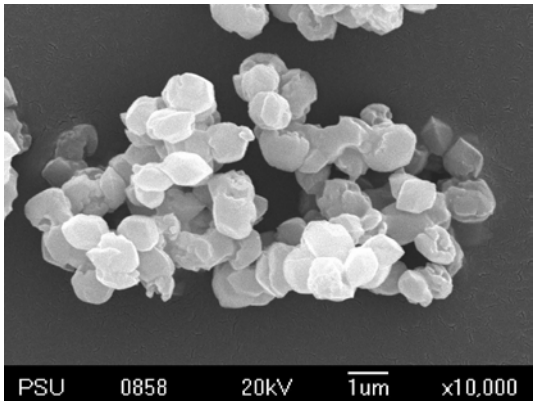

(e) *TiOX-03* x 5,000

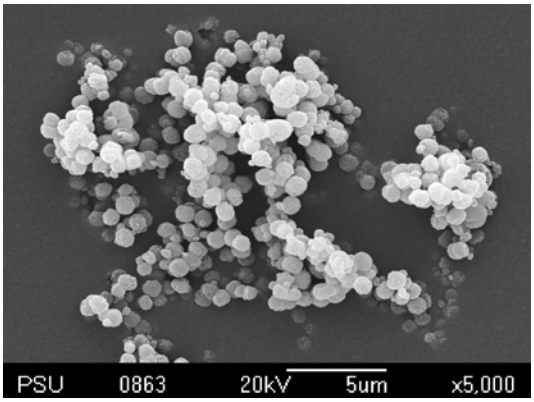

(f) *TiOX-03* x 10,000

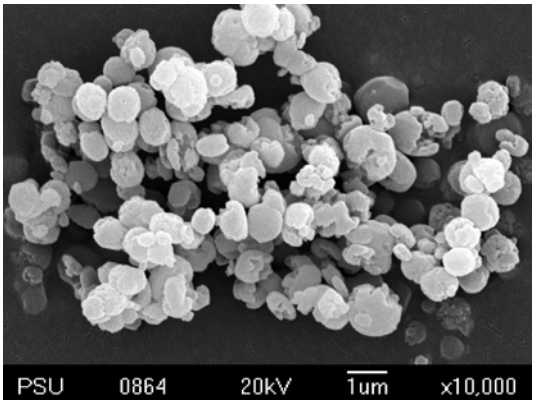

Figure 3.10 SEM photographs of the synthesized titanium oxalate complex; (a), (b) *TiOX-01*, (c), (d) *TiOX-02, and* (e), (f) *TiOX-03* sample. Each sample was photographed at low (5,000x) and high (10,000x) magnification

D. Compositional analyses

At first, titanium oxalate complex contains titanium, oxygen, and oxalate complex anion, $TiOC_2O_4.H_2O$, with one water molecule. As the ageing time increased, the powder was transformed to crystalline phase consist of two titanium, two oxygen, and oxalate complex anion, $Ti_2O_2(C_2O_4)(OH)_2.H_2O$ (*TiOX-03*), with one water molecule. In order to evaluate the content of each element (Ti, C, O, and S) in the synthesized titanium oxalate complex sample; all samples were analyzed for their composition by using EDX technique. The relative percentages of all constituents can be determined. The results are shown in Table 3.6 which show that the amount of S element decreased with increasing the ageing time. The percentage of oxalate group was determined by titration with a solution of potassium permanganate. In this experiment the oxalate content of the complex was determined. The complex was decomposed by addition of excess sulfuric acid.

$$TiOC_2O_4.H_2O + H_2SO_4 \rightarrow H_2C_2O_4 + TiO^{2+} + 3SO_4^{2-} + 3H_2O \qquad (3.3)$$

The oxalic acid thus released into the solution could be determined by titration with a standard solution of $KMnO_4$ which acted as an oxidant. The oxidation state of manganese in $KMnO_4$ was Mn^{7+} which was reduced to Mn^{2+} in hot acid solution (or else it was converted to MnO_2) by accepting five electrons from the oxalate ion which in turn acted as a reductant and was oxidized to CO_2. as shown in the reaction equation:

$$10e^- + 8H^+_{(aq)} + 2MnO^{4-}_{(aq)} \rightarrow 2Mn^{2+}_{(aq)} + 8H_2O_{(l)} + 5C_2O_4{}^{2-}_{(aq)} \rightarrow 10C_2O_{(g)} + 10e^- \quad (3.5)$$

The balanced equation is the sum of the balanced half-reactions. Note that the electrons on the reactant and product sides of the equation cancel each other:

$$2MnO^{4-}_{(aq)} + 5C_2O_4{}^{2-}_{(aq)} + 16H^+_{(aq)} \rightarrow 2Mn^{2+}_{(aq)} + 8H_2O_{(l)} + 10C_2O_{(g)} \qquad (3.6)$$

This method was utilized to obtain the percentage of oxalate group in the synthesized complexes. The accepted experimental result must be close to the calculated data. In practice, the experimental data are usually slightly different from the calculated data because of the impurity, the moisture, and how sensitive the samples to air. These affect the higher or lower quantitative values of the results.

(a) *TiOX-01*

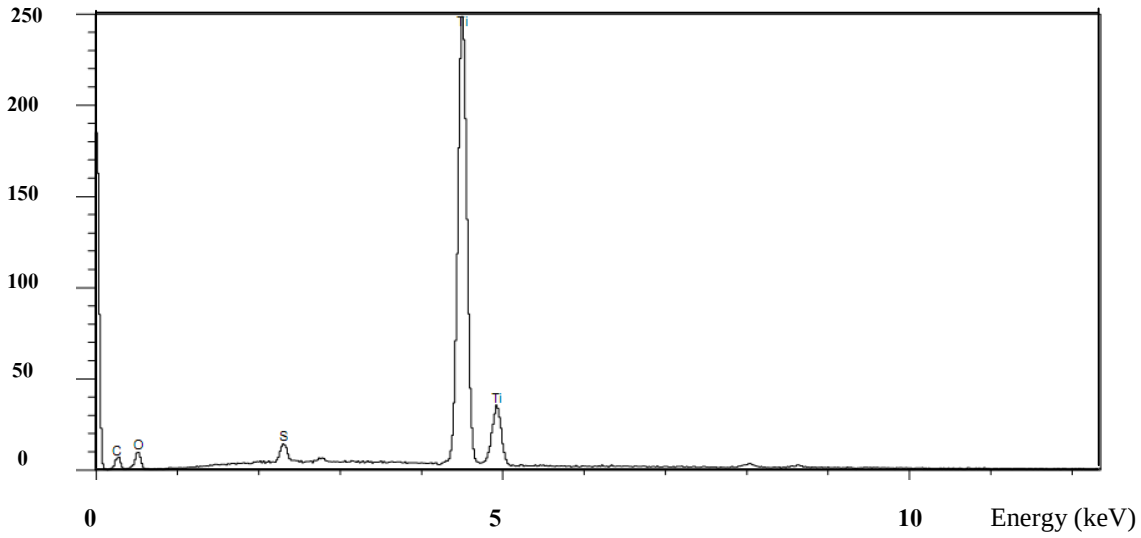

(b) *TiOX-03*

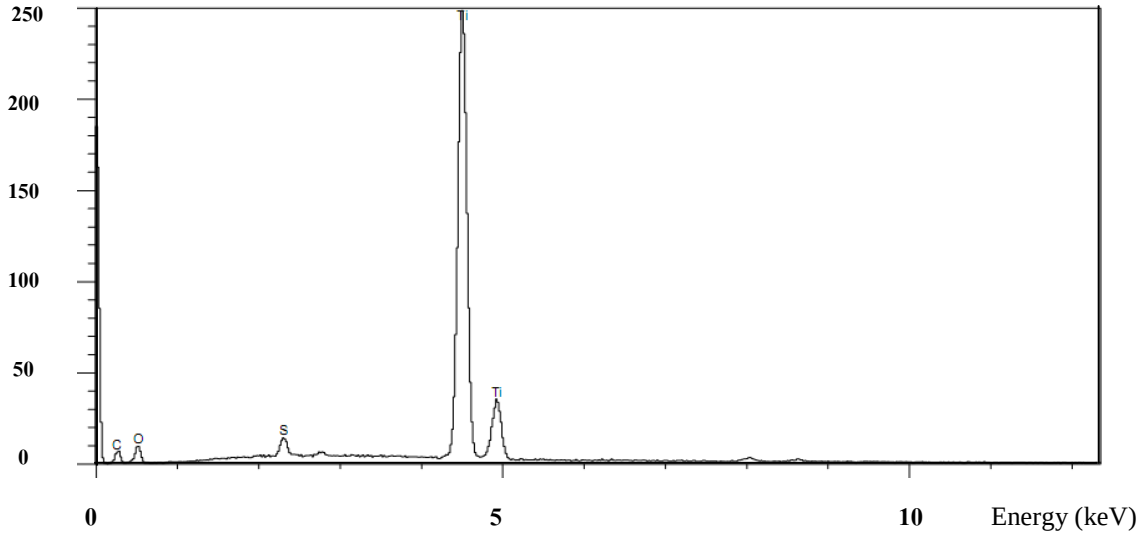

Figure 3.11 EDX spectra of the synthesized titanium oxalate complex; (a) *TiOX-01*, and (b) *TiOX-03* sample

Table 3.6 Oxalate contents from titration techniques of *TiOX-01* and *TiOX-03*

Compound	Amount of $C_2O_4^{2-}$* (%)
TiOX-01	40.12
TiOX-03	30.15

* Calculated from titration with a solution of potassium permanganate.

E. Thermogravimetric analysis (TGA)

Thermogravimetric analysis provides the analyst with a quantitative measurement of any weight change associated with a transition during heat treatment. For example, TGA can directly record the loss in weight with time or temperature due to dehydration or decomposition (Willard, *et al.*, 1974). Figure 3.12 displays TG curves of *TiOX-01* and *TiOX-03*.

a) *TiOX-01*

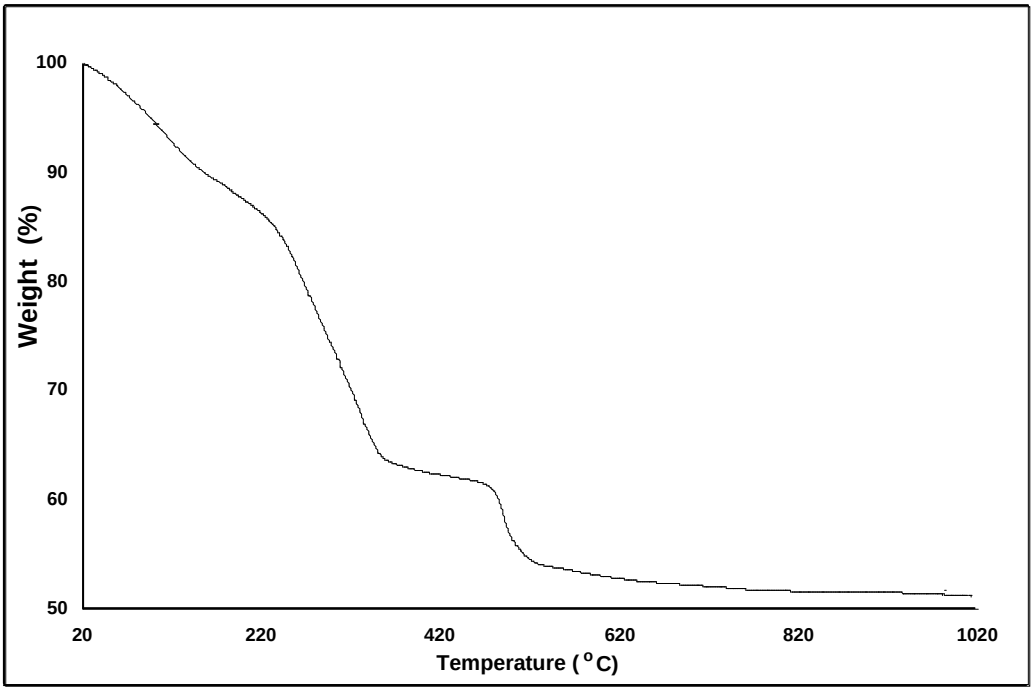

b) *TiOX-03*

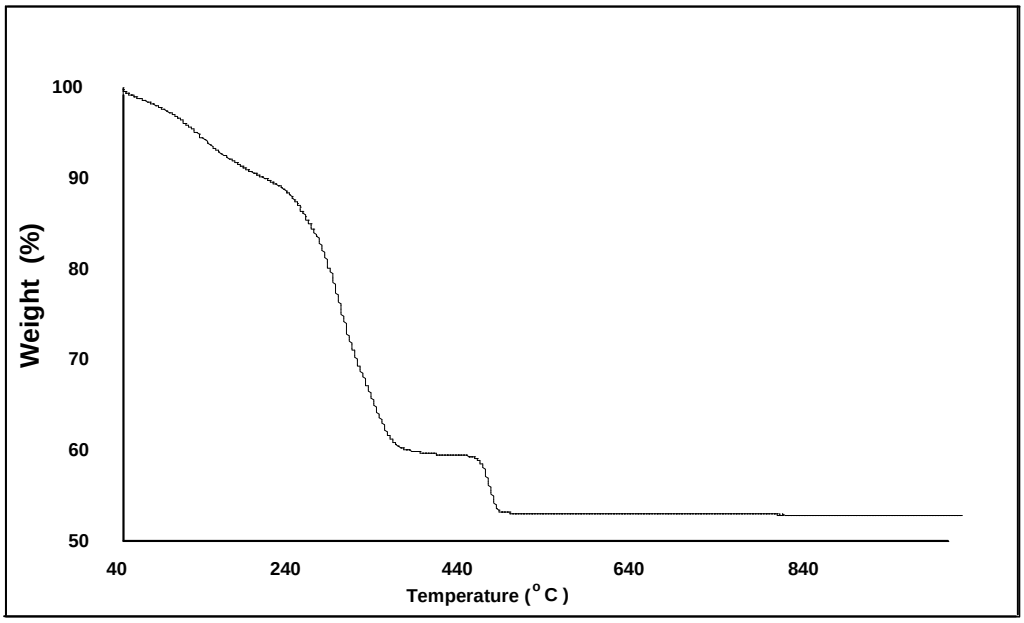

Figure 3.12 TGA curves of (a) *TiOX-01* and (b) *TiOX-03*

Table 3.7 Summary of the TG results obtained by heating from 40 °C to 1,000 °C at 10 °C/min in air

Complex	First transition (40 - 260 °C) Mass loss (%)	Second transition (260 - 456 °C) Mass loss (%)	Third transition (Above 456 °C) Mass loss (%)
TiOX-01	12.49	38.69 (40.12)*	2.60
TiOX-03	9.74	30.67 (30.15)*	6.58

* Calculated from titration with a solution of potassium permanganate.

In this work, the decomposition of titanium oxalate complex was identified by percentage of weight loss. The TGA curve indicates decomposition with total weight 46.99%. The initial weight loss (9.74%) in the temperature range 40-260 °C may be attributed to hydrated water released from $Ti_2O_2(C_2O_4)(OH)_2.H_2O$ (*TiOX-03*). The major weight loss of 30.67% in the temperature range 260-456 °C was due to the decomposition of oxalate to form TiO_2. Between 390-456 °C, the unit of TiO_2 is believed to grow into anatase-TiO_2 with no mass loss in TGA curves. The final weight loss 6.58% in the TGA curve at higher than 456 °C indicated transformation from anatase to rutile crystalline phase. This can be summarized that the process occurs in 3 steps according to the following reactions.

Step 1 = 9.74 % (40 - 260 °C)

$$Ti_2O_2(C_2O_4)(OH)_2.H_2O \rightarrow Ti_2O_2(C_2O_4)^{2+} + H_2O + 2OH^- \quad (3.7)$$

Step 2= 30.67 % (260 - 456 °C)

$$Ti_2O_2(C_2O_4)^{2-} \rightarrow 2TiO_2 + 2CO$$

By air oxidation; $2TiO + O_2 \rightarrow 2TiO_2$ (3.8)

By CO_2 reduction; $2TiO + 2CO_2 \rightarrow 2TiO_2 + 2CO^-$ (3.9)

Step 3 =6.58% (Above 456 °C)

$TiO_2 \rightarrow$ *Anatase*-TiO_2 (3.10)

This agreed with $TiOC_2O_4.H_2O$ (*TiOX-01*) where the thermal analysis *TiOX-01* showed the TGA plots are shown clearly decomposition of as-dried mixed oxalate precursor in following three steps:

1. removal of hydrated and adsorbed H_2O in the temperature range of RT–260 °C,

2. decomposition of oxalates between 260 and 456°C, and

3. between 390-456 °C, the unit of TiO_2 is believed to grow into anatase-TiO_2 with no mass loss in TGA curves.

Oxalate anion is a good ligand and can be coordinated with many transition and non-transition metals. Their thermal decomposition processes are relatively complicated because of the reduction property of $C_2O_4^{2-}$. The thermal decomposition of titanium oxalate complex was studied by Hee-Lack Choi, *et al*, 1999. The thermal decomposition processes of titanium oxalate complex was reported by Potdar, *et al*, 1999 and shows that the TG curves obtained for the as-dried precipitate indicates decomposition in three steps with total weight loss of 56.07%. Since the as-dried precipitate was used, it may contain some adsorbed water (Y) in addition to the hydrated water. Assuming final product as TiO_2 and total weight loss = 56.07%, the weight loss occurring at each step is calculated from the equation below:

$$TiO_2C_2O_4(H_2O)_2+Y \rightarrow TiO_2+[C_2O_3+(H_2O)_2+Y] \quad (3.11)$$

F. Differential scanning calorimeter (DSC)

DSC is thermal technique in which differences in heat flow into a substance and references are measured as a function of sample temperature while the two are subjected to a controlled temperature program (Skoog and Leary, 1992.). The DSC spectra of titanium oxalate complexes are summarized in Table 3.9.

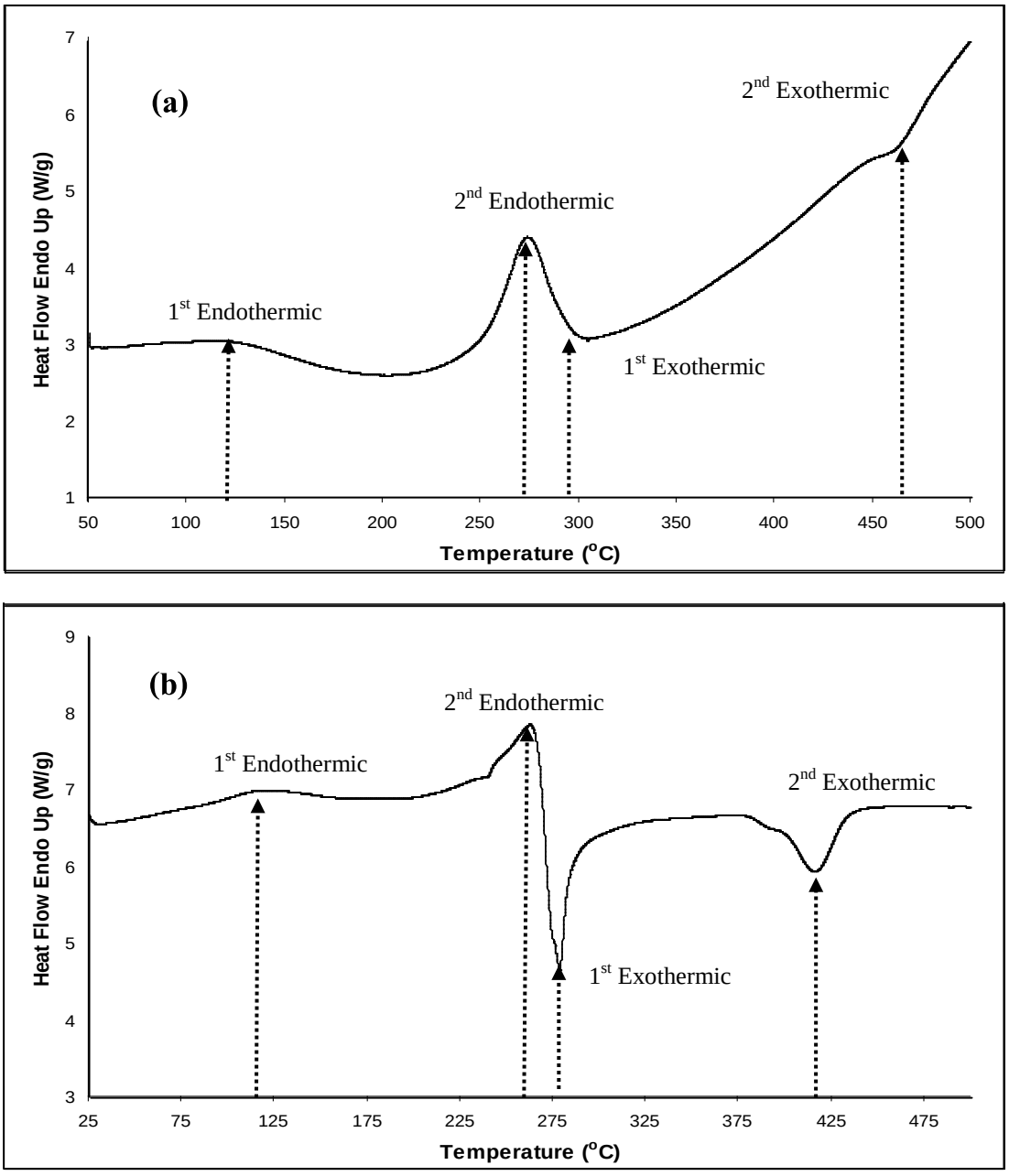

Figure 3.13 DSC spectra of (a) *TiOX-01* and (b) *TiOX-03*

.

Table 3.8 Summary of the DSC results obtained by heating from 25 ^{o}C to 500 ^{o}C at 10 ^{o}C/min in air

Complex	1st Endothermic		2nd Endothermic		1st Exothermic		2nd Exothermic	
	Area (J/g)	Temp (°C)	Area (J/g)	Temp (°C)	Area (J/g)	Temp (°C)	Area (J/g)	Temp (°C)
TiOX-01	-	120	251	274	-	-	24	464
TiOX-03	-	120	220	263	178	279	126	416

According to DSC curves of these as-prepared samples, it could be found that the endothermic peak around 125 °C assigned to the expulsion of free adsorbed water from sample which is more prominent in these synthesized samples (Liqiang, *et al*., 2003). This agreed with the TGA analysis which showed weight loss in these synthesized samples in first step. An endothermic peak at around 250 °C associated with the removal of water and combustion decomposition of the organic matters (Liqiang, *et al*., 2003). The exothermic peak at around 275 °C indicated the breakdown of oxalate and exothermic peak at around 425 °C indicated transformation from anatase to rutile crystalline phase of TiO_2 (Hee-Lack Choi, *et al.*, 1999).

G. Fourier-transformed infrared spectroscopy (FT-IR)

Figure 3.14 shows the FT-IR spectra of synthesized titanium oxalate complex products, *TiOX-01, TiOX-02, and TiOX-03*, respectively. The assigned modes of functional groups corresponding to Figure 3.14 listed in Table 3.9 that is responsible for vibration bands of titanium oxalate complex.

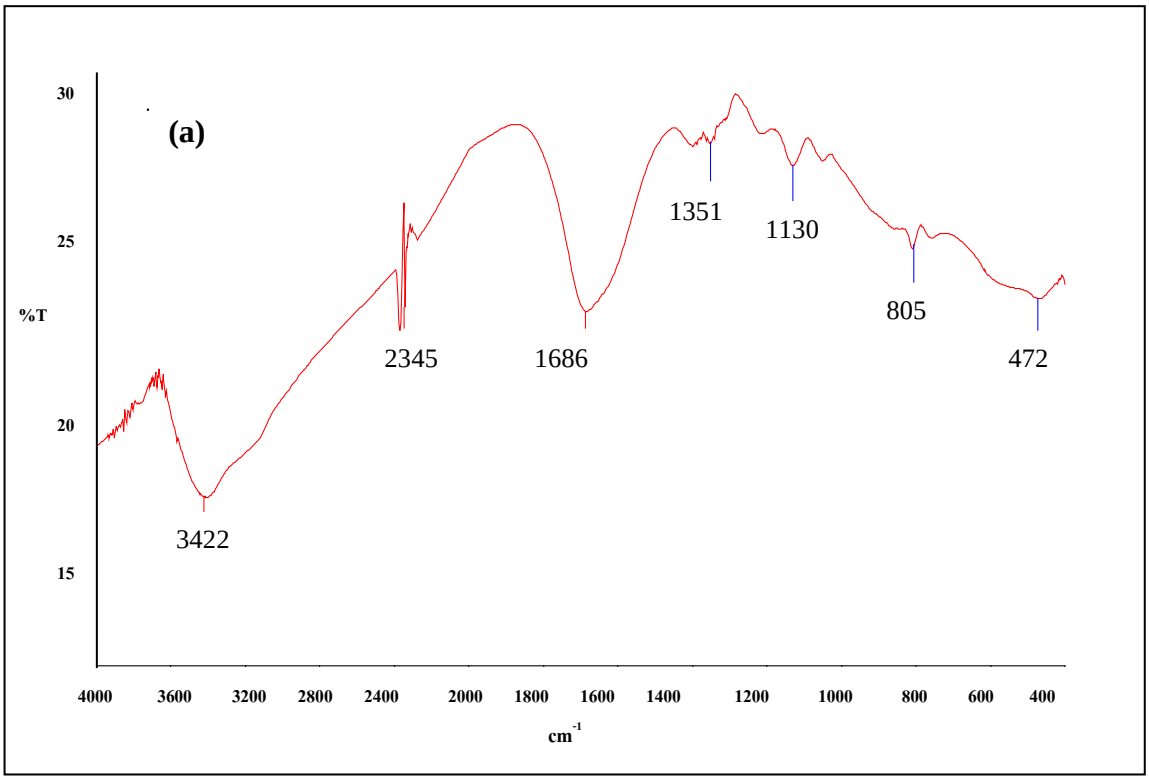
(a)
30
25
20
15
%T
3422
2345
1686
1351
1130
805
472
4000
3600
3200
2800
2400
2000
1800
1600
1400
1200
1000
800
600
400
cm-1

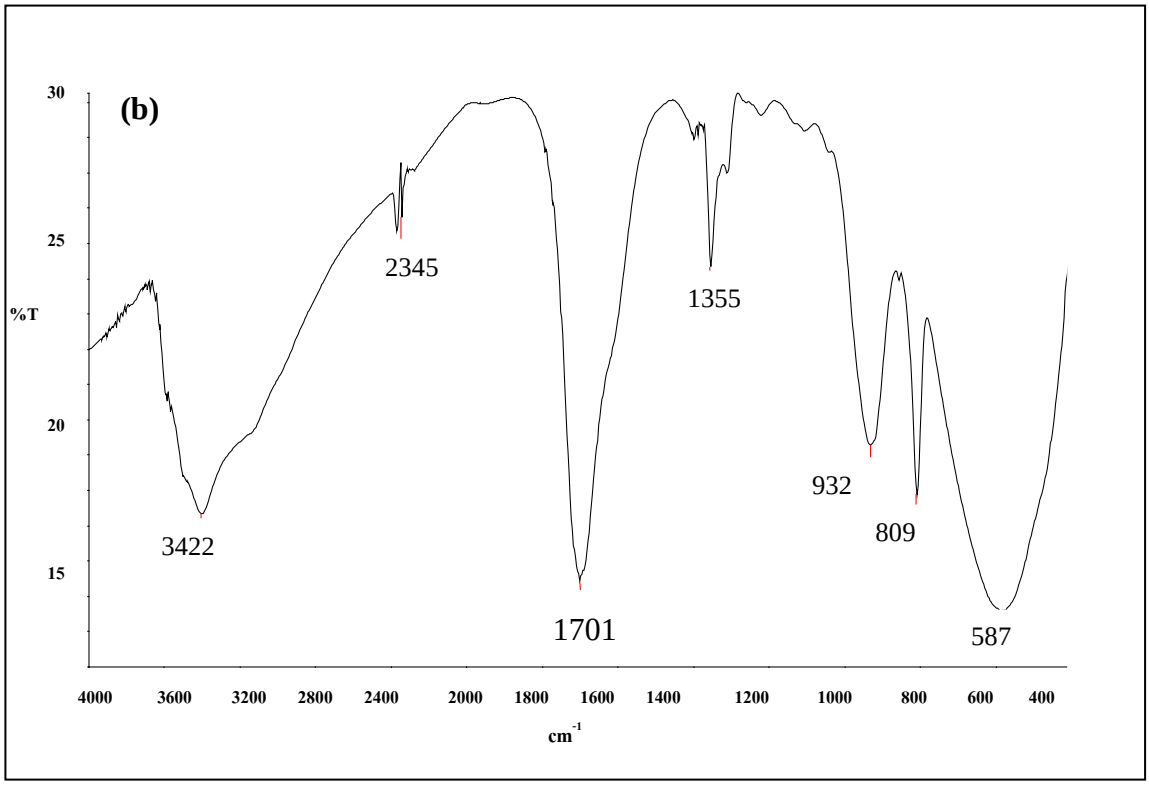
(b)
30
25
20
15
%T
3422
2345
1701
1355
932
809
587
4000
3600
3200
2800
2400
2000
1800
1600
1400
1200
1000
800
600
400
cm-1

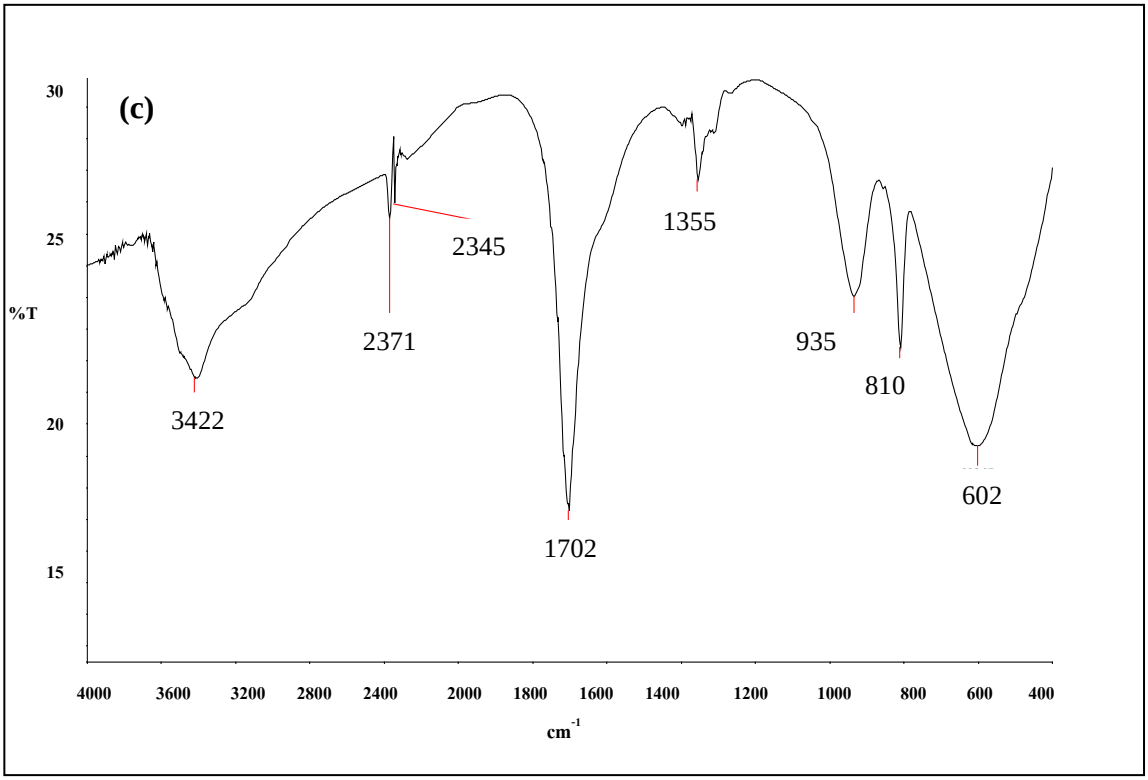

Figure 3.14 FT-IR spectra of the synthesized titanium oxalate complex; (a) *TiOX-01*, (b) *TiOX-02, and* (c) *TiOX-03*

It is well known that the $C_2O_4^{2-}$ ligand can coordinate to the metal as a monodentate as well as a bidentate one (Figure 3.15). Therefore, comparison of the infrared spectra of monodentate and bidentate metallic complex of this ligand will be of considerable interest.

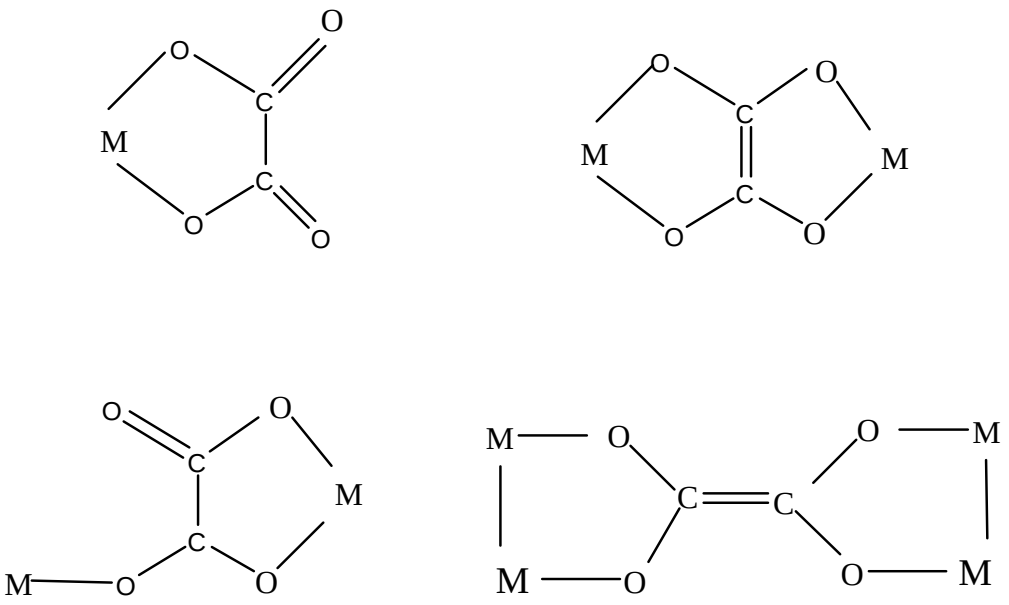

Figure 3.15 The main linkage types of oxalates ligand with metal (Cotton, *et al.*, 1999)

The infrared spectra of oxalate complexes have been studied extensively. Empirical band assignment had been made by using the result of normal coordinate analysis on the free oxalate ion. Free oxalate ion has high symmetry of V_h and exhibits 12 fundamentals (Nakamoto K., 1986). Among those, 9 are in-plane and 3 are out-of-plane vibrations. The numbers of infrared active in-plane modes are only 4 in V_h. If the symmetry is reduced to C_{2v} by coordination, all the 9 modes become infrared active. Whereas, Clark, *et al*., (2002) reported the oxalic ion was planar (D_{2h} symmetry) or twisted (D_2 or D_{2d} symmetry). The group theoretical predications for the Raman activity of the normal modes of the oxalate ion were that there should be 0, 8, and 5 coincidenced for D_{2h}, D_2, and D_{2d} symmetry, respectively. Atomic displacements of oxalate anion are shown in Figure 3.16.

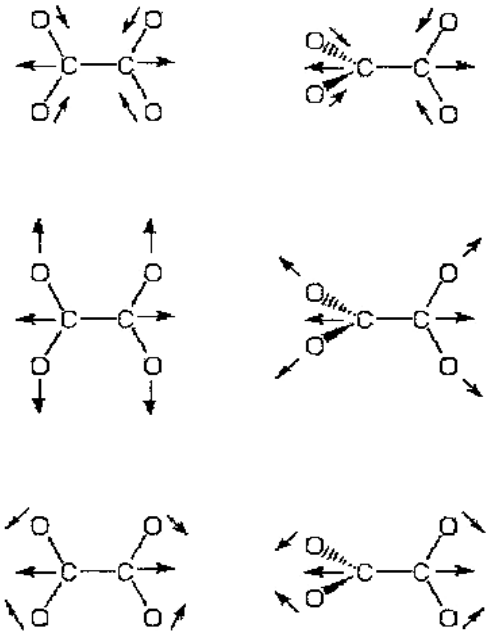

Figure 3.16 Atomic displacements in the totally symmetric normal modes of planar and 90^{o} twisted oxalate anion (Clark, *et al*., 2002)

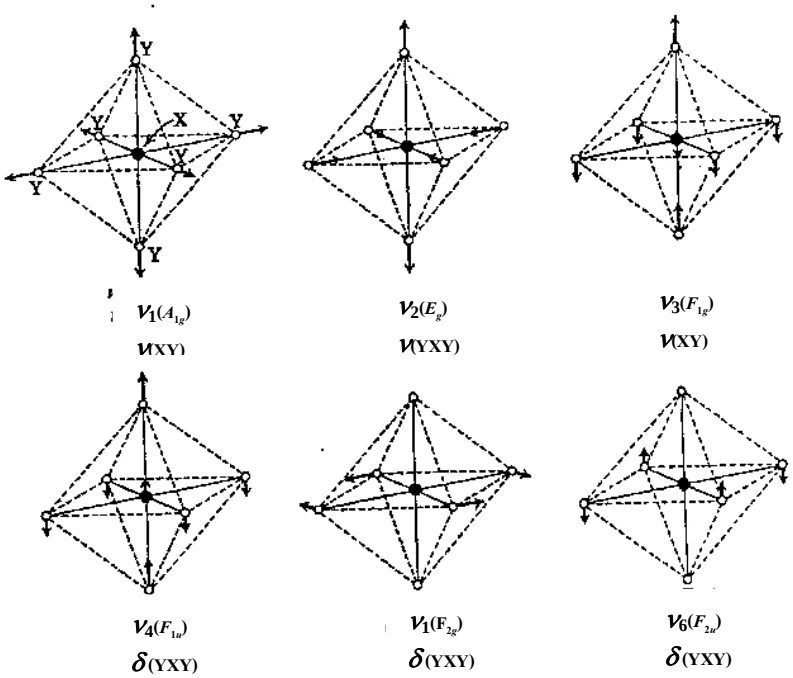

Figure 3.17 Normal modes of vibration in octahedral XY_6 molecules (Nakamoto K., 1986)

The oxalate complexes were distorted octahedral coordination. It could be explained as octahedral XY_6 molecules. Figure 3.17 illustrates the six normal modes of vibration of an octahedral XY_6 molecule. Vibrations ν_1, ν_2, and ν_5 are Raman active, whereas only ν_3 and ν_4 are infrared active. Since ν_6 is inactive in both, its frequency is estimated from an analysis of combination and overtone (Nakamoto K., 1986). In this work, the assignment of the FT-IR bands of titanium oxalate complex was identified and agreed with the work of Hee-Lack Choi, *et al*., (1999) which carried out normal coordination analysis on the 1:1 (Ti: $C_2O_4^{2-}$) model of titanium oxalate complex. Since the FT-IR spectra of the product complex are similar, discussion is confined to the most important vibration in the 400-4,000 cm^{-1} region in relation to the structure. Figure 3.14 shows the FT-IR spectra of the prepared titanium oxalate complexes samples. From these spectra, we can see the most relevant FT-IR obtained with the strong band at 1,680-1,710 cm^{-1} and 1,350 cm^{-1}, which is ascribed to C=O and C-O stretching mode, the presence of oxalate anion is predicted. The high wavenumber, 3,000-3,600 cm^{-1}, show the bands due to the presence of water. The sharp band at 3,600 cm^{-1} is stretching vibration of constitute on water. The broad band at 3,200 cm^{-1} is deformation vibration of hydration water. The observed band in the same range 935 cm^{-1} and below 500 cm^{-1} is associated with the characteristic vibrational modes of titanium oxalates complexes (ν_{Ti-O}, stretching mode of Ti-O bond) (Zhang, *et al*., 2002). The IR absorption bands of the products and the mononuclear and binuclear complexes *TiOX-01, TiOX-02*, and *TiOX-03*, together with their assignments are given in Table 3.9.

Table 3.9 Assignment of the FT-IR bands of synthetic titanium oxalate complexes

Sample	Wavenumber (cm^{-1})	Assignment	Functional groups/ Molecule	References
TiOX-01	3,600-3,000	ν_{OH}	H_2O	Wang, *et al*., 2000
	2,345	ν_{CO}	CO_2	Nakamoto, 1997
	1,686	ν_{CO}	C-O bridging	Nakamoto, 1997
	1,351	$\nu_{CO}+\nu_{CC}$	C-O + C-C	Nakamoto, 1997
	1,130	$\nu_{CO}+\delta_{OCO}$	C-O + O-C=O	Nakamoto, 1997
	805	δ_{OCO}	O-C=O	Nakamoto, 1997
	Below 500	ν_{Ti-O}	Ti-O bond	Velasco *et al*., 1999
TiOX-02	3,600-3,000	ν_{OH}	H_2O	Wang *et al*., 2000
	2,371 and 2,345	ν_{CO}	CO_2	Nakamoto, 1997
	1,702	ν_{CO}	C-O bridging	Nakamoto, 1997
	1,355	$\nu_{CO}+\nu_{CC}$	C-O + C-C	Nakamoto, 1997
	935	δ_{OCO}	O-C=O	Nakamoto, 1997
	810	δ_{CO}	C-O	Nakamoto, 1997
	Below 500	ν_{Ti-O}	Ti-O bond	Velasco *et al*., 1999
TiOX-03	3,600-3,000	ν_{OH}	H_2O	Wang *et al*., 2000
	2,345	ν_{CO}	CO_2	Nakamoto, 1997
	1,701	ν_{CO}	C-O bridging	Nakamoto, 1997
	1,355	$\nu_{CO}+\nu_{CC}$	C-O + C-C	Nakamoto, 1997
	932	δ_{OCO}	O-C=O	Nakamoto, 1997
	809	δ_{CO}	C-O	Nakamoto, 1997
	Below 500	ν_{Ti-O}	Ti-O bond	Velasco *et al*., 1999

The synthesized titanium oxalate sample was identified by the XRD pattern to be $Ti_2O_2(C_2O_4)(OH)_2.H_2O$, titanium oxide oxalate hydroxide hydrate, which matched with data in JCPDS No.00-048-1164. From FT-IR spectra, the strong bands

at 1,680-1,710 cm^{-1} and 1,350 cm^{-1}, ascribed to C=O and C-O stretching mode, supported the presence of oxalate anion. The TGA and DSC data also supported the presence of oxalate anion where the major weight loss in the temperature range 260-456 °C was due to the decomposition of oxalate to form TiO_2. The SEM images revealed that morphologies of the sample seem to be affected by the synthesized conditions. It is possible that a crystal phase might be formed after the dissolution of the initial particles which formed the clusters at first.

3.2 Photocatalytic activities of *TiOX-01* and *TiOX-03.*

In this work, iodine solution which was used as model for wastewater**,** was employed to evaluate the photocatalytic activity of as-prepared titanium oxalate complexes samples under UV light irradiation. Normally water solubility of iodine is determined by temperature (20^oC) and pressure (1 bar), and is relatively low. Iodine is better soluble in iodine solutions. Tincture of iodine is a disinfectant containing 2-7% elemental iodine along with potassium iodide or sodium iodide dissolved in a mixture of ethanol and water. The role of iodide and water in the solution is to increase the solubility of the elemental iodine; by turning it to the soluble triiodide anion (I_3^-).

$$I_{2\,(s)} + I^-_{(aq)} \rightarrow [I_3]^-_{(aq)} \qquad (3.12)$$

The dissolved iodine gives rise to a broad spectrum of colors. In aliphatic solvents, the color is violet, while in alcohols, ethers, and benzene it is brown or redish-brown. The use of UV-Vis spectrophotometry for characterization of triiodide is shown in Figure 3.18. The triiodide ion has two absorption bands at 290 and 367 nm (Gabes, *et al*., 1973).

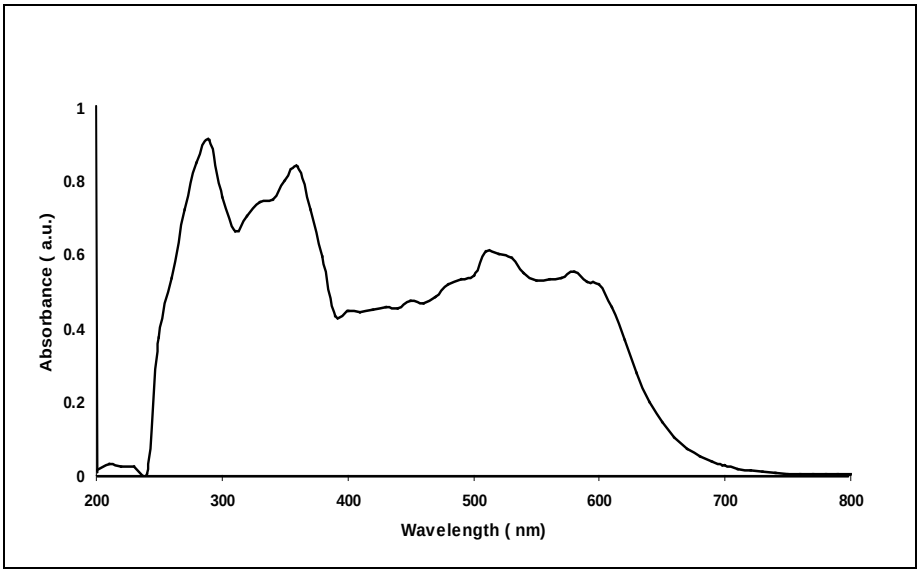

Figure 3.18 UV-Vis spectrum of iodine solution

3.2.1 Construction of calibration graph

Iodine solution concentrations were measured by using the standard calibration graph. The calibration graph is used to find the concentration of iodine solution at any stages during the experiment. In this work, the concentration of standard iodine solution were prepared in the range 1.0 x 10^{-4} M to 1.0 x 10^{-2} M. In order to construct reliable standard calibration graph of iodine solution, the concentrations were divided into two ranges: 1.0 x 10^{-4} M to 1.0 x 10^{-3} M, and 1.0 x 10^{-3} M to 1.0 x 10^{-2} M. The absorbance of iodine solution was measured with SPECORD S100 spectrophotometer at λ = 290 nm. The calibration graph was a straight line. The standard calibration graphs of, iodine solution in this range are shown in Figures 3.19 and 3.20.

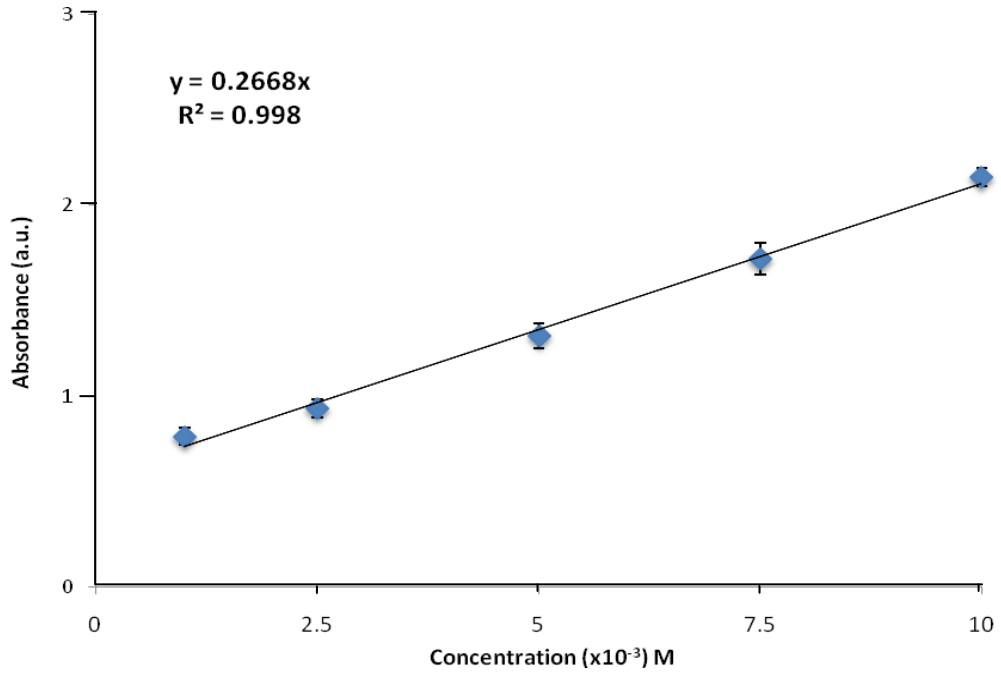

Figure 3.19 The standard calibration graph of iodine solution in the range of 1.0 x 10^{-3} M to 1.0 x 10^{-2} M (n = 3)

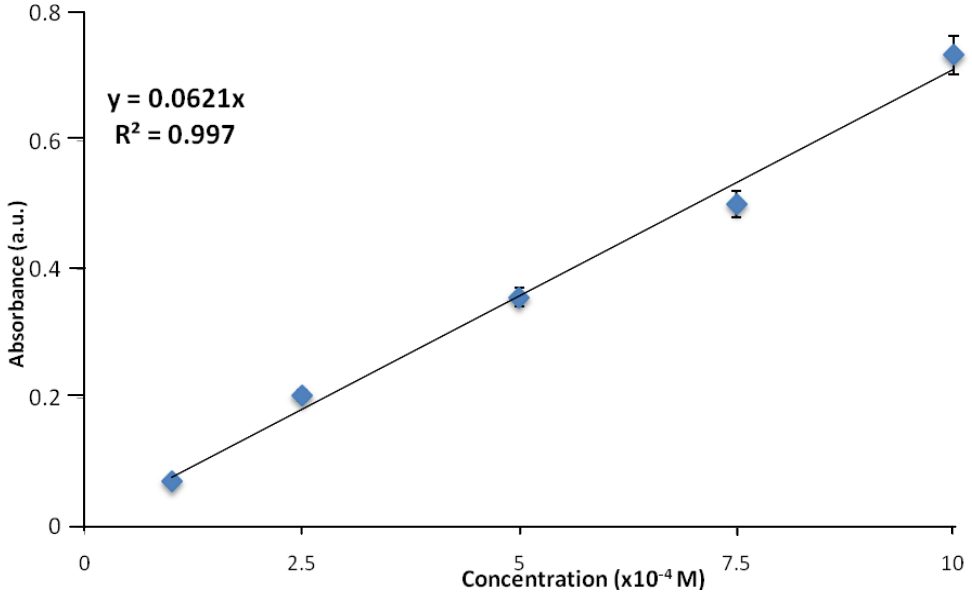

Figure 3.20 The standard calibration graph of iodine solution in the range of 1.0 x 10^{-4} M to 1.0 x 10^{-3} M (n = 3)

3.2.2 Photocatalytic activity tests procedure

In photodegradation process, there are two factors resulting in the decreasing of concentration of iodine solution: the adsorption of iodine solution onto the surface of titanium oxalate complexes, and the photoreduction-photooxidation of iodine solution. In the adsorption case, 3.1062 g of each titanium oxalate complex sample was placed in an Erlenmeyer flask which contained 100 mL of iodine solution the mixture was then continuously stirred in the closed compartment (0.9 m x 0.9 m x 0.9 m) to avoid interference from ambient light until the end of experiment, 6 hours. At time intervals (every 1 hour), 5 mL of decolorized iodine solution samples were collected and centrifuged to separate titanium oxalate particles prior to the spectral measurement. The changes in absorbance of mixture solution were recorded using UV-Vis spectrophotometer, (SPECORD S100, Analytik Jena GmbH, Germany) at 290 and 367 nm for triiodide ion (Gabes, *et al*., 1973). For the photochemistry reaction cases, the same amounts of reactants were used in the same reaction compartment. Prior to irradiation, the mixture solution was agitated with a magnetic stirrer in the dark for 1 hour to reach the adsorption equilibrium onto the surface of sample. Then the UV light source from 5 fluorescence blacklight (20 W, F20T12-BLB, GE, U.S.A.) tube was switched on and magnetically stirred for 5 hours. The percentage of iodine solution decolorized (adsorption study) or degraded (photocatalytic study) was determined from the following equation;

$$\%Decolorization = \frac{C_0 - Ct}{C_0} \text{X}100 \tag{3.13}$$

where C_0 is the initial concentration of iodine and C_t is the concentration of tincture iodine solution at specific sampling time.

In this experiment, the photocatalytic conditional reference material, Degussa P25-TiO_2, was used to compare the efficiency of decolorized iodine solution of as-prepared titanium oxalate complexes samples. In the comparison test, the synthesized titanium oxalate complex powders was used at fixed concentration (3.1062 g/L) because in our experimental conditions, only material sample expected to show high photocatalytic efficiency. Controlled experiments without UV-light and

without the synthesized titanium oxalate complex powders to ensure that degradation of the iodine solution was dependent on the presence of UV-light and the synthesized titanium oxalate complex powders**.**

3.2.2.1 Adsorption study of *TiOX-03*

The effect of adsorption in the dark was carried out in order to evaluate the photodegradation of iodine solution. To study the adsorption activity of *TiOX-03*, the catalyst *TiOX-03* was placed in the conical flask and the measured volume of iodine solution was added. The initial iodine solution was studied by varying concentration from $1x10^{-4}$ M to $1x10^{-3}$ M and $1x10^{-4}$ M to $1x10^{-3}$ M monitoring at wavelength 290 nm. Decolorization efficiency of *TiOX-03* is shown in Figure 3.21 and Table 3.10. In mixing *TiOX-03* with iodine solution, the adsorption of iodine solution on the *TiOX-03* surface took place instantly prior to the measurements. In this experiment, the adsorption time was 1 hour to allow the system to reach adsorption equilibrium.

The resulting data from Figure 3.21 and Table 3.10 indicated that the catalyst *TiOX-03* has low efficiency of decolorizing iodine solution by adsorption alone.

Table 3.10 The percentage of decolorization by *TiOX-03*

Concentration of iodine solution	*Decolorization by adsorption (% ± SD) with time (hours)				
	1	2	3	4	5
1×10^{-4} M	54.3 ± 1.1	55.7 ± 1.5	56.8 ± 1.9	56.3 ± 0.7	56.1 ± 0.2
5×10^{-4} M	24.8 ± 0.9	24.3 ± 1.3	25.7 ± 1.8	24.6 ± 0.8	25.7 ± 0.8
1×10^{-3} M	22.4 ± 0.5	22.4 ± 0.7	22.3 ± 0.9	22.4 ± 1.5	22.4 ± 3.3
2.5×10^{-3} M	14.6 ± 1.6	14.7 ± 3.0	14.9 ± 3.0	15.0 ± 3.1	15.1 ± 3.1
7.5×10^{-3} M	10.2 ± 1.2	10.5 ± 1.2	10.7 ± 1.3	10.8 ± 1.4	10.9 ± 1.4

n = 3

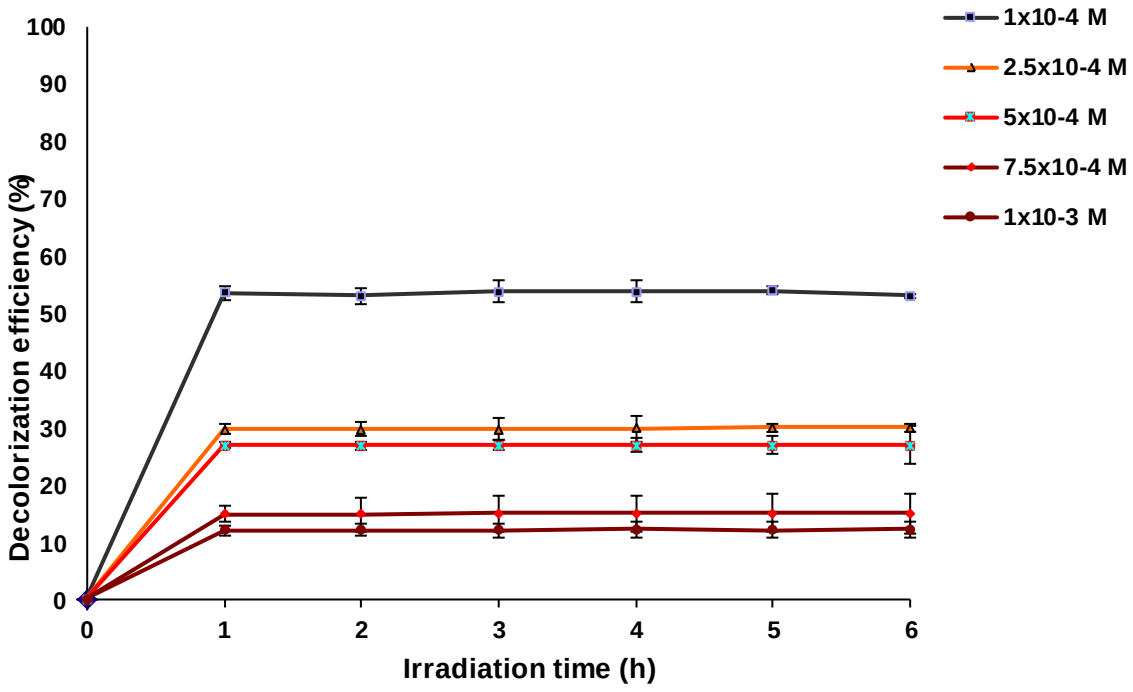

Figure 3.21 Decolorization by adsorption (in the dark) of iodine solution by crystalline titanium oxalate complexes [*TiOX-03*] at various concentrations (n = 3)

3.2.2.2 Photodegradation studies of *TiOX-03*

The photodegradation study of titanium oxalate crystalline complexes (*TiOX-03*) under UV light irradiation was investigated with iodine solution concentrations in the range 0.1-1.0 mM. The degradation efficiencies at five concentrations (included adsorption) are shown in Figure 3.22.

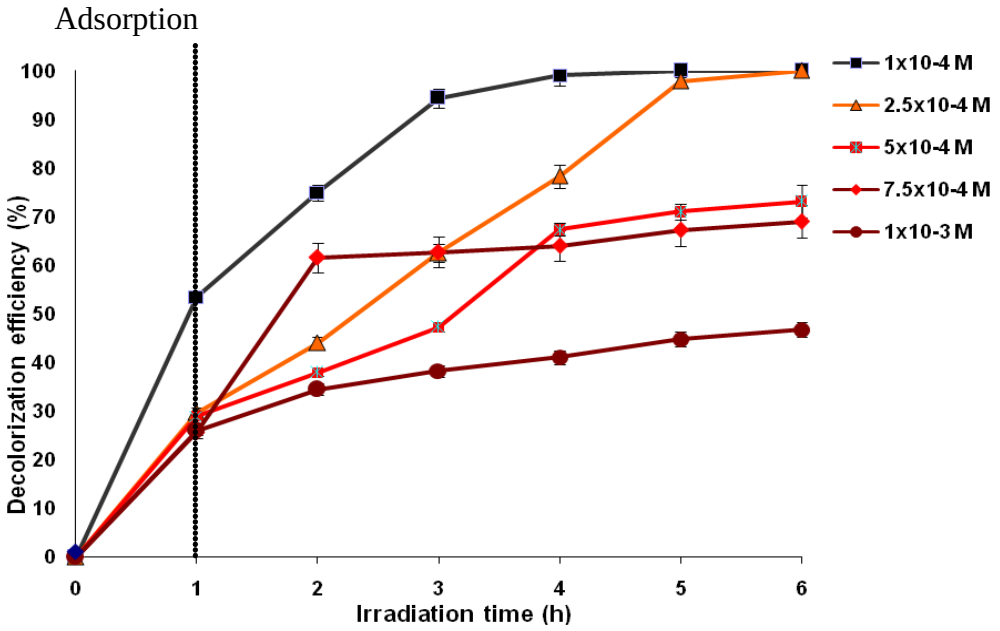

Figure 3.22 Photodegradation efficiency of tincture iodine by *TiOX-03* under UV light in various concentrations (n = 3)

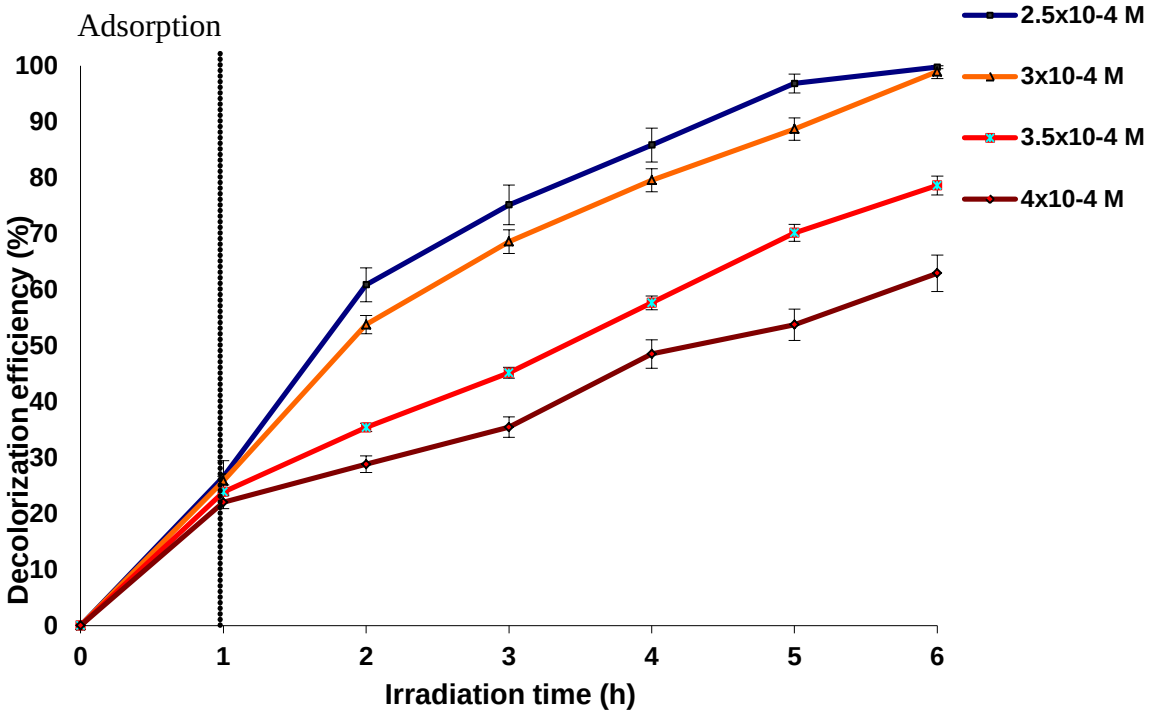

Figure 3.23 Photodegradation efficiency of tincture iodine by *TiOX-03* under UV light in various concentrations (n = 3)

From the above studies we found that the resulting data from Figure 3.21 indicated that the catalyst *TiOX-03* has low efficiency of decolorizing iodine solution by adsorption alone. It is clear, from Figure 3.22 and 3.23, that complete decolorizations of tincture iodine by crystalline titanium oxalate complexes were obtained when the dye concentrations were low (below 2.5 x 10^{-4} M) in 6 hours. This decolorization resulted solely from photodegradation and adsorption. The maximum initial concentration of aqueous iodine solution on the photodegradation by titanium oxalate complex which turned from dark-orange to colorless in 6 hours was 3 x 10^{-4} M. When the initial concentration of aqueous iodine solution was increased, the photodegradation by titanium oxalate complex significantly decreased.

3.2.2.3 Comparative studies of amorphous *TiOX-01* and crystalline *TiOX-03* with the Degussa P25.

The degradation efficiency of crystalline titanium oxalate complexes was comparatively studied with P25 TiO_2 in the photodegradation and adsorption of iodine solution under UV light and the results are shown in Figure 3.24. *TiOX-03* exhibited much higher photodegradation than that of Degussa P25 while *TiOX-01* has lower photodegradation than that of Degussa P25 in 6 hours. In the first 1 hour under dark condition, the adsorption efficiencies were in the order: Degussa P25 > *TiOX-03* > *TiOX-01*. The concentration of iodine solution decreased because of iodine solution was physical adsorbed on the surface sample, whereas, surface area of Degussa P25 is larger than the crystalline phase. After switching on the UV light, the photoefficiency of decolorization iodine solution in 3x10^{-4} M increased within 6 hours in order: *TiOX-03* > Degussa P25 > *TiOX-01*.

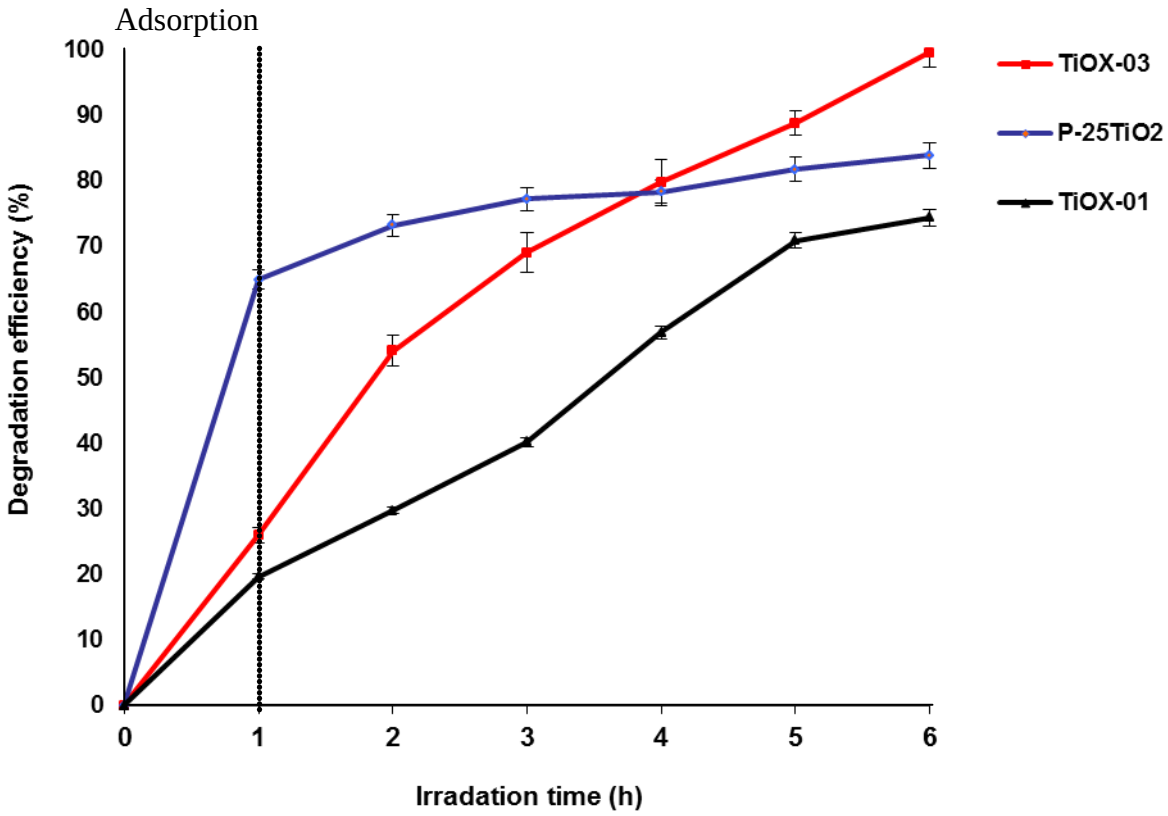

Figure 3.24 Photoefficiency of degradation tincture iodine by *TiOX-01* and *TiOX-03* compare with commercial P25-TiO_2 under UV light in $3x10^{-4}$ M (n = 3)

3.2.2.4 Effect of pH on the photodegradation activity.

In real life applications the photodegradation may be used in environment with varying conditions, hence, all the titanium oxalate complex samples were tested for their activities at varying pH values, 2.3, 5, 7 and 10. The natural pH of iodine solution in this work was 2.3. The influence of pH on the degradation of iodine solution ($3x10^{-4}$ M) under UV irradiation by the crystalline titanium oxalate complexes samples are shown in Figures 3.25. The results showed that there was a strong dependence on the pH of the solution during the heterogeneous photoprocess. It is known that when iodine is added to water, the following reaction results (www.lenntech, 2011):

$$I_{2\,(l)} + H_2O_{\,(l)} \rightarrow OI^-_{\,(aq)} + 2H^+_{\,(aq)} + I^-_{\,(aq)} \qquad (3.14)$$

I_2 molecules and water molecules react and yield substances such as hypoiodite (OI^-). The reaction can move both ways of the equilibrium, depending on the pH of the solution (www.lenntech, 2011). The order of activities is pH 10 > pH 7 > pH 5 > pH 2.3 under UV light irradiations.

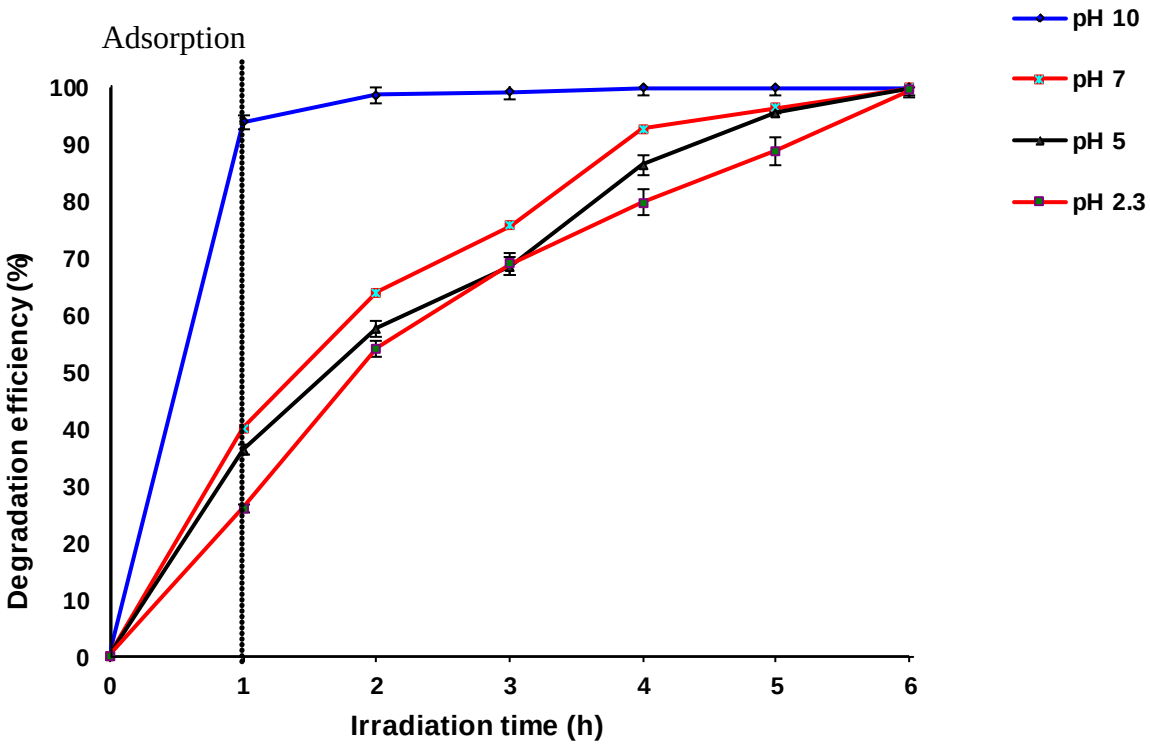

Figure 3.25 Effect of pH on photodegradation of iodine solution by $Ti_2O_2(C_2O_4)(OH)_2.H_2O$ [*TiOX-03*] under UV light ($3x10^{-4}$ M)(n = 3)

In general, as the pH of aqueous solution increases, the yield of hydroxyl radical in the photocatalytic reaction also increases. Moreover, pH values could also alter the surface electricity of photocatalyst, thus affecting the adsorption and desorption properties and abilities in mixing *TiOX-03* with iodine solution, the adsorption of iodine solution on the *TiOX-03* surface took place instantly prior to the measurements. The cause of this phenomenon was probably that oxalate at the first

ionization state showed a more favorable reaction rate with •OH (Kumar, *et al*., 2010). The degradation of iodine solution by titanium oxalate complex followed a different the increase of pH was less. The result of photodegradation of iodine solution by titanium oxalate complex more increased significantly at initial pH of 2.3 to 5 and 7. At the same time, the photodegradation efficiencies increase sharply during the photoreaction from initial pH of 10. These results indicate that another dominant is present pH of 10.

3.2.2.5 Effect of UV light intensity on the photodegradation activity.

The effect of UV light intensity on the photodegradation by titanium oxalate complex is shown in Figure 3.26. It can be seen that on increasing the light source intensity, the photodegradation efficiencies increased, due to high UV light intensity increase the photon influx.

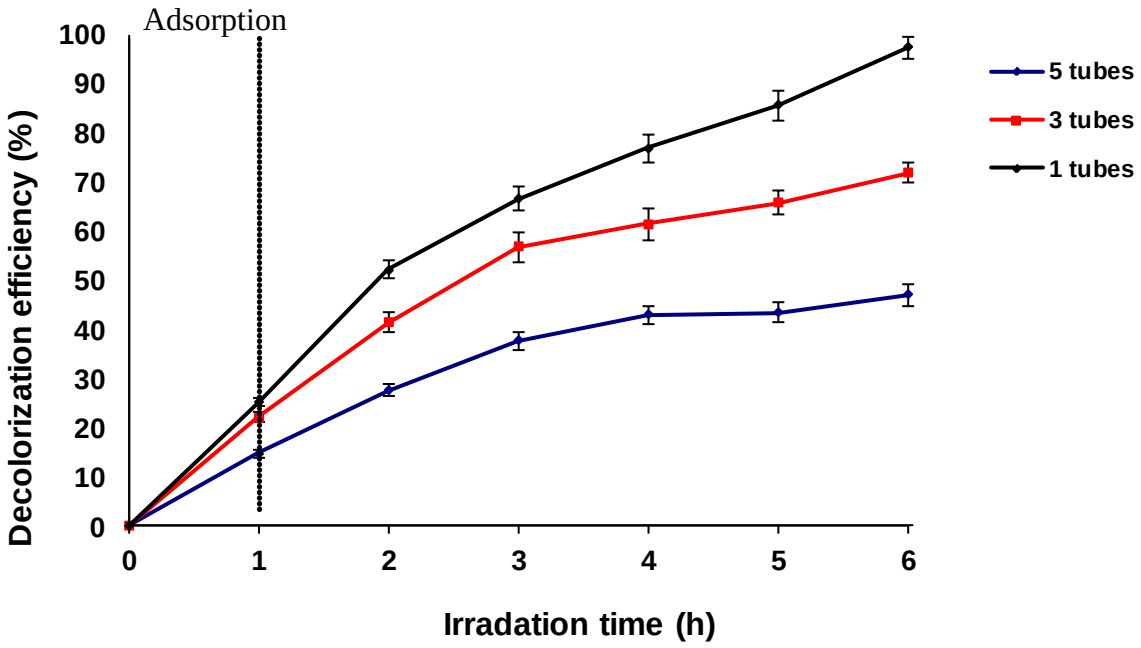

Figure 3.26 Effect of UV light intensity on the photodegradation of iodine solution by $Ti_2O_2(C_2O_4)(OH)_2.H_2O$ [TiOX-03] ($3x10^{-4}$ M) (n = 3)

The photocatalytic reaction rate depends largely on the irradiation absorption of the species involve in the photo degradation leading to an increase in the degradation with increasing light intensity during photodegradation (Toor, *et al*., 2006). With this in mind, as the UV light intensity increased, the photodegradation efficiencies of iodine solution in this study also increased.

3.2.2.6 Recyclability of the catalyst.

TiOX-03 could be used repeatedly to degrade the aqueous iodine solution under UV irradiation. The photodegradation activities decreased with number of repeated uses. During the first use these titanium oxalate complex were reacted with iodide in the photodegradation process along with iodine solution. However, the surface of used powders became off-white to pale yellow after several reuses compared to plain white of the new powders. The explanation for this observation is that when freshly prepared the titanium oxalate powder as well as some of iodine molecules were reacted and some iodine were still remained on the titanium oxalate complex surface. Hence, after the first use, the photodegradation efficiencies was decreased with higher number of iodine molecule in iodine solution, therefore, lower activity was observed in the second use and onward. The photodegradation efficiencies of the *TiOX-03* from the three repeating uses are shown in Figures 3.27.

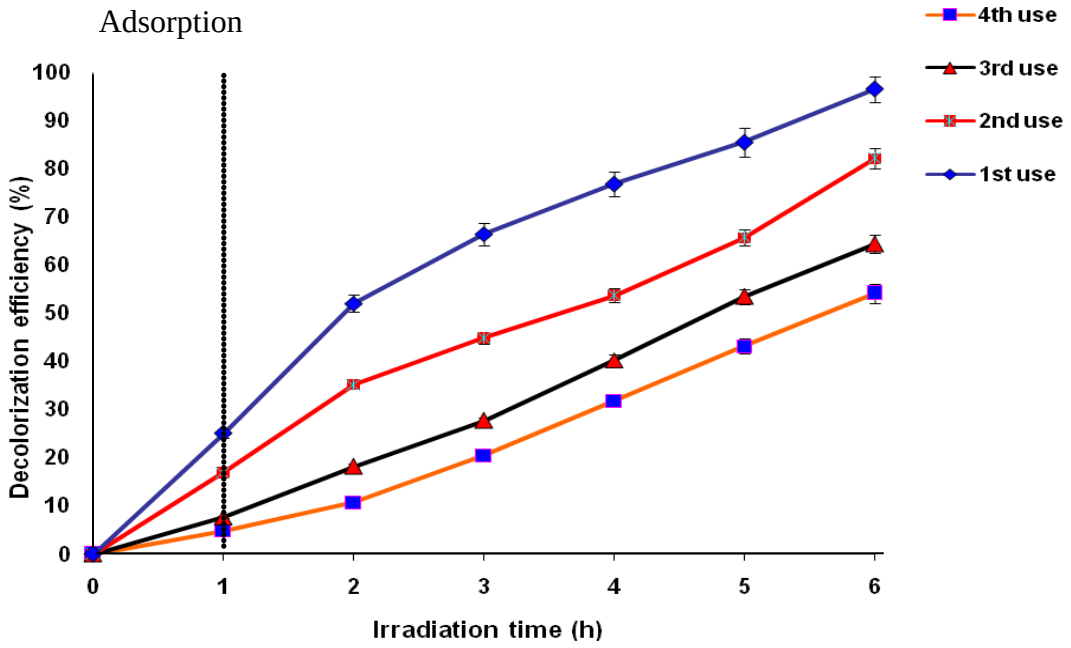

Figure 3.27 Photoefficiency of the reclyclability of *TiOX-03* on photodegradation of tincture iodine under UV light ($3x10^{-4}$ M) (n = 3)

From the conclusions above, we found that the titanium oxalate was successfully prepared using titanium oxysulfate dihydrate ($TiOSO_4.2H_2O$) as a precursor. Oxalic acid dihydrate ($H_2C_2O_4.2H_2O$) play the role as source of oxalate ligand. The X-ray diffraction spectra of the synthesized titanium oxalate complex (*TiOX-03*) at various aged periods are matched with compound of the chemical formula $Ti_2O_2(C_2O_4)(OH)_2.H_2O$, titanium oxide oxalate hydroxide hydrate, which exists in JCPDS No.00-048-1164. The initial formation of $TiOC_2O_4.H_2O$ (*TiOX-01*) has a poor crystallinity. As expected, with the ageing time increase, the initial precipitate goes to the phase with good crystallinity. In addition, the photodegradation of iodine solution, which was used as model for wastewater**,** was employed to evaluate the photochemistry parameters of as-prepared titanium oxalate complexes samples under UV light irradiation. The maximum initial concentration of aqueous iodine solution to be effectively photodegraded which turned from dark-orange to colorless in 6 hours was 3 x 10^{-4} M. In addition, the titanium oxalate complex could be reused to

degrade the iodine solution under UV irradiation but with short recycling life, for example, only three repeating uses for the *TiOX-03*.

CHAPTER 4
CONCLUSIONS

In this work, titanium(IV) oxalate was successfully synthesized in a polycrystalline form in the course of the study of precursor by adding $TiOSO_4.2H_2O$ solution to an ethanol solution of oxalic acid with aim to use it as a new precursor. The physico-chemical properties of the synthesized titanium(IV) oxalate compound were characterized by XRD, BET, TGA, DSC, SEM, EDX, and FT-IR techniques.

In the preparation, $TiOSO_4.2H_2O$ solution was poured into oxalic acid in ethanol solution, white powder was precipitated. The initial precipitate exhibited poor crystallinity. The powder turned into a crystalline phase after the ageing time was increased. The X-ray diffraction patterns of products prepared from various aged periods at 60°C and 70°C were obtained. The patterns of crystalline products matched with the compound of the chemical formula $Ti_2O_2(C_2O_4)(OH)_2.H_2O$, titanium oxide oxalate hydroxide hydrate, in JCPDS No.00-048-1164. The nitrogen adsorption isotherms of the amorphous titanium oxalate complex (*TiOX-01*) is of Type I (BDDT classification) indicating that the pore size is in the microporous region. For crystalline titanium oxalate complex (*TiOX-03*) the isotherm is a combination of Type I and IV (BDDT classification) with two distinct regions; at low relative pressure, the isotherm exhibits high adsorption, indicating that the sample contains micropore (Type I). However, at high relative pressure, the curve exhibits the presence of mesopores (Type IV). The present of micropore could be checked by plotting the adsorbed layer called "*t*-plot": *TiOX-01* showed linear t-plot not passing the origin indicating either micropore or mesopore was presence for this sample and *TiOX-03* complex showed linear part passing the origin indicating that it contained both micropore and mesopore structure, respectively. *TiOX-03* shows bimodal pore size distribution consisting of intra-particle pores (5-10 nm) and larger inter-particle pores (10-70 nm). Usually, there are two types of pores present in the bimodal pore size distribution. One is made from the intra-aggregated pores at lower P/P_o range (the pores within the hard aggregates) and the other is larger inter-aggregated pores in the higher P/P_o range arising from hard aggregated (the void between hard aggregates). From the SEM results the morphologies of the samples were affected by the synthetic conditions. The precipitate

of 1 hour consisted of clusters of the particles which disappeared with the ageing time and the morphology of the product consisted of a large size and porous particles of irregular shape. On the other hand, the amount and size of the round shape particles also decreased as ageing time increased. The particle sizes of samples were in the micrometer range; 1 μm for amorphous titanium oxalate complex, and less than 1 μm for crystalline titanium oxalate complex. It is believed that the crystal phase was formed after the dissolution of the initial particles which formed the clusters at first. EDX technique was used to confirm that titanium oxalate complex contained titanium, oxygen, and oxalate complex anion, $TiOC_2O_4.H_2O$, with one water molecule. After the ageing time increased, the powder was transformed to crystalline phase consisted of two titanium, two oxygen, and oxalate complex anion, $Ti_2O_2(C_2O_4)(OH)_2.H_2O$, with one water molecule. The purity of the complex can be determined by analyzing its constituents (Ti, C, O, and S). The relative percentages of all constituents can be determined in order to evaluate the content of each element (Ti, C, O, and S) in the synthesized titanium oxalate complex sample. The TGA and DSC techniques provided the analyst with a quantitative measurement of any weight change associated with a transition. The decomposition of titanium oxalate complex was identified by percentage of weight loss. In this study, the total weight loss of 47.11% was observed. The first weight loss (9.74%) in the temperature range 39-260 °C may be attributed to hydrated water released from $Ti_2O_2(C_2O_4)(OH)_2.H_2O$. The major weight loss of 30.67% in the temperature range 260-456 °C was due to the decomposition of oxalate to form TiO_2. Between 390-456 °C, the unit of TiO_2 is believed to grow into anatase-TiO_2 with no mass loss in TGA curves. The final weight loss 6.58%, the TGA curve at higher than 456 °C indicated transformation from anatase to rutile crystalline phase.

In summary the photodegradation of iodine solution which was used as model for wastewater**,** showed that the synthesized titanium oxalate complex could degrade the aqueous iodine solution via photocatalytic reaction under UV irradiation. The mechanism may be attributed to oxidation of oxalate ion ($C_2O_4^{2-}$) to carbon dioxide and reduction of iodine molecule (I_2) to iodide. The following reaction may occur:

$$Ti_2O_2(C_2O_4)(OH)_2.H_2O_{(aq)} + I_{2\,(aq)} \rightarrow 2\ TiOI(OH).H_2O_{(aq)} + 2\ CO_{2\,(g)} \quad (4.1)$$

The maximum initial concentration of aqueous iodine solution on the photodegradation by crystalline titanium oxalate complex (*TiOX-03*) which turned from dark-orange to colorless in 6 hours was 3 x 10^{-4} M. When the initial concentration of aqueous iodine solution was increased, the photodegradation by titanium oxalate complex significantly decreased. It was noticed that the presence of crystal phases in *TiOX-03* enhanced the photoefficiency of titanium oxalate complex (corresponding to 99.56% degradation) comparing with the sample of poorer crystallinity (only 74.46% degradation). In this part, all synthesized titanium oxalate complexes show higher photoefficiency than Degussa P25-TiO_2 sample. Furthermore, it has been good adsorption property and low photoefficiency property. As for the effect of UV light intensity on the photodegradation by *TiOX-03*, the increasing of the light source increased photodegradation efficiencies due to the high UV light intensity increase photon influx entering via photochemistry reaction. In addition, the titanium oxalate complex could be used repeatedly to degrade the iodine solution under UV irradiation. The photodegradation activities decreased with number of repeated used. The surface of powder became yellow after uses. This may result from the fact the trace impurities remained on the powder. The photodegradation efficiencies of the *TiOX-03* was rather short, i.e. approximately only from the three repeating uses.

REFFERENCES

Application of photochemistry from Wikipedia, the free encyclopedia. http://en.wikipedia.org/wiki/Photochemistry (accessed March 24, 13).

Albert Stwertka, 1998. "Guide to the Elements - Revised Edition", Oxford University Press, ISBN 0-19-508083-1. (1998).

Bally, R. D.; Hook, L. L. and Pennington, W. T. 1998. Chemistry Communication. 1181. (1998).

Balong, Z.; Baishun, C.; Keyu, S.; Shangjin, H.; Xiaodong, L.; Zongjie, D. and Kelian, Y. 2003."Preparation and characterization of nanocrystal grain TiO_2 porous microspheres", Applied Catalysis B: Environmental. 40 (2003), 253-258.

Banat, I. M.; McMullan, G.; Meehan, C.; Kirby, N.; Nigam, P.; Smyth, W.F. and Marchant, R. 1999. "Microbial decolorization of textile dyes present in textile industries effluent", Proceedings of the Industrial Waste Technical Conference. Indianapolis, USA. (1999), pp. 1–16.

Basic photosensitization from Nancy L. Oleinick. 2008. Department of Radiation Oncology. Case Western Reserve University School of Medicine. Cleveland, Ohio. (2008), 44106-4942. http://www.photobiology.info/Oleinick.html (accessed August 14, 12).

Bassaid, S.; Didier Robert, D. and Chaib, M. 2009. "Use of oxalate sacrificial compounds to improve the photocatalytic performance of titanium dioxide", Applied Catalysis B: Environmental. 5 (2009), 93-97.

Bragg, W. L. 1913. "The Diffraction of Short Electromagnetic Waves by a Crystal", Proceedings of the Cambridge Philosophical Society. 17 (1913), 43–57.

Boudaren, C.; Bataille, T.; Auffredic, J. P. and Louer, D. 2003. "Synthesis, structure determination from powder diffraction data and thermal behavior of titanium (IV) oxalate $[Ti_2O_3(H_2O)_2](C_2O_4).H_2O$", Solid State Sciences. 5 (2003), 175-182.

Carneiro, P. A.; Osugi, M. E.; Sene, J. J.; Anderson, M. A. and Boldrin Zanoni, M. V. (2004). "Evaluation of color removal and degradation of a reactive texile azo dye on nanoporous TiO_2 thin-film electrodes", Electrochimica Acta. 49 (2004), 3807-3820.

Chaiyapoom, L.; Wongnawa, S.; Pakawatchai, C.; Carmant, J. and Saithong, S. 2006. "The alexandrite-Like Cr-Doped Aluminum Oxalato Complexes", Inorganic Chemistry Commumcation. 9 (2006), 316-318.

Choychangtong, W. 2004. "Synthesis and Characterization of Titanium Dioxide", Master of Science Thesis, Prince of Songkla University, Songkhla, Thailand. (2004).

Clark, R. J. H. 1968. The Chemistry of Titanium and Vanadium. Amsterdam: Elsevier. (1968).

Coindet, J. 1820. J. F. Ann. Chim. 15 (1820), 49.

Cotton, F. A. and Wilkinso, G. 1972. Advance Inorganic Chemistry, 3rd ed. John Wiley & Sons, New York. (1972).

Cotton, F. A.; Wilkinso, G.; Murillo, C.A. and Bochman, M. 1999. Advance Inorganic Chemistry, 6rd ed. John Wiley & Sons, New York. (1999).

Daniele, P. G. 1983. "The Formation of Proton and Alkali Metal Complexes with Ligands of Biological Interest in Aqueous Solution: Thermodynamic of Li^+, Na^+, and K^+ Dicarboxylate Complex Formation", Thermochim. Acta. 62 (1983), 101- 112.

Davis, M. W.; Glasser, J.A.; Evans, J.W. and Lamar, R.T. 1993. "Field evaluation of the lignin-degrading fungus *Phanerochaete sordida* to treat creosote-contaminated soil", Environ. Sci. Technol. 27 (1993), 2572–2576.

Deana and John, A. 1995. The Analytical Chemistry Handbook. McGraw Hill, Inc., New York. (1995), 15.1–15.5.

Differential scanning calorimeter from Polymer Science Learning Center. Department of Polymer Science. The University of Southern Mississippi. http://www.pslc.ws/macrog/dsc.htm (accessed March 18, 12)

Douglas, A.; Skoog, F.; James Holler and Timothy Nieman. 1998. Principles of Instrumental Analysis, 5th Edition. New York. (1998), 805-808.

Evans, O. R. and Lin, C. 2002. "Photoassisted Bleaching Dyes Utilizing TiO_2 and Visible Light", Chemosphere. 46 (2002), 561-579.

Frank S. N. and Bard, A. J. 1977. Journal of American Chemical Society. 99 (1977), 303.

Fox M. A. and Dulay M. T. 1993. Chemical Review. 93 (1993), 341.

Gomes de Moraes, S.; Sanches Freire, R. and Duran, N. 2000. "Degradation and toxicity reduction of textile effluent by combined photocatalytic and ozonation processes", Chemospere. 40 (2000), 369-373.

Greenwood, N. N. and Earnshaw, A. 1990. In Chemistry of the Elements: Pergamon Press. (1990), Chapter 17.

Hee-Lack Choi and Chan Park. 1999. "Effect of ultrasonic treatment on ripening of titanium oxalate salt from solution", Journal of material science. 34 (1999), 3591-3596.

Hu, T. L. 1996. "Removal of reactive dyes from aqueous solution by different bacterial genera", Water Science Technology. 34 (1996), 89–95.

Hu, T. L. 1992. "Sorption of reactive dyes by Aeromonas biomass", Water Science Technology. 26 (1992), 357–366.

Iodine and water: reaction mechanisms, environmental impact and health effects, http://www.lenntech.com/periodic/water/iodine/iodine-and water.htm#ixzz0pVrHMe34 (accessed March 26, 12).

IUPAC Recommendation, 1994. Pure Appl. Chem. 66 (1994), 1739.

Jörgensen, S. M. 1870. J. F.Prakt. Chem. 2 (1870), 347.

Khalil, T.; Abou El-Nour, F.; El-Gammal, B and Boccaccini. 2001. "Determination of surface area and porosity of sol-gel derived ceramic powders in the system TiO_2-SiO_2-Al_2O_3", Powder Technology. 114 (2001), 106-111.

Kharkar, D. P. and Patel, C.C. 1957. Journal of Indian Intuition Science. 39 (1957), 41.

Kirby, N. 1999. "Bioremediation of textile industry wastewater by white rot fungi", DPhil Thesis, University of Ulster, Coleraine, UK. (1999).

Kiriakidou, F.; Kondarides, D.I. and Verykios, X. E. 1999. "The effect of operational parameters and TiO_2-doping on the photocatalytic degradation of azo-dyes", Catalysis Today. 54 (1999), 119-130.

Krebs, Robert E. 2006. The History and Use of Our Earth's Chemical Elements: A Reference Guide ,2nd edition. (2006).

Kulla, M. G. 1981. "Aerobic bacterial degradation of azo dyes. Microbial degradation of xerobiotics and recalcitrant compounds", In: Leisinger, T., Cook, A.M., Hutter, R., Nuesch, J. (Eds.), FEMS Symposium, 12. Academic Press, London. (1981), 387–399.

Kumar, B. V. R.; Sajan, C. P; Rai, K. M. L. and Byrappa, K. 2010. "Photocatalytic activity of TiO2:AlPO4-5 zeolites for the degradation of indigo carmine dye", Indian J chem Techn. 17 (2010), 191–197.

Kumar, M. N. V. R.; Sridhari, T. R.; Bhavani, K. D. and Dutta, P. K. 1998. "Trends in color removal from textile mill effluents", Colorage. 40 (1998), 25–34.

Landrum, G. A.; Goldberg, N. and Hoffman, R. 1997. Journal of Chemistry Society Dalton. 1997, 3605.

Lide, D. R. 2005. Handbook of Chemistry and Physics 86th ed. Boca Raton (FL): CRC Press. (2005)

Liqiang, J.; Xiaojun, S.; Weimin, C.; Zili, X.; Yaoguo, D. and Honggang, F. 2003. "The Preparation and Characterization of Nanoparticle TiO_2/Ti Films and Their Photocatalytic Activity", J. Phys. Chem. Solid. 64 (2003), 615-623.

Mansfield, E.; Kar, A.; Qiunn, T. P. and Hooker, S. A. 2010. "Quartz Crystal Microbalance for Microscale Thermogravimetric Analysis", Analytical Chemistry. (2010).

Muruganandham, M.; Shobana, N. and Swaminathan, M. 2005. "Optimization of solar photocatalytic degradation conditions of Reactive Yellow 14 azo dye in aqueous TiO_2", Journal of Molecular Catalysis A: Chemical. 246 (2005), 154-161.

Nagaveni, K.; Sivalingam, G. and Heged, M. S. 2004. "Solar photocatalytic degradation of dyes:high activity of combustion synthesized nano TiO_2", Applied Catalysis B: Environmental. 48 (2004), 83-93.

Nakamoto, K. 1978. Infared and Raman Spectra of Inorganic and Coordination Compound, 3rd ed, John Wiley & Sons, Inc., New York. (1978).

Nakamoto, K. 1986. Infared and Raman Spectra of Inorganic and Coordination Compound, 4rd ed, John Wiley & Sons, Inc., New York. (1986).

Nakamoto, K. 1997. Infared and Raman Spectra of Inorganic and Coordination Compound, 5rd ed, John Wiley & Sons, Inc., New York. (1997).

Niemantsverdriet, J. W. 1993. Spectroscopy in catalysis: Introduction. VCH Publishers. (1993).

Nigam, P.; Banat, I. M., Singh, D. and Marchant, R. 1996. "Microbial process for the decolorization of textile effluent containing azo, diazo and reactive dyes", Process Biochem. 31 (1996), 435–442.

Nigam, P. and Marchant, R. 1995. "Selection of the substratum for composing biofilm system of textile decolourizing bacteria", Biotechnol. Lett. 17 (1995), 993–996.

Ogawa, T. and Yatome, C. 1990. "Biodegradation of azo dyes in multistage rotating biological contractor immobilized by assimilating bacteria", Bull. Environ. Contam. Toxicol. 44 (1990), 561–566.

Photochemistry from Kendric C. Smith. Stanford University School of Medicine. http://www.photobiology.info/Photochem.html (accessed March 24, 12).

Pelletier, P. and Caventou. 1819. J. B. Ann. Chim. 10 (1819), 164.

Potdar, H. S.; Deshpande, S. B. and Date, S.K. 1999. "Chemical coprecipitation of mixed (Ba+Ti) oxalates precursor leading to $BaTiO_3$ powders", Material Chemistry and Physics. 55 (1999), 121-127.

Pungora and Erno. 1995. A Practical Guide to Instrumental Analysis, Boca Raton, Florida. (1995), 181–191.

Rajpure, K. J. and Bhosale, C. H. 2000. Chem. Mater. Chem. Phys. (2000).

Random, C.; Wongnawa, S. and Boonsin, P. 2004. "Bleaching of Methylene Blue by Hydrated Titanium Dioxide", Science Asia. 30 (2004), 149-156.

Robinson, T.; McMullen, G.; Marchant, R. and Nigam, P. 2001. "Remediation of dyes in textile effluent: a critical review on current treatment technologies with a proposed alternative", Bioresource Technology. 77 (2001), 247-255.

Rouquerol, F.; Rouquerol, J. and Sig, K. 1999. Adsorption by Powders and Porous Solids: Princiciples, Methodology and Application. Acadamic press. (1999).

Ryu, Z.; Zheng, J.; Wang, M. and Zhang, B. 1999. "Characterization of pore size distributions on carbonaceous adsorbents by DFT", Carbon. 37 (1999), 1257-1264.

Scanning Electron microscopy from Wikipedia, the free encyclopedia. http://en.wikipedia.org/wiki/Scanning_electron_microscope (accessed March 18, 12).

Serpone, N.; Lawless, D. and Khairudinov, R. 1995. "Size Effect Photophysical Properties of Colloidal Anatase TiO_2 Particles: Size Quantization or Direct Transition in This Indirect Semiconductor", J. Phys. Chem. 99 (1995), 16646-16654.

Sharma, Y. K.; Kharkwal, M.; Uma, S. and Nagarajan, R. 2009. "Synthesis and characterization of titanates of the formula $MTiO_3$ (M= Ma, Fe, Co, Ni and Cd) by co-precipitation of mixed metal oxalate", Polyhedral. 28 (2009), 579-585

Sivalingam, G.; Nagaveni, K.; Hegde, M. S. and Madras, G. 2003. Applied Catalyst B: Environmental. 45 (2003), 23-38.

Skoog, D. A. and Leary, J. J. 1992. Principle of Instrumental Analysis, 5th Edition, Philadelphia: Saunders College Publishing. (1992).

Sophie Lalleman; Murielle Bertrand and Edouard Plasari. 2011. "Physical simulation of precipitation of radioactive element oxalates by using the harmless neodymium oxalate for studying the agglomeration phenomena", Journal of Crystal Growth. (2011).

Streitweiser; Andrew Jr.; Heathcock and Clayton, H. 1976. Introduction to Organic Chemistry. Macmillan. (1976), 737.

Structure of oxalic acid dihydrate. (http://en.wikipedia.org/wiki/File:Oxals%C3%A4ure3.svg (accessed May 18, 12).

Structure of titanium isopropoxide.
(http://en.wikipedia.org/wiki/File:Ti(OiPr)4.png (accessed May 26, 12).

Structure of titanium oxide sulphate: Compound Summary.
(http://pubchem.ncbi.nlm.nih.gov/image/structurefly.cgi?cid=61684&width=400&height=400 (accessed June 16, 12).

Suzuki, E. 2002. "High-resolution scanning electron microscopy of immunogold-labelled cells by the used of thin plasma coating of osmium". 208 (2002), 153-157.

Svensson, P. H. and Lars Kloo. 2002. "Synthesis, structure and bonding in polyiodide and metal iodide-iodine systems", Chemical Review. 103 (2002), No.5.

Tincture of Iodine from Wikipedia, the free encyclopedia.
http://en.wikipedia.org/wiki/Scanning_electron_microscope
(accessed July 26, 12).

Tornqvist, E. G. M. and Libby, W. F. 1979. Inorganic Chemistry. 18 (1979), 1792.

Tsezos, M. and Bell, J. P. 1989. "Comparison of the biosorption and desorption of hazardous organic pollutants by live and dead biomass", Water Res. 23 (1989), 561–568.

UV-Vis spectroscopy from The Pennsylvania State University Materials Characterization Laboratory.
http://www.mri.psu.edu/facilities/mcl/techniques/uv-vis/uv-vistheory.asp
(accessed July 21, 12).

Velde van de, G. M. H.; Harkema, S. and Gellings, P. J. 1974. "The crystal and molecular structure of ammonium titanyl oxalate", Inorganica Chimica Acta.
11 (1974), 243-252. ISSN 0020-1693.

Velassco, M. J.; Rubio, F.; Rubio, J. and Oteo, J. L. 1999. "DSC and FT-IR analysis of the dry process of titanium alkoxide derived precipitates", Thermochimica Acta. 32 (1999), 91-97.

Wang Yuanbo; Qi Tao; Chu Jinglong and Zhao Wei. 2009. "Remove of iron from ilmenite by KOH leaching-oxalate leaching method", Rare Metal. 29 (2009), 9-15.

Wang, Z. C.; Chen, J. F. and Hu, X. F. 2000. "Preparation of nanocrystalline TiO_2 powders at near room temperature from peroxo-polytitanic acid gel", Material Letter. 43 (2000), 87-90.

Week, M. E. 1945. "In Discovery of the Elements", Journal of Chemical Education. 91 (1945), 304.

West, A. R. 1987. Solid State Chemistry and Its Application. John Wiley& Sons Ltd. (1987)

Wojciech Macyk; Konrad Szaciłowski; Grażyna Stochel; Marta Buchalska; Joanna Kuncewicz and Przemysław Łabuz. 2010. "Titanium(IV) complexes as direct TiO_2 photosentitizers", Coordination Chemistry Reviews. 254 (2010), 2687-2701.

Wunderlich, B. 1990. Thermal Analysis, Academic Press, New York. (1990), 137–140.

Yamamura, H.; Watanabe, A.; Shirasaki, S. and Tanada, M. 1985. Ceramics International. (1985)

Yanqing, Z.; Erwel, S.; Zhinzhan, C.; Wenjun, L. and Xingfang, H. 2001. "Influence of solution concentration on the hydrothermal preparation of titania crystallines", Journal of Material Chemistry. 11 (2001), 1547-1551.

Yu. V. Kolen' ko, A. A.; Burukhin, B.; Churagulov, R. and Oleinikov, N. N. 2004. "Phase Composition of Nanocrytalline Titania Synthesized under Hydrothermal Conditions from Different Titanyl Compounds", Inorganic Materials. 40 (2004), No. 8, 822-828.

Yu, J.; Yu, J. C.; Leung, M. K. P.; Ho, W.; Cheng, B.; Zhao, X. and Xhao, J. 2003. "Effects of acidic and basic hydrolysis catalysts on the photocatalytic activity and microstructures of bimodal mesoporous titania", Journal of Catalysis. 217 (2003), 69-78.

Zhang, Y.; Weidenkaff, A. and Reller, A. 2002. "Mesoporous Structure and Phase Transition of Nanocrystalline TiO_2", Mater. Lett. 54 (2002), 375-381.

Zhao, X. K. and Fendler, J. H. 1991. "Size Quantization in Semiconductor Particulate Films", J. Phys. Chem. 95 (1991), 3716-3723.

Zhou, G. and Li, W. 1989. The Abnormally Long C-C Bond in the Oxalate Ion. 99 (1989), 572.

Zhou, W. and Zimmerman, W. 1993. "Decolorization of industrial effluents containing reactive dyes by actinomyces", Microbiol. Lett. FEMS 107 (1993), 157–162.

APPENDICES

Photocatalytic activity tests

TABLE 1 The percentage of iodine solution concentrations in the range 0.1-7.5 mM decolorization by titanium oxalate crystalline complexes (*TiOX-03*).

Concentration of iodine solution	Decolorization efficiency by UV irradiation (% ± SD) with time (hours)		
	1	2	3
1 x 10^{-4} M	52.2 ± 1.1	73.1 ± 1.5	92.1 ± 1.9
5 x 10^{-4} M	28.2 ± 0.9	42.6 ± 1.3	60.6 ± 1.8
1 x 10^{-3} M	28.7 ± 0.5	37.5 ± 0.7	46.8 ± 0.9
2.5 x 10^{-3} M	24.3 ± 1.6	58.1 ± 3.0	59.2 ± 3.0
7.5 x 10^{-3} M	18.7 ± 0.9	25.2 ± 1.2	27.8 ± 1.4

TABLE 1 The percentage of iodine solution concentrations in the range 0.1-7.5 mM decolorization by *TiOX-03*. (Continued)

Concentration of iodine solution	Decolorization efficiency by UV irradiation (% ± SD) with time (hours)		
	4	5	6
1 x 10^{-4} M	96.7 ± 0.7	99.3 ± 0.2	99.7 ± 0.2
5 x 10^{-4} M	75.9 ± 2.3	97.1 ± 0.8	99.2 ± 0.8
1 x 10^{-3} M	66.7 ± 1.3	72.0 ± 1.5	76.6 ± 3.3
2.5 x 10^{-3} M	60.4 ± 3.1	63.5 ± 3.1	65.2 ± 3.3
7.5 x 10^{-3} M	29.8 ± 1.4	32.5 ± 1.6	33.8 ± 1.7

TABLE 2 The percentage of iodine solution concentrations in the range 0.2-0.4 mM decolorization by *TiOX-0*3.

Concentration of iodine solution	Decolorization efficiency by UV irradiation (% ± SD) with time (hours)		
	1	2	3
$2.5x10^{-4}M$	26.6 ± 2.8	60.9 ± 3.0	75.1 ± 3.5
$3x10^{-4}M$	25.9 ± 0.8	53.8 ± 1.6	68.6 ± 2.1
$3.5x10^{-4}M$	23.8 ± 0.5	35.4 ± 0.7	45.1 ± 0.9
$4x10^{-4}M$	22.0 ± 1.6	28.8 ± 3.0	35.4 ± 3.0

TABLE 2 The percentage of iodine solution concentrations in the range 0.2-0.4 mM decolorization by *TiOX-0*3. (Continued)

Concentration of iodine solution	Decolorization efficiency by UV irradiation (% ± SD) with time (hours)		
	4	5	6
$2.5x10^{-4}M$	85.9 ± 3.0	99.3 ± 1.7	99.7 ± 0.2
$3x10^{-4}M$	79.5 ± 2.0	88.7 ± 2.0	98.9 ± 1.2
$3.5x10^{-4}M$	57.6 ± 1.3	70.1 ± 1.5	78.6 ± 1.7
$4x10^{-4}M$	48.5 ± 3.1	53.7 ± 3.1	62.9 ± 3.3

TABLE 3 The percentage of iodine solution decolorization by crystalline titanium oxalate complexes was comparatively studied with P25 TiO_2.

Sample	Decolorization efficiency by UV irradiation (% ± SD) with time (hours)		
	1	2	3
TiOX-01	19.8 ± 0.3	29.9 ± 0.5	40.3 ± 0.7
TiOX-03	24.7 ± 1.1	51.4 ± 2.3	65.5 ± 3.0
P-25	65.5 ± 1.4	73.8 ± 1.6	77.9 ± 1.7

TABLE 3 The percentage of iodine solution decolorization by crystalline titanium oxalate complexes was comparatively studied with P25 TiO_2. (Continued)

Sample	Decolorization efficiency by UV irradiation (% ± SD) with time (hours)		
	4	5	6
TiOX-01	57.1 ± 0.9	71.2 ± 1.2	73.8 ± 1.2
TiOX-03	75.8 ± 3.5	86.7 ± 1.9	97.1 ± 2.1
P-25	78.9 ± 1.7	82.4 ± 1.8	84.6 ± 1.9

TABLE 4 The influence of pH on the percentage degradation of iodine solution ($3x10^{-4}$ M) decolorization by *TiOX-03*.

pH iodine solution	Decolorization efficiency by UV irradiation (% ± SD) with time (hours)		
	1	2	3
2.3	26.1 ± 0.7	54.2 ± 1.4	69.1 ± 1.8
5	35.9 ± 0.4	57.1 ± 0.6	68.0 ± 0.8
7	41.0 ± 0.8	65.4 ± 1.3	77.4 ± 1.5
10	92.7 ± 1.2	97.2 ± 1.2	97.8 ± 1.2

TABLE 4 The influence of pH on the percentage degradation of iodine solution ($3x10^{-4}$ M) decolorization by *TiOX-03*. (Continued)

pH iodine solution	Decolorization efficiency by UV irradiation (% ± SD) with time (hours)		
	4	5	6
2.3	80.0 ± 2.1	89.0 ± 2.4	98.7 ± 1.3
5	85.7 ± 1.0	94.9 ± 1.1	99.2 ± 1.1
7	95.0 ± 1.9	96.7 ± 0.3	99.7 ± 1.7
10	98.5 ± 1.3	98.6 ± 1.3	98.6 ± 1.3

TABLE 5 The effect of UV light intensity on the percentage degradation of iodine solution ($3x10^{-4}$ M) decolorization by *TiOX-03*.

UV light tube	Decolorization efficiency by UV irradiation (% ± SD) with time (hours)		
	1	2	3
1	14.6 ± 0.7	27.5 ± 1.3	37.7 ± 1.8
3	22.0 ± 1.1	41.3 ± 2.1	56.7 ± 2.9
5	25.0 ± 0.9	52.1 ± 1.9	66.5 ± 2.4

TABLE 5 The effect of UV light intensity on the percentage degradation of iodine solution ($3x10^{-4}$ M) decolorization by *TiOX-03*. (Continued)

UV light tube	Decolorization efficiency by UV irradiation (% ± SD) with time (hours)		
	4	5	6
1	40.8 ± 1.9	43.3 ± 2.0	47.0 ± 2.2
3	61.3 ± 3.1	65.7 ± 2.5	71.9 ± 2.0
5	76.8 ± 2.8	85.5 ± 3.1	99.7 ± 2.1

TABLE 6 The percentage degradation of iodine solution ($3x10^{-4}$ M) decolorization on the number of repeated uses time of *TiOX-03*.

Repeated uses time	Decolorization efficiency by UV irradiation (% ± SD) with time (hours)		
	1	2	3
1	16.7 ± 0.4	35.2 ± 0.9	44.9 ± 1.1
2	7.6 ± 0.2	18.2 ± 0.5	25.7 ± 0.7
3	4.8 ± 0.1	10.8 ± 0.3	20.5 ± 0.7

TABLE 6 The percentage degradation of iodine solution ($3x10^{-4}$ M) decolorization on the number of repeated uses time of *TiOX-03*. (Continued)

Repeated uses time	Decolorization efficiency by UV irradiation (% ± SD) with time (hours)		
	4	5	6
1	53.7 ± 1.3	65.6 ± 1.7	82.1 ± 2.1
2	40.2 ± 1.1	53.5 ± 1.5	64.3 ± 1.9
3	31.8 ± 1.1	43.2 ± 1.5	54.1 ± 1.2

VITAE

Name Mr. Tanin Tudrabiab

Student ID 5210220028

Educational Attainment

Degree	Name of Institution	Year of Graduate
B. Sc. (Chemistry)	Prince of Songkla University	2004

Scholarship Awards during Enrollment

1. Outstanding poster presentation award from the Pure and Applied Chemistry International Conference 2011(PACCON 2011)
2. Center of Excellence for Innovation in Chemistry (PERCH-CIC)
3. Teaching Assistant, Department of Chemistry, Prince of Songkla University

List of Publication and Proceedings

1. Tudrabiab, T., Wongnawa, S. 2011. PHOTOCHEMISTRY OF IODINE SOLUTION AND TITANIUM OXALATE COMPLEX. Proceedings of the Pure and Applied Chemistry International Conference 2011 (PACCON 2011). Miracle Grand Hotel, Bangkok, Thailand. January, 5-7, 2011. pp. 248-251.

2. Tanin Tudrabiab and Sumpun Wongnawa, 2011. Photochemistry of Iodine Solution and Titanium Oxalate Complex. Proceedings of the 7th Invitation to the International Congress for Innovation in Chemistry (PERCH-CIC Congress VII). Jomtein Palm Beach Hotel & Resort, Pattaya, Chonburi, Thailand. May 4-7, 2011. pp. 82.